Sensitivity of Urban Buildings to Tunneling-Induced Settlements

PhD DISSERTATION

PhD Dissertation by:

Carles Camós i Andreu

Supervised by:

Dr. Climent Molins i Borrell

UNIVERSITAT POLITÈCNICA DE CATALUNYA BARCELONATECH

Departament d´Enginyeria de la Construcció

Barcelona, February 2015

SENSITIVITY OF URBAN BUILDINGS TO TUNNELING-INDUCED SETTLEMENTS

PhD Dissertation by

Carles Camós i Andreu

Supervised by

Dr. Climent Molins i Borrell

This research has received the financial support of the *Ministerio de Educación y Ciencia* through the research project SUBTIS (*Study of the Sensitivity of Urban Buildings to Tunneling Induced Settlements*, ref. num. BIA2009-13233), the European Regional Development Fund (ERDF) and the *Col·legi d'Enginyers de Camins, Canals i Ports de Catalunya*.

Keywords: Tunneling, settlement, building damage, equivalent beam, numerical simulation, structural reliability, Bayesian updating, allowable settlements

Printed in Barcelona, Catalonia, February 2015

"The probability of success is difficult to estimate;

but if we never search the chance of success, is zero"

(Giuseppe Cocconi and Philip Morrison, 1959)

Agraïments - Acknowledgements

Des d'aquestes línies voldria reconèixer tota una sèrie de gent sense les quals, tòpics a part, no hagués aconseguit mai escriure totes les pàgines que vénen a continuació. I per començar, és evident que sense el suport i l'estima dels meus pares i de la meva germana, tot això no hauria estat possible.

Vull agrair al supervisor d'aquesta tesi, Climent Molins, la confiança constant que m'ha mostrat per emprendre el que ell em va deixar ben clar des del primer dia que seria una aventura. Han estat gairebé 6 anys de treball conjunt entre la tesina, el projecte de final de carrera i la tesi doctoral, d'on me n'emporto moltes bones coses. Des d'aquí agraeixo també l'ajut de l'Oriol Arnau, una persona que va passar-se hores assegut al meu costat amb una paciència infinita per tal de fer-me entendre que tot plegat era una qüestió de convergència, i que si allò divergia, alguna cosa no estava fent bé. Bromes a part, gràcies per tot!

Part of this thesis was developed in the Engineering Risk Analysis Group of the Technische Universität München (Munich, Germany). This experience definitely marked a milestone in my life, for which I want to thank my supervisors there, Olga Špačková and Daniel Straub for all the gathered knowledge. I will always keep with me the friendship of the rest of ERA members, Giulio, Patty, Iason, Killian, Jesús, Wolfang, Ji, Karen and Anneliese.

Im Laufe meines Forschungsaufenthalts am Techno Innovation South Tyrol (TIS) in Bozen hatte ich das Vergnügen mit Johannes Brunner und Daniel Reiterer zusammenarbeiten zu dürfen. Ich danke ihnen für deren wertvollen Hilfe und Unterstützung in der Ausarbeitung dieser Doktorarbeit.

Han estat diversos anys de trobar-me dia a dia amb gent collonuda. Gràcies a tots els companys del Departament per fer-ho tot plegat simplement molt agradable: Mireia, Clara, Luca, Tasos, Ahmed, Yohei, Francesc, Maria del Mar, Júlia, Marta, Giorgio, Pau, Ana, Albert, Liao, Sandra, Alexis, Barbara, Prashan i Razmic. I a part de fer-ho agradable, la Mercè, les dues Carme's i la Montse ho han fet a més, ben fàcil. Des d'aquí vull donar també les gràcies al Professor Pere Roca, a l'Alessandra di Mariano i a la Teresa Yubero per la seva atenció, predisposició i ajuda que m'han mostrat en tot moment.

I a tots els meus amics que em suporteu cada dia, i a vosaltres Anna, Xevi i Fra, infinites gràcies per tot.

Summary

Tunneling construction represents an alteration to the distribution of soil pressures that will almost inevitably generate ground subsidence, which can endanger the adjacent buildings in urban areas. The risk of building damage can be substantially reduced with a comprehensive preliminary damage assessment during tunnel design phases, in combination with excavation techniques that minimize ground subsidence.

The present research aims to increase the knowledge concerning the analytical and numerical techniques for building damage prediction related to tunneling. The thesis starts with the study of a real case of masonry building affected by the construction of the L9 metro line tunnel in Barcelona. Data available made possible to develop 2D and 3D numerical models of the building. The latter includes also the soil, the lining and interface models to simulate the contact between the building and the ground. The predicted crack patterns and opening widths in walls were verified by comparison to real damage reports. The case study also allowed a back analysis of the classical analytical prediction techniques based in the equivalent beam concept from Burland and Wroth.

Analytical predictions of building damage are typically done for building walls aligned transversally or longitudinally with respect to the tunnel axis. These buildings are statistically representative, since many urban tunnels follow the tracks of avenues or streets. However, there is a significant number of buildings randomly aligned with respect to tunnel axes, in particular when using a Tunnel Boring Machine. For these buildings, the application of the classical analytical methodology can be done only with approximations, which can lead to unrealistic damage assessments. For this reason, a novel equation for the determination of ground strain has been developed. This equation allows the application of the classical settlement Gaussian profiles and the equivalent beam method in 3D, i.e. for buildings located in whichever position with respect to the

tunnel axis. In addition, the model allows considering the position of the tunnel heading, which increases the realism of the settlement trough generated by tunnel construction.

Another detected issue during the present research was the high sensitivity of both analytical and numerical damage predictions to certain parameters related to the characterization of ground. In the case of analytical predictions, the modeling of settlement troughs by Gaussian curves offers numerous mathematical advantages. However, the simplicity of this approximation leads to substantially different estimations of damage for small variations of the governing parameters. For this reason, the use of reliability-based methods can be useful for the assessment of building damage. In this way, the present thesis shows the development of a probabilistic model for the prediction of tunneling-induced damage. A procedure to determine the maximum allowable settlements that are used as monitoring threshold values of the construction process is also included. Furthermore, it is shown how the prediction of ground behavior and the allowable settlements can be updated with a Bayesian method by incorporating measurements made during the construction.

Resum

La construcció de túnels representa una alteració de la distribució de pressions del sòl que, de manera pràcticament inevitable, genera assentaments en superfície. Aquests poden provocar danys en edificis, especialment en zones urbanes. No obstant, aquest risc es pot reduir substancialment mitjançant la correcta predicció dels danys en les fases de disseny del túnel, juntament amb l'ús de tècniques d'excavació que minimitzin els assentaments induïts.

La present recerca aprofundeix en la metodologia de predicció de danys en edificis afectats per la construcció de túnels urbans. La tesi comença amb l'estudi d'un edifici real d'obra de fàbrica afectat per la construcció del túnel de la línia L9 del metro de Barcelona. Mitjançant les dades disponibles, s'han realitzat models numèrics en 2D i 3D de l'edifici. Aquest últim inclou a més el sòl, el túnel i un conjunt d'elements d'interfície que simulen el contacte entre l'edifici i el terreny. Els patrons de fissuració predits pel model han estat comparats amb aixecaments dels danys fets durant les obres. L'estudi d'aquest cas ha permès també l'aplicació i verificació de les tècniques de predicció de danys en edificis basades en el concepte de la biga equivalent ideat per Burland i Wroth durant la dècada dels 70.

Les prediccions analítiques de dany en edificis es duen a terme generalment assumint els edificis posicionats transversalment o longitudinalment respecte l'eix del túnel. El nombre d'edificis que compleix aquesta hipòtesi és estadísticament representatiu, ja que molts túnels segueixen la traça dels carrers o les avingudes de les ciutats. Tot i així existeix un gran nombre d'edificis alineats arbitràriament respecte l'eix del túnel, especialment quan la construcció del túnel es realitza mitjançant l'ús de tuneladores (*Tunnel Boring Machines* – TBM). Per aquests edificis, l'aplicació de la metodologia

analítica clàssica es pot efectuar només mitjançant aproximacions, la qual cosa pot implicar estimacions poc realistes dels danys. Per aquest motiu, s'ha desenvolupat una nova equació per al càlcul de la deformació del terreny. Aquesta equació permet l'aplicació dels perfils Gaussians d'assentament clàssics i del model de la biga equivalent en 3D, és a dir, en edificis ubicats en qualsevol posició respecte l'eix del túnel. A més, el model permet considerar la posició del front d'excavació, incrementant així el realisme del camp d'assentaments generat per la construcció del túnel.

Un altre aspecte important detectat durant la recerca és l'extrema sensibilitat de les prediccions dels danys segons els valors dels paràmetres relacionats amb la caracterització del terreny. La modelització del camp d'assentaments mitjançant perfils Gaussians ofereix una sèrie d'avantatges matemàtics, però tot i així, la simplicitat del model comporta diferències notables en l'estimació dels danys si s'efectuen petites variacions dels paràmetres d'entrada. És per això que les tècniques de fiabilitat estructural poden ser útils per a l'estimació dels danys. En aquesta línia, la tesi mostra un model probabilístic per a la predicció dels danys provocats en edificis degut a la construcció de túnels. L'aplicació de tècniques de fiabilitat estructural permet a més la determinació dels llindars d'assentament que s'utilitzen durant el procés constructiu. En cas de tenir mesures prèvies d'assentaments de la zona d'estudi, es mostra també com el comportament del terreny i aquests valors llindars poden actualitzar-se a través d'un mètode Bayesià.

Table of Contents

Table of Figures

List of Tables

1. Introduction

In 2005, a ground collapse in the neighborhood of *'El Carmel'* (Barcelona) occurred during the construction of a maneuver queue tunnel of the L5 metro line. Due to the excessive convergence detected in the tunnel, an inverted arch was constructed for safety reasons in a sandstone zone. However, an undetected discontinuity in the ground entailed the generation of a hole of 35m deep and 30m of diameter (Figure 1.1). Although no human losses were caused, hundreds of residents had to be rehoused and ground stabilization works were prolonged for months.

Figure 1.1. Ground collapse in the neighborhood of 'El Carmel' (Barcelona) Source: El Periódico de Catalunya.

The accident of *'El Carmel'* created a huge technical and political distrust in the country, in addition to outrage for the dangerous tendency of cutting prices devoted to public infrastructure at the expense of reducing safety measures. This kind of events evidence the importance of safety in excavation processes of urban tunnels, wherein reliable assessments of building damage at design stages play a crucial role.

1.1 BACKGROUND

With time, tunnel construction has become an essential aspect in the integration of infrastructures in the cities, mainly because of the general lack of space on urban surface. The construction of new and more efficient metro and railway lines, roads and supply infrastructures, have been made possible by the continuous evolution of tunneling technology. However, excavation processes represent an alteration to the distribution of soil pressures that will almost inevitably generate ground subsidence (Burland, 2008). Its severity is related to the type of ground, the depth and diameter of the tunnel, the construction technology and human factors. In the case of urban areas, ground deformations are critical since they can endanger buildings and other structures located in the vicinity of the tunnel.

The associated risk with tunneling activity can be substantially reduced with the use of excavation techniques that minimize subsidence and with the performance of exhaustive damage assessments during design phases. If estimated damages exceed the tolerable predefined limits, modifications on the tunnel design should be taken into account, as well as the implementation of mitigation measures and building strengthening in the zones with a higher risk of damage (Deulofeu *et al.*, 2007; Giardina, 2013).

The prediction of building damages is difficult due to the limited knowledge of geotechnical conditions and the existing uncertainty in predicting the response of the structure to the settlements. This response is usually addressed by the application of analytical and empirical approaches developed in the 70s and 80s. These approaches are based on the equivalent beam concept, which models a certain building as a linear elastic beam conforming to a settlement profile (Burland and Wroth, 1974; Boscardin and Cording, 1989). The magnitude of the tensile strains generated on the beam is further compared to limiting strain values, which in turn define the categories of severity of the affection.

The equivalent beam model is based on hypotheses that facilitate its common application, but that may turn the method somewhat uncertain (Gesto and Gens, 2008). Although the literature in this field and its use in engineering practice are extensive, back analyses that allow the appropriate assessment of such methods are rather scarce. For this reason, it is of major importance to verify the reliability of these approaches by comparing their predictions with real cases of damage occurred due to tunneling. Moreover, designers are often unaware of certain aspects that may be critical on the damage predictions and that could lead to deviated estimations. For example, analytical predictions of building damage are typically done for building walls aligned transversally or longitudinally with respect to the tunnel axis. These buildings are statistically representative, since many urban tunnels follow the tracks of avenues or streets. However, a significant number of buildings are randomly aligned with respect to tunnel axes, in particular when using a Tunnel Boring Machine (Guglielmetti *et al.*, 2008). For these buildings, the application of the classical analytical methodology can be done only with approximations, which can lead to unrealistic damage assessments. Moreover, the position of the tunnel face is usually not taken into account. This can be critical in the predictions because maximum damage can be generated when the tunnel heading is approaching the building.

More detailed damage predictions can be performed by the use of numerical analyses including the buildings, the soil, the tunnel and the simulation of the excavation process. The use of Finite Element Models (FEM) allows for instance the determination of cracking patterns on walls, as well as the estimation of cracks' widths. Most of the guidelines given in works from the 1990s and 2000s (Lourenço, 1996; Augarde, 1997; Burd *et al.*, 2000; Rots *et al.*, 2005) are still valid in the current numerical models. Nevertheless, the improvement of computer features allows performing more complex and detailed models, which in turn need the comparison to real case studies in order to state the validity of their predictions.

It is important to remark that both analytical and numerical prediction methods are however very sensitive to certain parameters related to the ground description. For example, settlement troughs are typically modeled by Gaussian curves in the case of analytical methods, which offer numerous mathematical advantages. Even so, the simplicity of this model leads to substantially different estimations of damage for small variations of the governing parameters (Kym *et al.*, 2001). For this reason, the application of reliability-based methods seems to be reasonable when performing assessments of

building damage. Moreover, it should be evident that a realistic assessment of the associated uncertainties is crucial in the decision making during all phases of tunnel construction projects (Špačková and Straub, 2013).

1.2 RESEARCH OBJECTIVES

The present research aims to increase the knowledge concerning the analytical and numerical techniques for the prediction of building damage related to tunneling. The adequate achievement of the main goals is planned through the sequential accomplishment of the partial targets listed below:

- Characterization of a real case of building damage produced by tunneling works.
- Development of 2D and 3D models of the building and comparison between the predicted and real damage.
- Validation of the damage prediction done with the classical analytical methodology, based on the equivalent beam method.
- Development of a 3D analytical model for the prediction of building damage.
- Study of the influence of the building wall location with respect to the tunnel axis on the estimated damage.
- Development of a probabilistic model for the prediction of building damage.
- Use of this model for the reliability-based determination of maximum allowable settlements and their updating with prior measurements gathered during the excavation process.

1.3 DISSERTATION OUTLINE

The present dissertation is organized as a compilation of three research journal papers and an extension of a conference paper. Each paper has been edited and presented as an individual chapter in a thesis format.

Chapter 2 studies the structural response of a group of masonry buildings subjected to real ground movements experienced during the construction of the L9 Metro tunnel in Barcelona, bored by a TBM-EPB. The real structural damage presented in the buildings is compared with the predictions given 1) by the equivalent beam and 2) by the application of a non-linear 2D Finite Element macro-model. Main model parameters were determined by means of characterization experiments developed on the site and in the laboratory.

This chapter represents also a review of the state-of-the-art regarding the research field of this thesis.

Chapter 3 presents a 3D Finite Element macro-model of the case study shown in Chapter 2. The numerical model simulates the tunnel face advance with a phased analysis. The behavior of masonry is simulated with the Total Strain Rotating Crack model. Interface elements are included to simulate the contact between the building and the soil. Results allow verifying the differences in the resulting damage when taking into account the tunnel face advance and the bent layout of the tunnel, which further increase the 3D effects.

Chapter 4 proposes a novel equation for the determination of ground horizontal strain. This equation departs from the expressions of the classical Gaussian settlement profiles. The novel formulation allows the modeling of the tunnel advance and the application of the equivalent beam method in 3D. The results show significant variations of estimated damage according to the wall position with respect to the tunnel axis. A parametric analysis is further performed to create a non-linear regression model that allows direct estimation of the maximum tensile strain generated in a building by tunneling subsidence.

Chapter 5 shows the development of a probabilistic model for the prediction of tunneling-induced damage. The novel equation proposed in Chapter 4 is used for this purpose. Moreover, the chapter shows a Bayesian method for updating the predicted settlements when measurements are available. The probabilistic model is used for determining maximum allowable settlements, which are used as threshold values for monitoring the construction process. The proposed methodology is applied to the group of masonry buildings shown in Chapter 2.

The work of Chapter 5 was carried out in the Engineering Risk Analysis Group of the Technische Universität München (TUM, Munich, Germany), under the supervision of Prof. Dr. Daniel Straub and Dr. Olga Špačková.

An overview of the dissertation outline is shown in Figure 1.2.

1.4 PUBLICATIONS

1.4.1 Publications conforming the present dissertation

The research papers presented as chapters of the thesis are listed in the following.

Chapter 2

- *'A Case Study of Damage on Masonry Buildings Produced by Tunneling Induced Settlements'*

  Authors: Carles Camós, Climent Molins and Oriol Arnau.
  International Journal of Architectural Heritage, 8, 602-625. 2014.

Chapter 3

- Extension of *'A 3D Temporal Evolutionary Numerical Model of a Masonry Building in Barcelona Subjected to Tunneling Induced Settlements'*

  Authors: Carles Camós and Climent Molins.
  EURO:TUN 2013, 3rd International Conference on Computational Methods in Tunneling and Subsurface Engineering. Bochum, Germany.

Chapter 4

- *'3D Analytical Prediction of Building Damage Produced by Tunneling Subsidence'*

  Authors: Carles Camós and Climent Molins.
  Submitted to the Journal of Tunnelling and Underground Space Technology.

Chapter 5

- *'Probabilistic Approach to Assessing and Monitoring Settlements Caused by Tunneling'*

  Authors: Carles Camós, Olga Špačková, Daniel Straub and Climent Molins.
  Submitted to the Journal of Tunnelling and Underground Space Technology.

1.4.2 Other publications developed in the framework of the thesis

- *'Development of a probabilistic model for the prediction of building damage due to tunneling induced settlements'*

  Authors: Carles Camós, Olga Špačková, Daniel Straub and Climent Molins.
  4th International Symposium on Geotechnical Safety and Risk (2013), Hong Kong, China.

- *'Study of the sensitivity of different building structures to tunneling induced settlements'*

  Authors: Climent Molins and Carles Camós.
  2nd International Conference on Structures and Architecture (2013). Guimaraes, Portugal.

- *'Estudio de las cubetas de asientos producidas por la tunelación y simulación de la respuesta estructural de edificios afectados'*

  Authors: Carles Camós, Climent Molins, Oriol Arnau and Vicente Alegre.
  V ACHE Conference (2011), Barcelona, Spain.

- *'Clasificación de los tipos constructivos y estructurales de los edificios para el estudio de su sensibilidad frente a los efectos de la tunelación'*

  Authors: Isabel Serrà, Carles Camós, Climent Molins and Mariel Chirino.
  V ACHE Conference (2011), Barcelona, Spain.

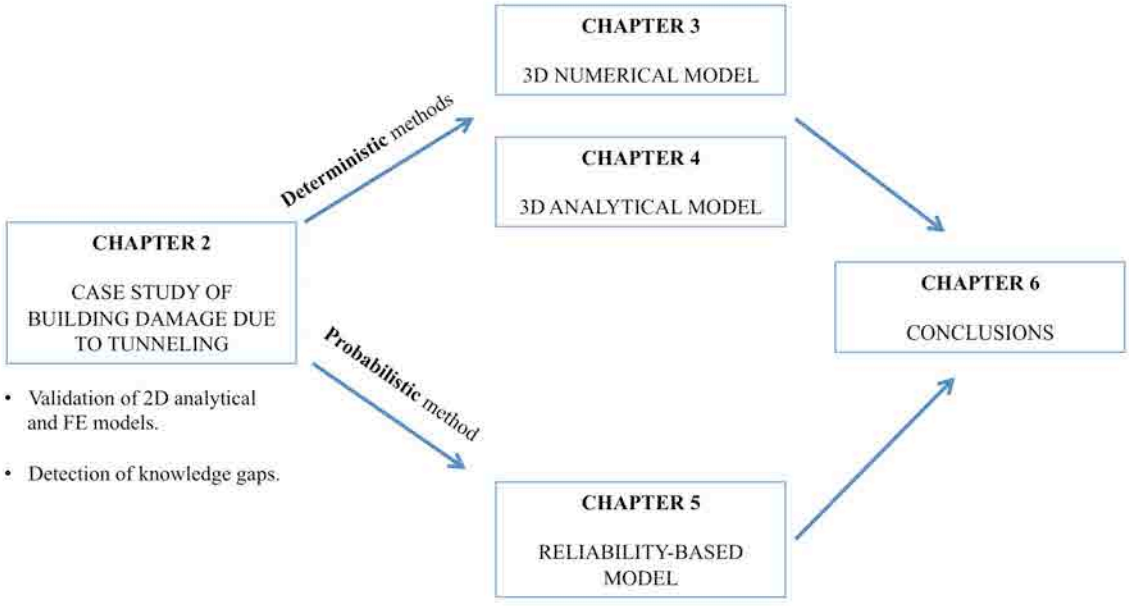

Figure 1.2. Dissertation outline.

2. Case Study of Damage on Masonry Buildings Produced by Tunneling-Induced Settlements

Abstract: This chapter analyzes the structural response of a group of masonry buildings subjected to real ground movements experienced during the construction of the L9 Metro tunnel in Barcelona, bored by a TBM-EPB. The studied one-story small dwellings represent a common building typology frequently used in those days in Barcelona's outskirts (more than 1000 were erected). Real settlement profiles are compared with the ones provided by empirical methods, which estimate the shape and the area of the trough according to the ground properties and the volume loss (inherent to the tunneling construction method). The real structural damage presented in the buildings is compared with the predictions given by two different methods: 1) the equivalent beam and its subsequent refinements, and 2) the appliance of a non-linear Finite Element macro-model. Main model parameters have been determined by means of characterization experiments developed on the site and in the laboratory, thus giving a much higher significance to the analysis. The obtained predictions present a high correspondence with the real damage registered, particularly in crack patterns and widths.

Keywords: Tunneling, settlements, building, structural damage, equivalent beam, numerical simulation.

2.1 INTRODUCTION

Underground constructions, such as tunnels and excavations, are essential to integrate transportation infrastructures in our cities. Tunneling always produces settlements in ground surface that can affect the architectural heritage along its track. The significance of the ground movements is closely related to the diameter of the tunnel section, the tunnel depth and the particular conditions of the surrounding ground (bearing capacity of materials, presence of groundwater and the construction method employed). The prediction of the value and location of settlements is an essential task of the design process in order to set out the proper instrumentation to control the surface settlements evolution and thus, to minimize the damage likely to occur in buildings (Standing, 2008).

The classical methodology of subsidence prediction is still widely used. It is based on empirical approaches that describe the settlement profile transverse to the tunnel axis by means of Gaussian shape curves (Peck, 1969; Attewell *et al.*, 1986; Rankin, 1988) (Figure 2.1). Apart from settlements, tunneling also produces horizontal ground displacements, which can induce tensile and compressive strains in building foundations.

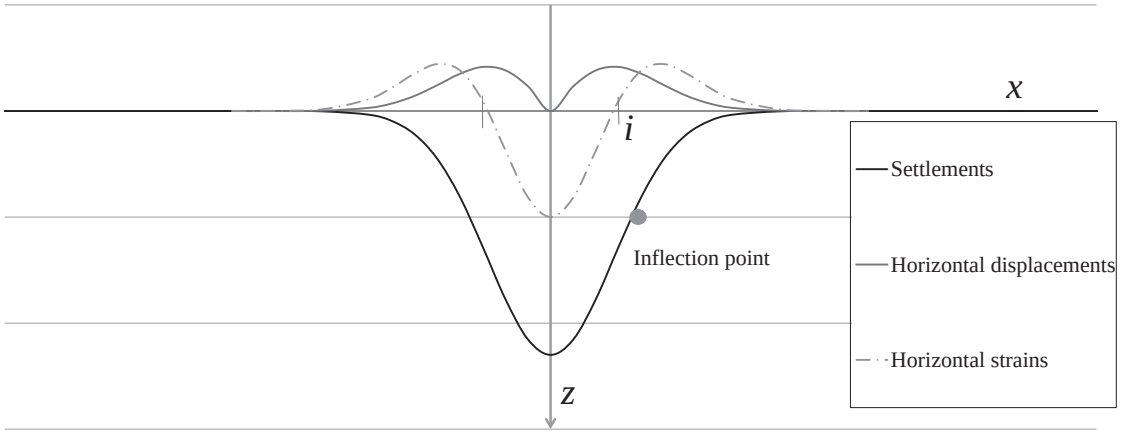

Figure 2.1. Illustration of transverse settlement trough, horizontal displacements and strain profiles.

Once the foreseeable ground movements are determined in *greenfield* conditions (meaning *no presence of buildings and pavements*), the determination of damage on buildings is commonly estimated by using an equivalent weightless elastic beam, which models the walls of the building assuming that they conform perfectly to the settlement shape (Burland and Wroth, 1974). The maximum tensile strains in this beam are calculated according to the expressions of the deflection in a centrally loaded beam,

having both bending and shear stiffness (Timoshenko, 1957). In addition, the influence of horizontal tensile strain coming from ground can be introduced by superposition according to the approach of Boscardin and Cording (1989).

The maximum strains ε_{max} obtained in the equivalent beam are further compared with strain thresholds ε_{lim} that define different categories of damage associated with masonry buildings (Table 2.1 - Burland *et al*., 1977). This classification gives the description of the typical damage likely to occur in terms of degree of severity, typical damage and ease of repair.

This methodology has been mainly used in preliminary phases of design and quite often the results obtained have still been conservative. In the majority of cases, real damage was less than the assessed. The reason for this is that, in calculating the tensile strains, the building is assumed to have no stiffness so that it conforms to the *greenfield site* subsidence trough (Burland, 2008). For this reason, Potts and Addenbrooke (1997) assessed the influence of the inherent stiffness of a building and introduced a set of factors in order to take into account the interaction with the supporting ground and hence, obtaining apparently more reliable strains within a building.

Table 2.1. Classification of building damage (Burland et al., 1977).

Category of damage	**Normal degree of severity**	**Typical damage**	**Tensile strain ε_{max} (%)**	$\varepsilon_{lim}(\%)$
0	Negligible	Hair cracks less than 0.1mm	0 – 0.050	0.050
1	Very slight	Fine cracks up to 1mm	0.050 – 0.075	0.075
2	Slight	Cracks easily filled up to 5mm	0.075 – 0.150	0.150
3	Moderate	Cracks from 5 to 15mm	0.150 – 0.300	0.300
4	Severe	Extensive repair works. Cracks from 15 to 25mm	> 0.300	-
5	Very severe	Partial or complete rebuilding. Cracks > 25mm	-	-

Today, the equivalent beam approach represents a first stage methodology commonly used in tunnel design to establish which buildings may require a detailed evaluation due to their sensitivity to tunneling induced settlements. Commonly, when drilling a tunnel, many recognition campaigns are carried out to distinguish whether possible structural pathologies can be related to tunneling, thus creating huge databases of information.

Additionally, the machine operational parameters recorded by different sensors installed in the shield, give a real-time control of the construction works and allow the suitability assessment of these classical approaches in damage prediction.

The equivalent beam approach is based on a series of hypotheses that facilitate its common application but can turn the method somewhat uncertain (Gesto and Gens, 2008). Also, very few examples of numerical damage prediction can be found in the literature (Lourenço, 1996; Burd *et al.*, 2000; Rots *et al.*, 2005). However, back analyses that allow the appropriate assessment of such methods are very difficult to found in the bibliography. For this reason, it is of major importance to check the reliability of these approaches by comparing their predictions with real cases of damage occurred due to tunneling.

The present paper focuses on the structural response of a group of masonry buildings subjected to tunneling subsidence experienced during the construction of the L9 Metro tunnel in the neighborhood of *Bon Pastor* (Barcelona). The one-story small dwellings erected (more than 1000), represent a common building typology frequently used in those days in Barcelona's outskirts. The analysis is carried out in the façade of a group of six dwellings located at *Sanet* street (Figure 2.2). This particular set of buildings was selected due to its proximity to the tunnel track and the elevated amount of settlements occurred during the construction of the Metro tunnel. Due to the relationship of these buildings to the history of the city, a sample will be preserved.

Initially, the real settlement profile is compared with the results provided by the state-of-the-art analytical expressions. The equivalent beam method and its subsequent refinements are then applied to predict the expected damages in the dwellings, which precision is stated by comparing with the real damage survey. However, techniques such as the equivalent beam can give only a broad classification of damage, which can be useful only for preliminary assessment. When a more detailed evaluation is pretended, numerical simulation has to be used to precisely estimate the location, pattern and width of cracks according to a given ground trough. Therefore, numerical tools have to be previously calibrated according to real cases. For this reason, and to complete the back analysis of the present case study, a numerical tool is applied to assess the reliability of FE methods in predicting building damage induced by tunneling subsidence. A detailed comparison of the results produced by the different methods allows achievement of practical conclusions on the application of those methods appraised in this paper. All

these analyses become especially significant since comprehensive geometric survey and mechanical characterization of the constituent materials of the buildings were carried out, providing realistic parameters to the advanced models used in damage prediction.

2.2 CASE STUDY

2.2.1 Introduction

The Metro Line 9 in Barcelona is a reference tunneling project due to its total length of shield driven tunnels of more than 40km and large excavation diameters (9,4m and 12,0m), encountering a wide variety of geological and hydrological conditions (Deulofeu *et al*., 2007). The case study corresponds to a neighborhood located at the north of the city, over an area of soft alluvium soils of the *Besòs* river delta. This zone represents one of the four main residential complexes built in 1929 in order to relocate workers coming from southern Spain for the construction works developed for the World Exposition celebrated in the city. Today, a reconstruction of the neighborhood is being done with the demolition of the oldest houses and the relocation of tenants in several new buildings, achieving the most substantial improvement for the neighborhood with the arrival of the Metro Line L9 in 2010.

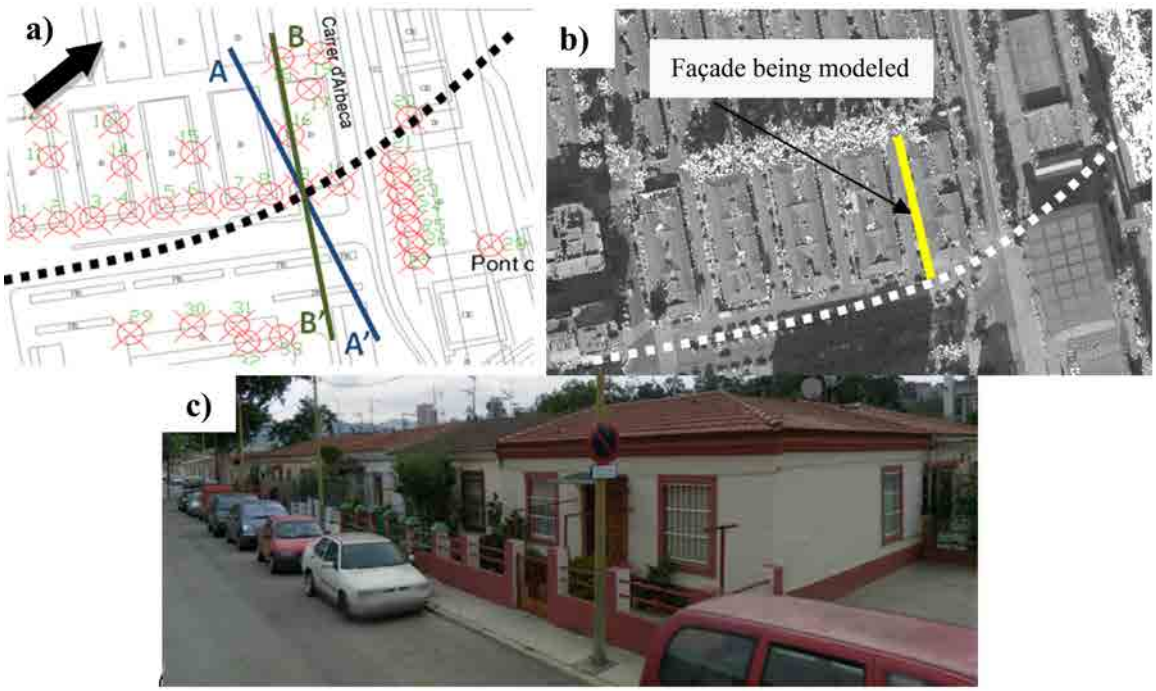

Figure 2.2. (a) Illustration of monitoring points, tunnel track and studied sections in Bon Pastor (BCN); (b) Aerial view of façade being modeled (Source: © Google Earth); (c) Street view of the dwellings (Source: © Google Earth).

The key factors in the present analyses are: (1) the poor bearing capacity of the soil, (2) the presence of groundwater, (3) the low depth of the tunnel (z_0) (23m from surface to tunnel axis) together with the high diameter of the tunnel (d) (12m) and (4) the initial state of the adjacent buildings (constructed at the end of 1920's). Therefore, a rigorous planning of instrumentation was placed in the zone to continuously register ground and building movements (Figure 2.2). Note that a value of z_0 equal to 15m was used in Camós *et al*. (2014) according to the data available at that time. Gathered data from construction projects a posteriori showed that tunnel run deeper at the particular section of study.

Data available for the research included the measurements from total stations of 30 retro-reflective prisms installed on building façades to control vertical and horizontal movements produced by the underpass of the TBM. After discarding the prisms out of the tunnel influence zone and the data noise, the measurements from 15 prisms were used to determine ground movements in the area. These measurements were taken daily for a period from several weeks before the tunnel face underpass to four years after. This period was established to control the stabilization of ground movements due to long-term effects such as consolidation, which can increase settlements with time.

2.2.2 Geometric, mechanical and chemical survey of the buildings

A comprehensive inspection was carried out, which included a characterization of the materials' structural properties and a geometrical survey. It was found that most of the dwellings had a squared plant of dimensions about 8x8m and a terrace in the front part. Façades are mainly built with ceramic brick masonry, with unit dimensions of 29x14x4cm. However, in several façades it is also possible to find solid concrete blocks of 30x20x20cm or even a mixture of clay brick and concrete block masonries. The façade wall under analysis (Figure 2.2b and Figure 2.3) is composed of ceramic bricks and it is 20cm. This value is the sum of 14cm of a row of horizontal ceramic bricks, 2cm of lime mortar and 4cm of another row of bricks set up vertically (Figure 2.4). Partition walls are 4cm thick (the bricks are laid on the stretchers). Sloping roofs sustained by timber beams are mainly used, although most of these beams have been replaced by pre-stressed concrete beams due to the rotting that many presented. These structures are supported by columns of brick masonry forming an 'L' shape in section to save material consumption. In addition, partition walls are attached to these brick masonry columns.

Penetrometer tests are applicable to estimate the in-place strength of mortar, according to a given relationship experimentally established between penetration resistance and mortar strength. Several of these tests were carried out to determine the *in situ* strength of mortar in the façade and in a central column supporting the roof (Table 2.2) according to the ASTM C-803 standards (2010).

As it can be observed in Table 2.2, mortar used in columns presented a high average strength (28.7MPa) with low scatter (CV=10.4%). On the other hand, the mortar used in walls had a lower strength of 1.7MPa with a high scatter of results (CV=75.9%). However, this is misleading because such high value of the coefficient of variation is derived from the low average value of this mortar. The notable difference of strength between the mortar used in walls and in columns suggested a different composition of them.

X-ray diffraction (XRD) techniques are applicable to provide the structural analysis of polycrystalline samples of unknown materials. XRD analyses were performed in both mortars extracted from the façade wall and from columns. Phase identification was accomplished by comparing the peaks and relative intensities of the XRD patterns for each sample. Figure 2.5 shows an example of diffraction pattern from the mortar used in the columns, indicating a relative high presence of larnite larnite (Ca_2SiO_4) and porlandite ($Ca(OH)_2$) with quarz sand (SiO_2). In the pattern of the mortar used in the façade wall there was a total absence of porlandite. This fact, in addition to the much higher strength shown in the mortar of columns, lead to the conclusion that a cement type mortar was used, whereas a lime type was used in the façade wall. This difference in composition can be noticeable by the naked eye due to the darker grey color of cement mortar (Figure 2.6 (a-b)).

The compressive strength of the ceramic bricks from the façade has been determined according to the procedures of EN 772-1 (2002), thus providing realistic parameters to the models as for Young and shear modulus and compressive strength in both axes. The results of three specimens are shown in Table 2.3. Afterwards, the measured strengths of mortar and bricks are employed to determine the characteristic strength of masonry according to the expressions from the Eurocode 6 (EN 1996-1-1:2005) for solid clay brick. This characteristic value has been further converted to an average value (4.90 MPa) according to the transformation proposed by Melchers (1999). The vertical modulus of

elasticity is determined by the expression of Kaushik *et al*. (2007), giving a result rounding off till 2680 MPa.

Assuming the same compressive strength of bricks in columns than in façade, these values increased up to 11.40MPa and 6270MPa in columns. It must be kept in mind that the latter assumption is conservative, since the chemical analysis have shown a higher quality of bricks used in columns but no entire bricks could be extracted from there to carry out a compressive strength test. The present characterization of materials has been employed in the predictions of damage on buildings due to the underpass of the TBM. In contrast, it was not possible to carry out tests to determine the tensile strength and hence, these values had to be assumed from the literature.

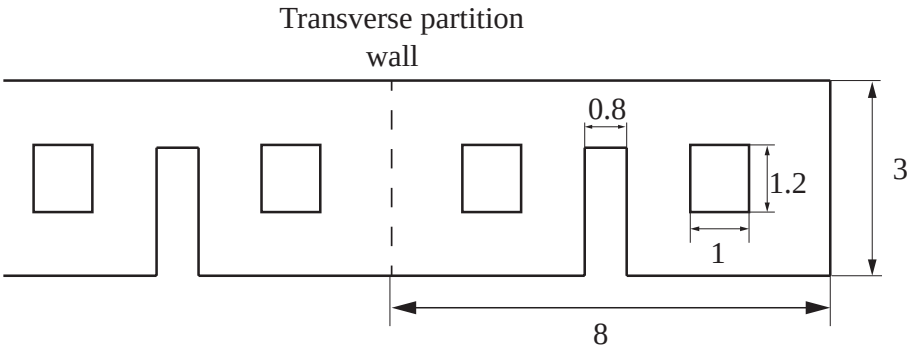

Figure 2.3. Elevation (in m) of the dwellings.

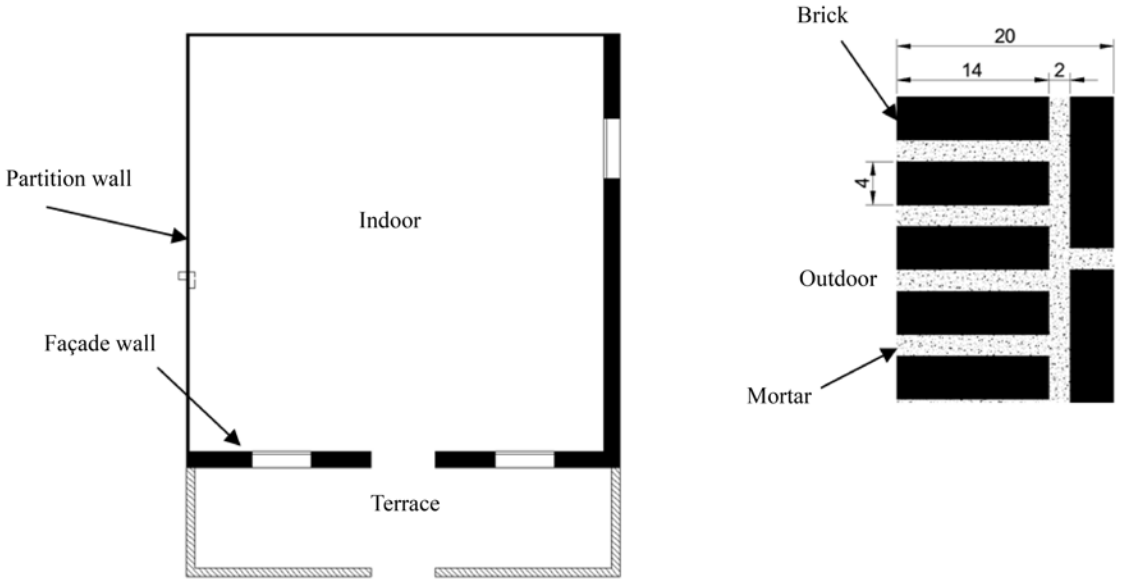

Figure 2.4. Plan of the dwellings and section (in cm) of the façade.

Table 2.2. Penetrometer test results in façade.

Reading #	Façade and partition walls		Column	
	Microm. reading	Strength (MPa)	Microm. reading	Strength (MPa)
1	0.554	0.2	0.816	24.4
2	0.582	1.2	0.887	31.1
3	0.571	0.3	0.867	29.3
4	0.594	2.4	0.876	30.1
5	0.601	2.8		
6	0.602	3		
Mean (MPa)		**1.7 MPa**		**28.7 MPa**
C.V. (%)		**75.9%**		**10.4%**

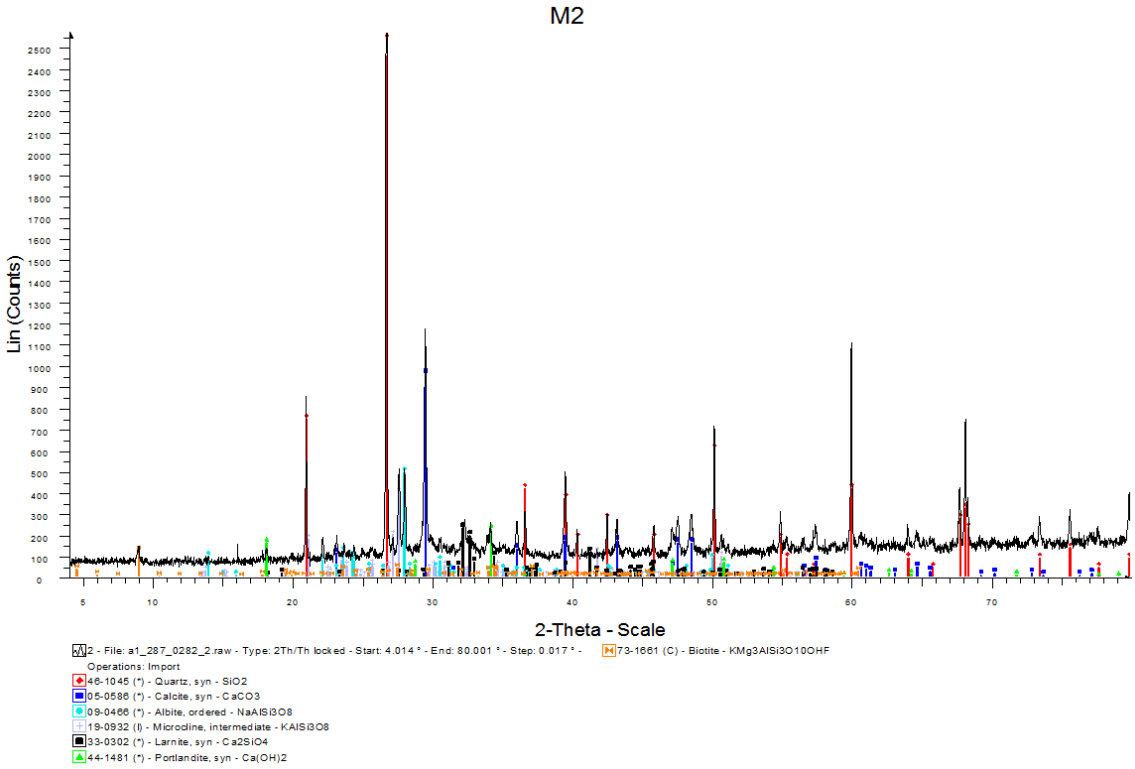

Figure 2.5. Diffraction pattern of a cement mortar sample using X-Ray diffraction (note the presence of porlandite).

Table 2.3. Compression strength tests for ceramic brick samples.

Sample	Mean length (mm)	Mean width (mm)	Mean thickness (mm)	Load (kN)	Compressive strength (MPa)
1	289	139	41	445.34	11.06
2	210	139	39	570.66	19.55
3	152	140	43	506.15	23.69
Mean					**18.01 MPa**
C.V.					**35.6%**

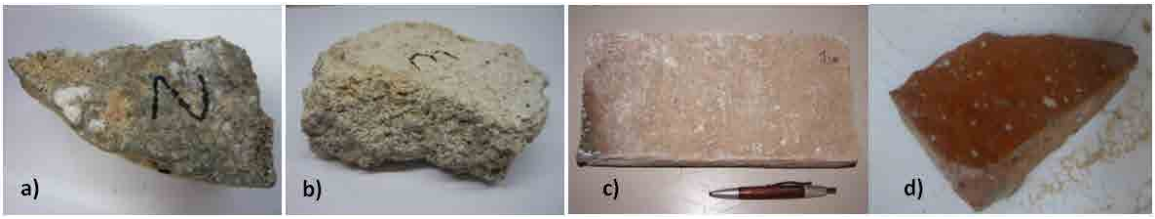

Figure 2.6. Photographs of (a) fragment of cement mortar used in columns, (b) fragment of lime mortar used in walls, (c) clay brick used in walls, and (d) fragment of clay brick used in columns.

2.2.3 Prediction of ground movements

Ground movements in section A-A' (Figure 2.2) are studied to test the suitability of the methods used in the prediction of settlements and horizontal movements. The approaches from Peck (1969), Attewell *et al.* (1986) and Rankin (1998) are used, assuming a Gaussian distribution curve for the transverse profile of the trough. The soil in the zone of study is characterized by the interbedding of sediment layers with a high variety of grain particle distributions (grained sands, gravels and blocks in a sandy matrix, clay and silts and coarse sands and gravels) (Deulofeu *et al.*, 2007). According to this type of soil, the trough width parameter K is chosen equal to 0.3 (Burland, 2008). The maximum settlement (S_{max}) will occur above the tunnel axis and its magnitude depends on the ground volume loss (V_L), which is inherent to the construction method employed. Typical values for tunnels bored by TBM-EPB are in the range of 0.3% - 0.6% with maximum values of 1.0% (Gatti and Cassani, 2007). In granular soils, higher values are expected, mainly when bored under the ground water table. Therefore, an average volume loss of 0.7% is considered.

Maximum settlement (S_{max}) can be estimated using the approach from Peck (1969), Attewell *et al.* (1986) and Rankin (1988), given by:

$$S_{max} = \frac{V_L \cdot d^2}{3.192 \cdot i} \tag{2.1}$$

where i represents the location of the inflection points given by (O'Reilly, 1982):

$$i = K \cdot z_0 \tag{2.2}$$

For a tunnel of 12m diameter (d) and 23m depth (z_0), the location of the points of inflection (i) will be at a distance equal to half-depth (6.9m) from tunnel centerline, giving a maximum estimated settlement value of 46mm.

The predicted settlement profile in section A-A' corresponds to the dashed line in Figure 2.7, whereas the small triangles correspond to the real measured values of settlement projected in section A-A', with a maximum value of 41mm. Therefore, the prediction of maximum settlement was notably well adjusted to reality, with only a difference of about 12%. The continuous line corresponds to the Gaussian curve, which best fits the real settlements (Kim *et al*. 2001), thus showing the acceptable adjustment of the settlement profile to a Gaussian shape.

It must be kept in mind that these calculations estimate the maximum immediate settlement when tunnel face is under the buildings, and do not take into account long-term effects such as ground consolidation, which could increase subsidence with time. In this particular case, the maximum settlement value rose up to 54mm, 4 years after the TBM underpass.

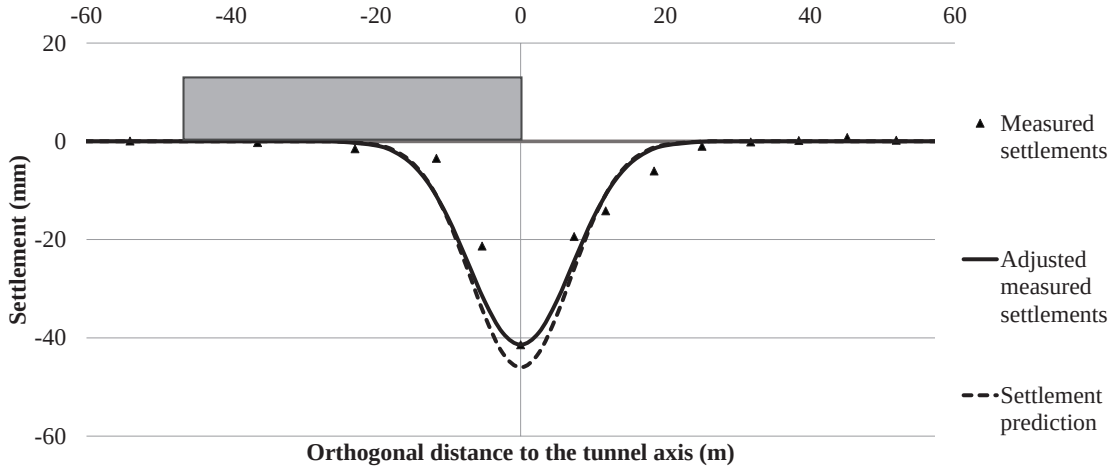

Figure 2.7. Immediate settlement profile (predicted, measured and adjusted).

Horizontal displacements (U) and strains (ε_h) along section A-A' (continuous lines in Figure 2.8 and Figure 2.9) were predicted according to the expression given by O'Reilly (1982), assuming that the overall movement of ground is directed towards tunnel axis:

$$U = \frac{S \cdot x}{z_0} \tag{2.3}$$

$$\varepsilon_h = \frac{dU}{dx} \tag{2.4}$$

where x is the orthogonal distance from tunnel axis. It can be seen that the two plots are notably different from real measurements projected along section A-A' (small rhombus). It must be taken into account that real data of horizontal movements at ground level were not available. For this reason, only measurements from prisms located at mid-height of dwellings are used. Therefore, the comparison between predictions and real measurements must be taken with care since the foundations will partly constrain the complete transmission of the horizontal ground strains. However, in the case of vertical displacements of ground, available measures taken by other instruments placed at ground level in the proximity of the buildings did show similar values to the ones registered by the prisms at mid-height. Moreover, the adjustment of these measurements to a Gaussian profile (as in green-field conditions) allows assumption of a notable flexible behavior of the building in the vertical direction which could not be assumed in the horizontal axis.

The determination of deflection ratios implies the projection along the façade (section B-B') of settlements along section A-A'. The façade of the buildings is aligned θ =26° with respect to the reference section A-A'. Moreover, tunnel track (dashed line) in this zone runs in curve. Therefore, settlement profile in B-B' will not follow exactly the shape of a Gaussian probability density function. However, for large radius of curvature of the tunnel track, the shape will be very similar to a probability density function. For this reason, one can imagine a group of lines parallel to the tunnel track, thus joining points subjected to equal settlements. Then, if a settlement is calculated in section A-A', the lecture can be transferred by simple trigonometry to section B-B' (for instance, between points *a-b*, assuming null curvature between the two sections (tunnel track radius is equal to 300m).

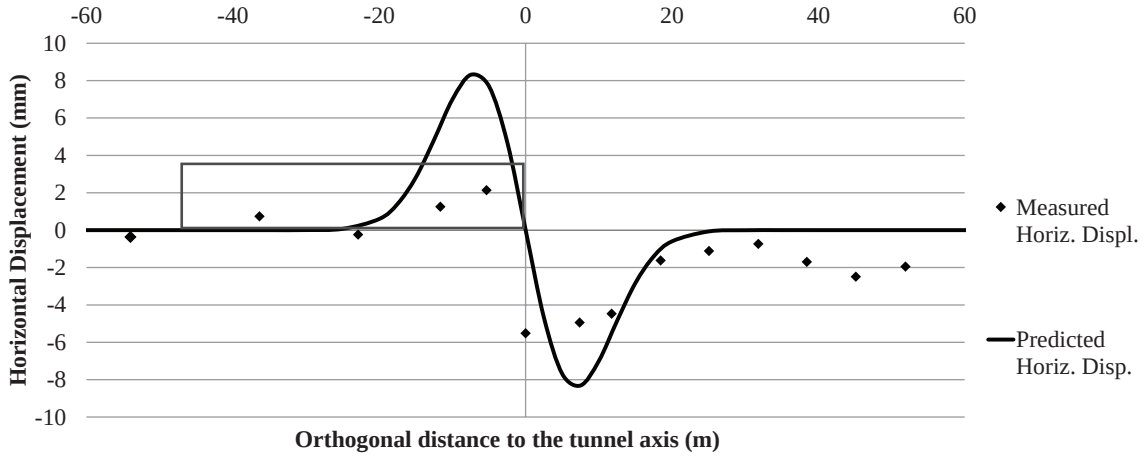

Figure 2.8. Horizontal displacements in monitoring section.

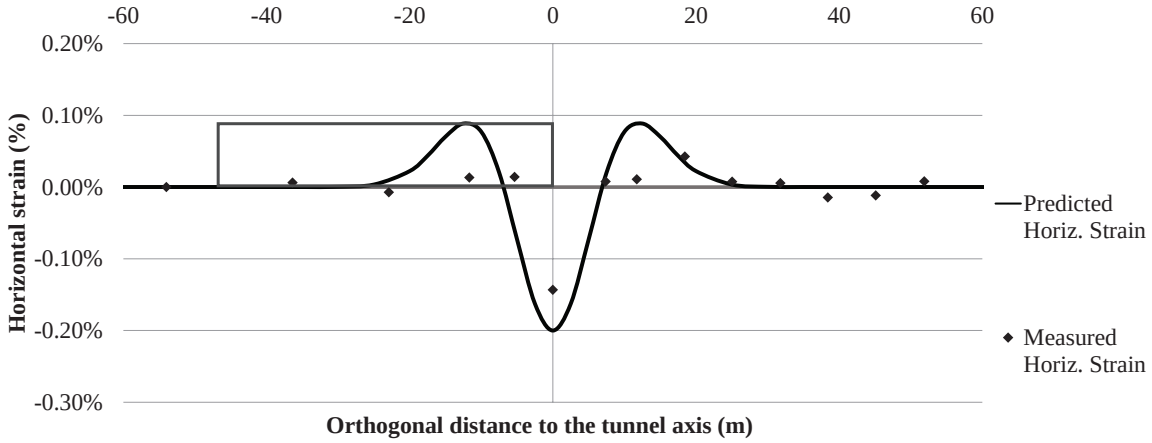

Figure 2.9. Horizontal strain according to horizontal displacements measured in ground.

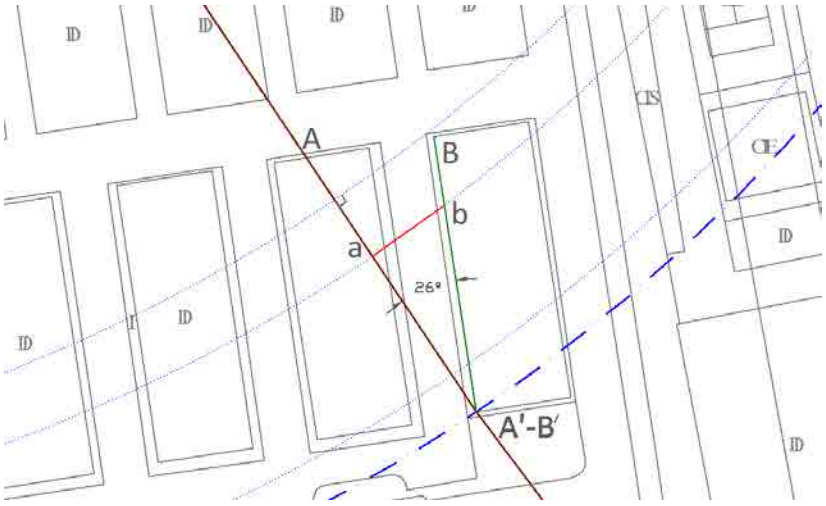

Figure 2.10. Projection of settlements from the transverse plane to tunnel axis to the building plane.

The settlement profile S in a section B-B' which is slightly rotated θ degrees with respect to A-A' can be well described by the Gaussian curve:

$$S = S_{max} \cdot exp\left(-\frac{m^2}{2i^2}\right) \tag{2.5}$$

with

$$m = \frac{x}{cos\theta} \tag{2.6}$$

If θ =0°, the settlement profile corresponds to the section A-A'.

2.3 PREDICTION OF DAMAGE ON BUILDINGS USING THE CLASSICAL METHODOLOGY

2.3.1 Determination of deflection ratios

A first estimation of the damage on the group of dwellings due to the TBM underpass is carried out using the equivalent beam method. This approach assumes that the parts of the buildings under sagging (upward concavity of the settlement profile) and hogging (downward concavity) can be treated as independent beams. Therefore different, deflection ratios (Δ/l) for each part must be considered (Figure 2.11). These ratios are determined in four steps: (1) assessment of the settlement profile, (2) plot of the straight lines joining the inflection point and the maximum and minimum settlements affecting the total length of the building, (3) determination of the maximum differences between these lines and the settlement profile (relative deflection, Δ) and (4) division of these values by the respective lengths of sagging and hogging.

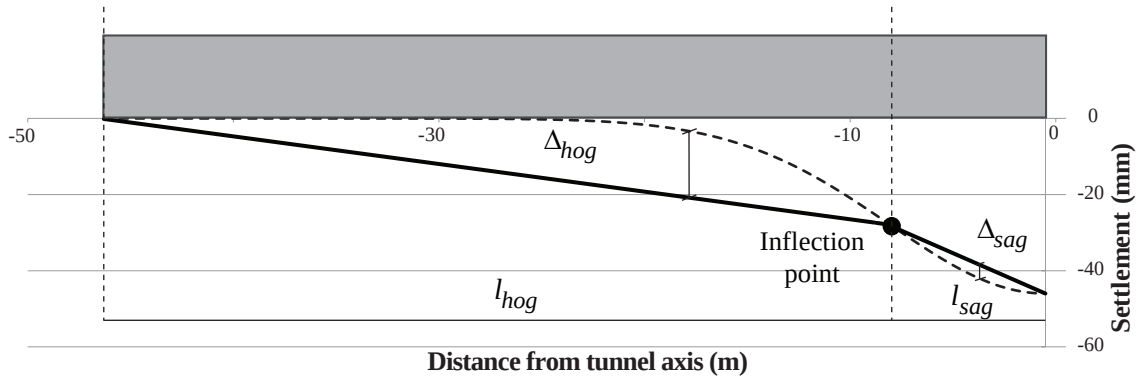

Figure 2.11. Illustration of the determination of the deflection ratios in sagging and hogging.

Considering the predicted settlement profile of Figure 2.7 and projecting it to the section B-B' of the façade, the length of the building affected by sagging deflection is l_{sag} =7.7m, whereas in hogging is l_{hog} =38.3m. The values of relative deflection (Δ) are 3.73mm in sagging and 17.46mm in hogging. Therefore, the deflection ratios in both modes of deflection match up to Δ/l =0.05%.

2.3.2 Burland and Wroth (1974) and Boscardin and Cording (1989) approach

Bending and shear strains on the equivalent beam under deflection are given by Eq. (2.7) and (2.8), where Δ/l is the deflection ratio, l is the distance between two reference points and Δ is the relative deflection between these two points and t corresponds to the height of the neutral axis. Two extreme modes of deformation (bending only ε_{bmax} and shear only ε_{dmax}) are assumed to ascertain which type is limiting, where ε_{bmax} and ε_{dmax} are the maximum tensile strain due to bending and shearing respectively, a is the height of the fiber were strains are calculated, H is the beam height, I is the inertia per unit length and E/G is the ratio between the elastic and shear moduli of the material.

$$\varepsilon_{bmax} = \frac{\frac{\Delta}{l}}{\left(\frac{l}{12t} + \frac{3I}{2alH}\frac{E}{G}\right)} \tag{2.7}$$

$$\varepsilon_{dmax} = \frac{\frac{\Delta}{l}}{\left(1 + \frac{Hl^2}{18I}\frac{G}{E}\right)} \tag{2.8}$$

Maximum tensile strains are calculated at each part of the beam for a height (H) equal to 3m, inertia per unit length equal (I) to 2.25m^4/m and a relationship E/G =2.5 (Devriendt, 2003), typical for structures assumed to be linear elastic, isotropic and homogeneous, based upon Poisson ratios of 0.2 to 0.3.

The equivalent beam method requires to take an independent decision about the position of the neutral axis (t) in each part of the building. In hogging, due to the inability of the masonry in the upper part of the wall to withstand significant tensile stresses, the neutral axis is likely to be nearer to the foundations (t_{hog} =3m). In sagging mode, however, the lower part of the masonry wall tends to be capable of withstanding tensile stress and therefore the neutral axis can be considered as being at mid-height of the wall (t_{hog} =1.5m) (Mair *et al.* 1996).

Tensile stresses in the wall mainly occur due the deflection induced to the beam. Moreover, in certain parts of the building, ground movements can induce additional stresses increasing the level of damages. The influence of horizontal ground strain (ε_h) can be introduced by superposition using the approach of Boscardin and Cording (1989), giving expressions for the extreme fiber strain in bending (ε_{br}) and in shear (ε_{dr}):

$$\varepsilon_{br} = (\varepsilon_{bmax} + \varepsilon_h) \tag{2.9}$$

$$\varepsilon_{dr} = \varepsilon_h \left(1 - \frac{E}{4G}\right) + \sqrt{\frac{\varepsilon_h^2}{16}\left(\frac{E}{G}\right)^2 + \varepsilon_{dmax}^2} \tag{2.10}$$

As it could be seen in Figure 2.9, the ground strain predicted is not constant along the building length and hence, the designer has to choose arbitrarily a particular value, which is in fact somewhat unreal. Considering the maximum value of ground strain could lead in an overestimated damage category, since the coordinate corresponding to the maximum ground strain could not match the coordinate where the tensile strains in the equivalent beam are maximum (however, these values corresponding to different points of the beam are combined in the same Mohr's circle). To avoid overestimation, an intermediate value of ground strain will be considered in both modes of deflection:

a) **Hogging part:** The building length being long, the strain value at ground level is negligible for approximately half of its length. If the average was taken, it might lead to an underestimation. The value is therefore taken as the average calculated for the most critical sections (approximately from coordinates x =-25m and x =-7.7m in Figure 2.11).
b) **Sagging part:** The study of Boscardin and Cording (1989) only examined cases where the lateral strains were positive (tensile strains). The nature of strain in sagging zones is compressive, thus giving a favorable contribution for damage resistance a priori. Therefore, the approach of Boscardin and Cording might not be applied in sagging. A conservative approximation is taken considering null ground tensile strain in this part of the buildings and hence the favorable contribution of compressive strains to damage reduction is not considered.

Strain results given by the equivalent beam are shown in Table 2.4. The major damage is given by bending in the part subjected to hogging deflection, with an assessed damage equal to Category 2 (Slight). According to the classification given by Burland *et al.* (1977) and Boscardin and Cording (1989), this category implies the onset of cracking that

could be easily filled. Cracks could be visible externally and some repointing might be required to ensure weather tightness. The typical crack widths are up to approximately 5mm. As it is further shown in Section 2.6, this description of damage agrees with actual crack width as observed during the tunneling.

Table 2.4. Equivalent beam strains results.

Burland andWroth (1974) and Boscardin and Cording (1989) approaches

	Δ_{max}/L	$\varepsilon_{h,mean}$	ε_{bmax}	ε_{dmax}	ε_{br}	ε_{dr}	**Assessed category of damage**
Sagging	(+) 0.05 %	0.000 % (*)	(+) 0.074 %	(+) 0.018 %	(+) 0.074 %	(+) 0.018 %	**VERY SLIGHT (CAT. 1)**
Hogging	(-) 0.05 %	(+) 0.052 %	(+) 0.046 %	(+) 0.001 %	(+) 0.126 %	(+) 0.052 %	**SLIGHT (CAT. 2)**

(*) Note that ground strain is considered negligible since the approach of Boscardin and Cording (1989) only applies to cases of tensile lateral strains.

2.3.3 Modification factors from Potts and Addenbrooke (1997)

As it was mentioned in the introduction, the application of the equivalent beam method from Burland and Wroth assumes that the building conforms perfectly to the greenfield site subsidence trough. However, in practice, the inherent stiffness of the building will be such that its foundations may interact with ground and thus reduce the deflection ratio and horizontal strains. Therefore, the modification factors from Potts and Addenbrooke (1997) are here applied, updating the deflection ratios and the horizontal ground strains.

These factors (M) depend on the eccentricity (e/B) of the tunnel respect the building centerline (where e is the difference of distance between the tunnel axis and building centerline and B is the building half-length) and to the relative axial (α^*) and bending (ρ^*) stiffness of the structure:

$$M^{DRsag} = \frac{(\Delta/L)_{sag}}{(\Delta/L^g)_{sag}} \tag{2.11}$$

$$M^{DRhog} = \frac{(\Delta/L)_{hog}}{(\Delta/L^g)_{hog}} \tag{2.12}$$

$$M^{\varepsilon_{hc}} = \frac{\varepsilon_{hc}}{\varepsilon_{hc}^g} \tag{2.13}$$

$$M^{\varepsilon_{ht}} = \frac{\varepsilon_{ht}}{\varepsilon_{ht}^{g}} \tag{2.14}$$

$$\alpha^{*} = \frac{EA}{E_s B} \tag{2.15}$$

$$\rho^{*} = \frac{EI}{E_s B^4} \tag{2.16}$$

Where B is 23m, E is the modulus of elasticity of the beam, taken as 2500MPa in first approximation, A is the cross-section area per unit length (out-of-plane direction) equal to 3m^2/m, I is the inertia per unit length equal to 2.25m^4/m (considering a wall 1m wide), E_s is a representative soil stiffness. According to the type of ground with grained sand and clay and silts, typical from a river delta (Calavera, 2000), the subgrade reaction modulus of ground can be taken as 0.09N/mm^3. Assuming a 30cm width continuous foundation, E_s can be estimated in 27MPa. Then, the relative stiffness measures are α^{*} =12.1 and ρ^{*} =0.0007 (1/m).

The design curves for horizontal strain modification factors for a given tunnel eccentricity ($e/(2B)$) can be found in Potts and Addenbrooke (1997). The eccentricity in this case is 0.5, since the tunnel is located under the corner of the set of buildings. The resulting modification factors for these relative stiffness measures are: M^{DRsag} =0.5 and M^{DRhog} =1.2. For the horizontal ground strain in compression and tension regions, factors are $M^{\varepsilon_{hc}}$ ≈0.01 and $M^{\varepsilon_{ht}}$ ≈0.01, giving the strain results shown in Table 2.5.

Table 2.5. Equivalent beam strains results (modification factors applied).

Application of Potts and Addenbrooke (1997) factors

	Δ_{max}/l	$\varepsilon_{h,mean}$	ε_{bmax}	ε_{dmax}	ε_{br}	ε_{dr}	**Assessed category of damage**
Sagging	(+) 0.03	0.000 %(*)	(+) 0.044 %	(+) 0.011%	(+) 0.044 %	(+) 0.011 %	**NEGLEGIBLE (CAT. 0)**
Hogging	(-) 0.06	(+) 0.0005 %	(+) 0.051 %	(+) 0.001 %	(+) 0.052 %	(+) 0.001 %	**VERY SLIGHT (CAT. 1)**

Once again, bending deflection is dominating instead of shear. However, the resulting category of damage is *'Negligible'* in sagging and Very slight in hogging. This reduction of the predicted damage is mainly given by the dramatic reduction of the horizontal strain coming from ground. Potts and Addenbrooke showed in their numerical analysis that the tensile strains could be reduced in a 90% respect to those calculated assuming *greenfield*

conditions. Nevertheless, as it will be seen in Section 2.6, the assessed category of damage using this approach is clearly underestimated compared to the real damage occurred. According to Potts and Addenbrooke design charts, the modification factor for horizontal strain in tension and compression is low (<0.01) for realistic axial stiffness of buildings (i.e. $\alpha^* > 10$) (Dimmock, 2008), and also for the case study. Therefore, not all the walls would be represented in these design charts and hence the results obtained by this approach should be considered with care.

2.4 NUMERICAL SIMULATION USING A FINITE ELEMENT METHOD: RANKINE-HILL MACRO-MODEL

2.4.1 Introduction

The structural behavior of the set of dwellings subjected to subsidence is simulated by using a FE model in DIANA software (Diana 9.4.4, 2005, TNO DIANA BV, Delft, The Netherlands). The modeling consists in a two-dimensional non-linear plane stress analysis using the macro-model Rankine-Hill proposed by Lourenço (1996), which includes cracking effects in tension and crushing in compression. Plastic strain contours make possible to obtain the crack patterns of the structure, which will be already compared with the damage survey done during the construction of L9.

2.4.2 Description of the model

The geometry of the model is represented by Figure 2.4. The dimensions of each dwelling are 3m height and 8m wide. All of them have two windows of dimensions 1.2m x 1m and a door of 2m x 0.80m, repeating this pattern of openings along the six dwellings.

In the present numerical analysis, the entire façade is considered as a ceramic brick masonry wall 20cm thick. Although a two-dimensional plane stress model is assumed, certain assumptions will be done at the level of the transverse walls. The effect of the out-of-plane elements such as transverse partition walls of 4cm brick masonry has been introduced using thicker elements in these zones, thus increasing their stiffness. An extra thickness of 30cm is given (having 50cm width in total in these elements, 20cm corresponding to the façade itself width + 30cm of length out of plane).

When the equivalent beam method was previously used, ground movements were assumed to follow a Gaussian profile according to relative simply hypotheses. Therefore, when doing the prediction of damage, the evaluation was approximately the global

quality of both ground movements and the structural damage assessment. However, when using the numerical approach, it would be desirable to pay attention mainly to the quality of the numerical model in order to assess the reliability of FE methods as a damage prediction tool. It was therefore decided to work with the real ground movements instead of using predictions given by classical methods. Since the available real measurements of settlements are limited, an interpolation process is carried out based on a Gaussian trough according to literature (Peck, 1969; Attewell *et al*. 1986; Rankin, 1988).

The analysis is performed considering plane stress. Thus, only in-plane actions are taken into account (self-weight, roof load, settlements and horizontal movements from ground). Self-weight was determined according to the typical value of masonry density (1800kg/m^3). Following the Spanish regulations, the typical self-weight value for a tile roof with false ceiling (constructed with gypsum mortar and canes) can be estimated in 2.5kN/m^2. This load is acting in a roof surface of 8x8m and thus giving a uniform load on the façade of 10kN/m.

The mesh consists of 11790 4-nodes quadrilateral isoparametric plane-stress elements (Q8MEM). The element width was set up at 0.1m, thus giving a perfectly rectangular mesh, which made possible to obtain results with an acceptable precision for this case study.

A model based in the mathematical approach of Winkler (Muzás, F., 2002) is here used to represent the behavior of the soil. Interaction between soil and foundations in the vertical direction is simulated by a set of non-linear springs, whose compression stiffness (K_s) has been estimated according to the subgrade reaction modulus of ground, taken as 0.09N/mm^3 for the present type of soil with grained sand and clay and silts, typical from a river delta (Calavera, 2000). A continuous foundation of 30cm has been assumed, since no real dimensions were available. This set of springs remain inactive (K_s =0) for tensile strains in order to simulate the gapping phenomenon. The modeling in the horizontal direction is performed in a similar way, now setting out linear springs also with the same constant K_s. Horizontal springs remain inactive in zones where soil-foundation contact is lost.

The material response has been adopted according to the values obtained experimentally (Table 2.6). The ratio between the vertical and the horizontal modulus of elasticity of masonry (E_y/E_x) is taken as 0.8, according to Samarashinge *et al*. (1982). For the ratio

between vertical and horizontal maximum compression strength (f_{cy}/f_{cx}), a value of 1.5 was proposed by the same authors and Sandoval (2011). Other values needed for the analysis have been assumed according to general properties of masonry and previous studies from Barbosa (2010) (Table 2.6, where G is the shear modulus, ν is the Poisson's ratio, G_{fx} and G_{fy} are the fracture energies in the horizontal and vertical direction respectively, and f_{tx} and f_{ty} are the horizontal and vertical tensile strength of masonry).

Table 2.6. Model parameters. (*) determined according to experimental values // (**) assumed values.

E_x (*)	E_y (*)	G(*)	υ(**)	Density(**)	K_s (**)
3350 MPa	2680 MPa	1070 MPa	0.20	1800 kg/m^3	2700 N/mm
f_{tx} (**)	f_{ty} (**)	G_{fx} (**)	G_{fy} (**)	f_{cx} (*)	f_{cy} (*)
0.10 MPa	0.05 MPa	2.0 N·mm/mm^2	2.0 N·mm/mm^2	3.20 MPa	4.90 MPa

2.5 RESULTS

2.5.1 Introduction

The deformed shape of the structure when ground movements are applied can be seen in Figure 2.12, giving the contour of plastic strains (ε_{p_1}) of Figure 2.13. As it can be seen, the most unfavorable plastic strains are concentrated in the corners of doors and windows, since they represent stress concentration points. The maximum value of plastic strain (2.12%) is reached in the corner of the left window of the second dwelling, which is subjected to hogging. The maximum value in sagging is equal to 1.31%. According to the plastic strains values, it is possible to determinate crack widths in the wall. Considering an element side size of 0.1m, the expected crack opening computed by the FE model is 2.12mm in hogging and 1.31mm in sagging.

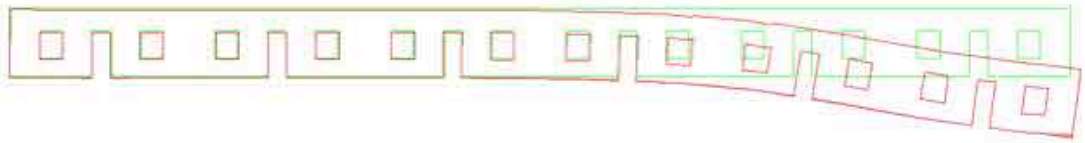

Figure 2.12. Illustration of the deformed shape when ground movements are applied (Amplification factor = 74.5).

However, the high difference between maximum and minimum plastic strains in Figure 2.13, may hide lower strains that could develop smaller cracks. Therefore, in Figure 2.14,

plastic strains in a range from $0.9 \cdot 10^{-4}$ to $0.9 \cdot 10^{-3}$ are shown. As it can be seen, several diagonal strains appear in the first dwelling that could not be appraised in Figure 2.13.

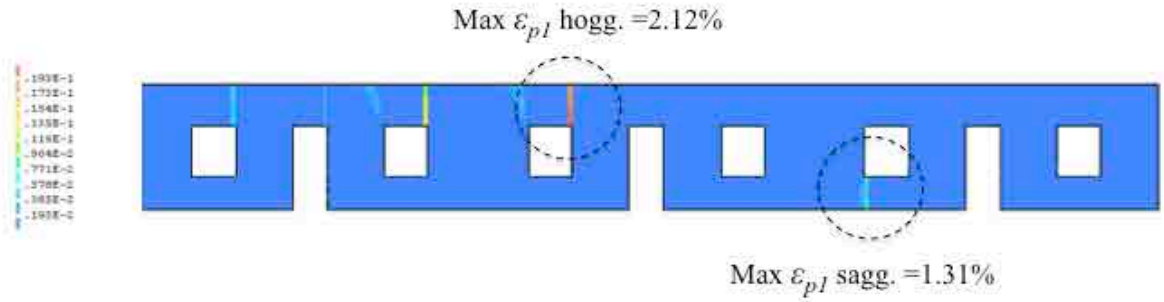

Figure 2.13. Contour plot of maximum plastic strains/crack patterns (three last dwellings from right).

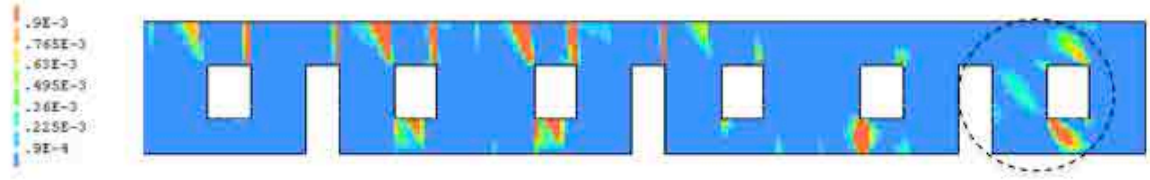

Figure 2.14. Contour plot of maximum plastic strains/crack patterns (in 5 levels from $0.9 \cdot 10^{-4}$ to $0.9 \cdot 10^{-3}$).

The FE analysis showed a critical dependence on the horizontal movements (U) from ground that tunneling can induce. In this case study, horizontal movements reached a maximum value of 2.4mm, becoming critical due to the produced distortion effects that substantially modify the distribution of the strain field. Therefore, the determination of the modulus of elasticity in the horizontal direction takes a remarkable importance. Higher is the modulus, higher stresses will be generated for the same field of strains. As a consequence, the accommodation of the building to the imposed profile of the ground implies a stress redistribution that will lead in an increment of plastic strains in zones where non-elastic effects had started, thus increasing the crack widths.

2.6 COMPARISON BETWEEN REAL DAMAGE AND PREDICTIONS

2.6.1 Description of real damage occurred

Damage ocurred during the construction of the tunnel consisted of several diagonal and vertical cracks, starting from corners of windows and doors till the lintel of the façade (Figure 2.15). Several shorter cracks appeared in the ledges of the façade windows.

Horizontal cracking appeared in the base of the lateral wall of the set of dwellings. In particular, this wall played an important role, since it avoided a higher descent of the façade corner. Real crack widths were comprised between 1 and 3mm. According to the chart of Burland *et al.* (1977), the overall damage in the building can be classified as Slight (Category 2).

Figure 2.15. Photographs of damage occurred in buildings due to tunneling (three last dwellings).

2.6.2 Comparison of real damage with non-linear numerical simulation and equivalent beam results

The crack patterns described by the FE analysis (Figure 2.13 and Figure 2.14) are in notable agreement with most of the cracks registered in the survey. As regards to the predicted crack widths, the numerical model values are 2.19mm in hogging and 1.39mm in sagging. Both measures are within the range of real craking occurred. According to the classification of visible damage to walls from Burland *et al.* (1977), the predicted categories of damage by numerical simulation would be Slight (Category 2) for both parts. This fact agrees with reality and it can be globally said that the numerical tool shows a high degree of reliability in damage prediction due to tunneling.

The predicted categories of damage using the equivalent beam approach from Burland and Wroth (Sec. 2.3.2) were Slight (Category 2) in hogging and Very Slight (Category 1) in sagging (Table 2.4). Therefore, the global prediction of damage in the building agrees with reality but, however, there is a difference in the prediction of damage in the part under sagging. This fact shows the inconvenience of the approaches when considering

compressive strains coming from ground. On the other hand, the application of the modification factors from Potts and Addenbrooke (1997) has predicted a negligible onset of damage in the structure. The survey show that this assessment is clearly underestimated.

*Table 2.7. Comparison of real damage with non-linear numerical simulation and equivalent beam results (*crack width, **maximum tensile strain)*

	Reality		**Numerical Non - Linear Analysis**		**Equivalent beam**	
Sagging	1-3*mm**	Category 2 Slight	1.3*mm**	Category 2 Slight	0.074 %**	Category 1 Very slight
Hogging	1-3*mm**	Category 2 Slight	2.2*mm**	Category 2 Slight	0.126 %**	Category 2 Slight

2.6.3 Comparison of linear elastic numerical simulation and the equivalent beam

By definition, the equivalent beam method assumes linear elasticity. Then, classification of damage is based on the calculation of a maximum tensile strain in the elastic beam. This value is latter compared with the limiting values of category of damage on buildings. For this reason, it is of interest to compare the predictions given by a linear analysis of the structure using numerical simulation and the results from the application of the equivalent beam to ascertain the equivalence of using both methods.

The distribution of principal strains (ε_x) of the structure subjected to the predicted ground movements (recall Figure 2.7 and Figure 2.8) assuming linear elastic behavior of masonry is presented in Figure 2.16. In this case, the springs are not used, since ground movement is directly imposed in the foundations. The self-weight and the vertical loads coming from roof are disregarded. In the hogging part, the strain coming from ground is assumed to be constant and equal to 0.069% (as it was also assumed in the equivalent beam calculations, section 4.2). In sagging, ground strain is assumed to be null and hence, the horizontal displacements are constant in this part.

The maximum principal strain obtained value is equal to 0.270%, located in the zone under hogging. If one takes into account this value, the predicted category of damage would be Moderate, with a critical affection on the serviceability of building. The reason of such high value lays in its location (in a window corner). As infinitely elasticity is

assumed, this points acts as a concentrator of stresses. Therefore, principal strains close to openings can be overestimated and should be considered with circumspection.

If these local values are disregarded and strain measures are taken in the extreme fibers of the façade (out of the openings influence), the resulting maximum values of principal linear elastic strains are then equal to 0.120% in the hogging zone and 0.062% in sagging (Figure 2.16). The resulting damage categories are Slight (Category 2) for hogging and Very slight (Category 1) for sagging.

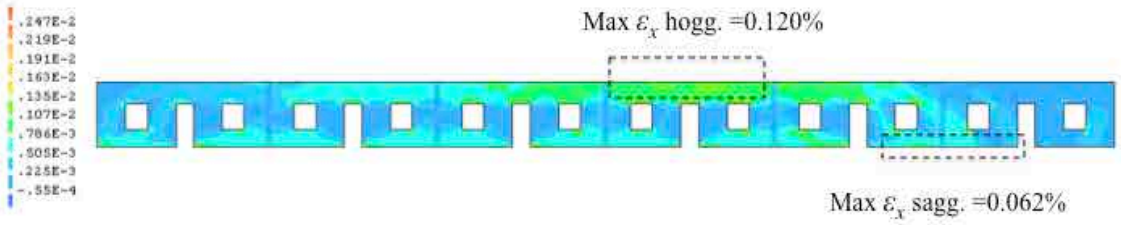

Figure 2.16. Contour plot of the distribution of principal strains.

Table 2.8. Comparison of linear elastic numerical simulation and the equivalent beam results.

	Numerical Elastic Linear Analysis		**Equivalent beam**	
Sagging	0.062 %	Category 1 Very slight	0.074 %	Category 1 Very slight
Hogging	0.120 %	Category 2 Slight	0.126 %	Category 2 Slight

There is a clear similarity of maximum tensile strain values between the numerical prediction of the linear analysis and the assessment done with the equivalent beam method (without the application of modification factors) (view Table 2.8). The predicted damage in hogging is Slight (Category 2), which matches with the prediction of the non-linear numerical analysis and the reality. The predicted damage in sagging is classified as Very Slight (Category 1) for both methodologies. As it was mentioned in Sec. 2.6.1 and Sec. 2.6.2, the real damage occurred in this part of the building was classified as Slight (Category 2). Therefore, the predicton is quite underestimated by both methods but however, the global prediction of damage in the buildings is correctly done.

2.7 CONCLUSIONS

According to the monitoring data, it has been stated that the shape of the settlement trough can be well described as a normal Gaussian probability densitiy function for the transverse profile. Prediction of maximum settlement has given a difference of only 12%

of the real measured value. Contrarly to the usual *greenfield* approximation, the prediction of the horizontal displacements requires the consideration of the interaction between the building and the soil. In practice, the presence of buildings and pavements tends to reduce the amount of vertical and horizontal movements of ground.

Damage prediction performed with the equivalent beam method generaly agrees with the reality. The application of the modification factors of Potts and Addenbrooke assumes that no significant horizontal strain is induced in the building due to its axial stiffness. As a consequence, the categories of damage assessed by this method in the case study are completely out of reality.

The macro-model proposed by Lourenço (1996) which uses two yield surfaces allowing to considering cracking and crushing effects, has predicted a crack pattern in accordance with the damage survey. The plastic strain distributions clearly show that the presence of openings in the façade has a notable importance in the onset of cracking. The estimation of the maximum crack opening is consistent with the damage survey, thus showing the reliability and suitability of the method. In general, the part of the building likely to be affected with more severity is the one subjected to hogging.

Numerical linear elastic simulations of the structure provided similar results of damage than the approach of Burland and Wroth (1974). However, principal strains must be checked in zones out of the influence of openings, which can amplify stresses in corners up to unrealistic values of strain.

In general, the equivalent beam has been proved to be a useful tool in damage prediction due to tunneling which can be used in first stage of assessment of damage. Buildings likely to be more sensitive to tunnel subsidence can be successfully evaluated in more detail using the presented numerical FE Model.

Acknowledgements

The authors would like to thank GISA (*Gestió d'Infraestructures S.A.*) and the *Patronat Municipal de l'Habitatge de Barcelona* for the information provided. This research has received the financial support from the *Ministerio de Educación y Ciencia* through the research project SUBTIS (*Study of the Sensitivity of Urban Buildings to Tunneling Induced Settlements,* ref. num. BIA2009-13233), the ERDF (European Regional Development Fund) and the *Col·legi d'Enginyers de Camins, Canals i Ports de Catalunya* to carry out this research.

3. 3D Numerical Analysis of a Masonry Building Subjected to Tunneling Subsidence

Abstract: The present chapter analyzes the structural response of a group of one-story buildings subjected to ground movements experienced during the construction of the L9 Metro Line tunnel in Barcelona, which was bored by an Earth Pressure Balance - Tunnel Boring Machine (EPB-TBM). A 3D phased numerical model is developed to predict the building damage resulting from subsidence generated by the construction of a curved tunnel beneath. The model includes the building, the soil, the tunnel lining and interface elements to simulate the contact between walls and ground. The generation of ground loss is achieved with a step-by-step lining contraction method. Main model parameters have been determined by means of characterization experiments developed on the site and in the laboratory, which gives a higher significance to the analysis. Damage predictions given by numerical model are validated with the real structural damage occurred.

Keywords: Tunneling, settlements, structural damage, curved tunnel, numerical model, 3D, Finite Element Model, step-by-step pressure method, phased analysis.

3.1 INTRODUCTION

Primary assessments of building damage due to tunnel construction usually start with the use of analytical and empirical approaches that estimate a category of damage in the buildings. Gaussian profiles are used for approximation of the settlement trough, whereas

the equivalent beam method is employed to model the building response to settlements (Peck, 1969; Attewell *et al*. 1986; Burland and Wroth, 1974; Burland *et al*., 1977; Boscardin and Cording, 1989; Rankin *et al*., 1988 – see Chapters 2 and 3).

Nevertheless, building damage mechanisms generated by tunneling subsidence can combine a mixture of shear deformation, arching and bending behavior (Graham, 2002) that the equivalent beam method can barely model. Moreover, it has been seen that the longitudinal component of the settlement field (which is usually not taken into account in the analytical approaches) can cause important cracking damage (Netzel, 1999). Its effect is particularly important when the tunnel face is approaching to the building.

For this reason, the use of Finite Element methods in 2D and 3D becomes optimal for achieving more detailed predictions of damage, for instance, when performing assessments about the location and width of crack patterns (Lee and Rowe, 1990; Eisenstein *et al*., 1994; Lourenço, 1996; Augarde, 1997; Liu, 1997; Burd *et al*. 2000; Rots *et al*., 2005; Roca *et al*. 2010).

The continuous improvement of computer features facilitates the resolution of more complex issues and situations. Recent works performed in Giardina (2013) and Kappen *et al*. (2013) showed 3D, phased, fully coupled FEMs with non-linear material properties of buildings subjected to subsidence generated by tunneling construction.

The present research shows a 3D phased numerical model of a real case of one-story masonry dwellings from the 1920's in the neighborhood of *Bon Pastor* (Barcelona) (Figure 3.1). These buildings are located over a curved tunnel section of the L9 metro bored by a TBM-EPB. The tunnel section of 300m radius, 12m diameter, 0.35m of segment thickness and 17m of overburden was bored in deltaic ground conditions due to the vicinity of the *Besòs* river. Important ground subsidence was generated, with a maximum monitored settlement of about 40mm, which entailed the appearance of several cracks in the buildings.

The tunnel lining, the soil and the excavation process are simulated in the model, thus doing a step forward on the research carried out in Camós *et al*. (2014), Gálvez (2012) and Camós *et al*. (2012), where primary 2D and 3D numerical simulation were performed. Available monitoring data of ground movements, damage survey and material properties give a higher significance to the analysis.

Figure 3.1. View of one-story masonry dwellings from the 1920's located in the outskirts of Barcelona (Source: © Google Earth).

3.2 DESCRIPTION OF THE CASE STUDY

3.2.1 Background

The L9 Metro line in Barcelona is a reference urban tunneling project in Europe due to its length (more than 40km), large excavation diameters (9.4m and 12m) and the wide variety of geological and hydrological conditions encountered. Nowadays, 8km of the line are already in service in the north part of the city, precisely where the group of buildings is located.

The set of one-story masonry buildings selected for this study represent a common building typology frequently used in the 20's due to the construction of residential complexes for workers coming from southern Spain due the World Exposition that took place in Barcelona during the 1929. The poor bearing capacity of the soil, the presence of groundwater, the low depth of the tunnel and the initial structural state of the adjacent buildings are key factors in the present study (Camós *et al*. 2014).

3.2.2 Geometrical survey and characterization of materials

The masonry dwellings have a squared plant and a terrace in the front part. The structural components at each dwelling comprise the façade, which acts as a load bearing wall, two interior bearing walls and three columns. The façade has a thickness of 200mm, the interior bearing walls, 140mm, and the rest of partition walls, 40mm.

The in-place strength of mortar was determined by means of penetrometer tests. These tests showed a notable difference of quality between the mortar used in the façade and in the columns. Further X-Ray diffraction (XRD) analyses confirmed the different composition of the mortar: a lime mortar with 1.7MPa of compressive strength and C.V.=76% was used for the façade and a cement mortar with 28.7MPa of compressive strength and C.V.=10% for the columns.

The compressive strength of ceramic bricks was also tested, giving 18MPa (C.V.=35.6%). The estimated characteristic compressive strength was equal to 4.90MPa and the vertical modulus of elasticity was 2680MPa. For columns, these values raised up to 11.40MPa and 6270MPa respectively. For further details on the determination of these magnitudes, see Chapter 2.

3.3 DESCRIPTION OF THE NUMERICAL MODEL

3.3.1 Introduction

The numerical model simulates the structural behavior of a group of 12 dwellings distributed in two rows of 6 houses over an area of 235m x 98m and 35m depth of alluvium soil. Such a high extension of soil is taken to avoid the transmission of boundary effects produced by the model limits.

The dwellings subjected to the highest settlements (i.e. located closer to the tunnel axis) correspond to dwellings DW1 to DW3 (see Figure 3.2). These buildings are modeled in more detail by using non-linear material models and include the partition walls and columns. Note that DW2 and DW3 are symmetric. DW1 corresponds to an old restaurant of the neighborhood and therefore some of the partition walls were not present. The façade of DW4 is also included and modeled with a non-linear material. The rest of walls are modeled schematically in linear elastic regime in order to transfer boundary conditions to the most detailed part of the model. According to the damage survey, these walls were not affected by the tunnel construction.

The dimensions of each dwelling are 3m of height and a squared plant around 8m x 8m. The façade of each dwelling contains two windows of 1.2m x 1m and a door of 2m x 0.80m (see Figure 2.4). Note that the plant of the houses can be slightly different from house to house. For this reason, the geometry of DW2 (7.8m x 7.7m) has been taken as reference for the whole set of buildings.

The soil and the tunnel lining are modeled in linear elastic regime. The contact between the building walls and the soil is simulated by means of interface elements, which govern the transmission of vertical and horizontal movements to the walls.

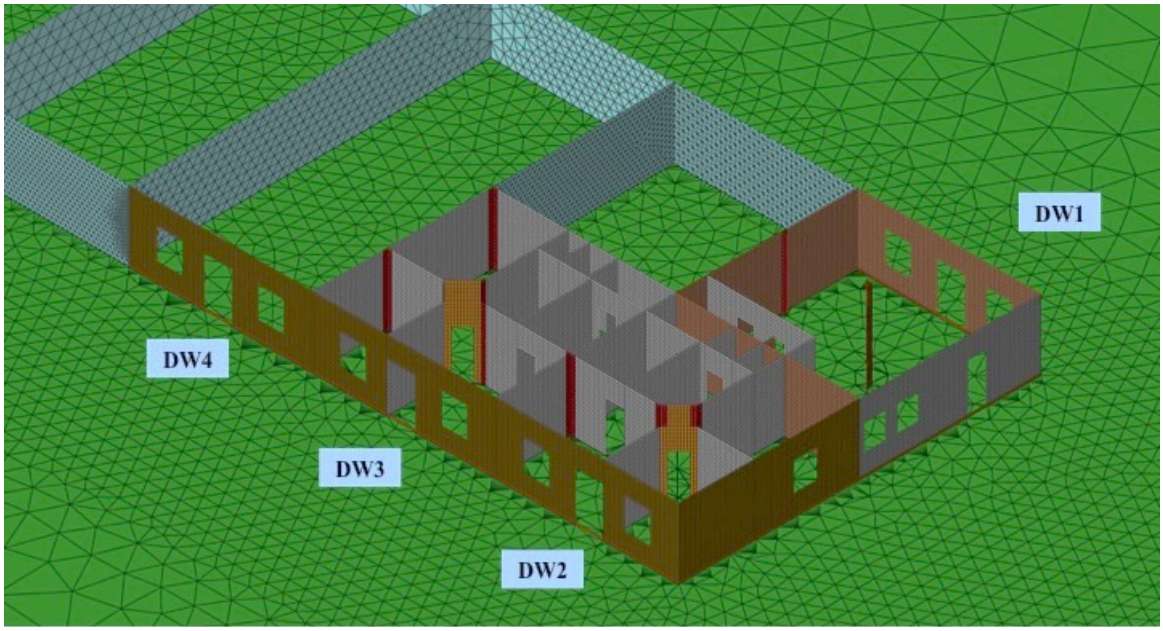

Figure 3.2. Model view of dwellings DW1 to DW4.

3.3.2 Model mesh

The model was developed with the pre- and postprocessor FX+ for DIANA® v.3.3.0 and the Finite Element software DIANA® v9.5. The model mesh is conformed by 4 different element types. The building walls corresponding to the non-linear part are modeled by 34244 4-node quadrangular shell elements, which allow the determination of plastic and cracking strains (Q20SH type). The rest of wall elements (10614 in total) are triangular with 3 nodes (T15SH type), which perform only linear elastic analysis. Element size is 100mm for the quadrangular elements and it is increased till 600mm in the zones out of the influence of the tunnel.

The lining mesh is conformed by 5527 Q20SH elements of 900mm sided. The ground is modeled using 130877 three-side iso-parametric solid pyramid elements (TE12L type). The soil mesh increases density in the zone of the vicinity of the building and the tunnel (Figure 3.3). The soil and the lining are directly connected.

The contact between the non-linear elastic building walls and the soil is simulated with 1292 4-node line interface elements (L12IF type). The part of the building modeled in linear elastic regime is directly attached to ground.

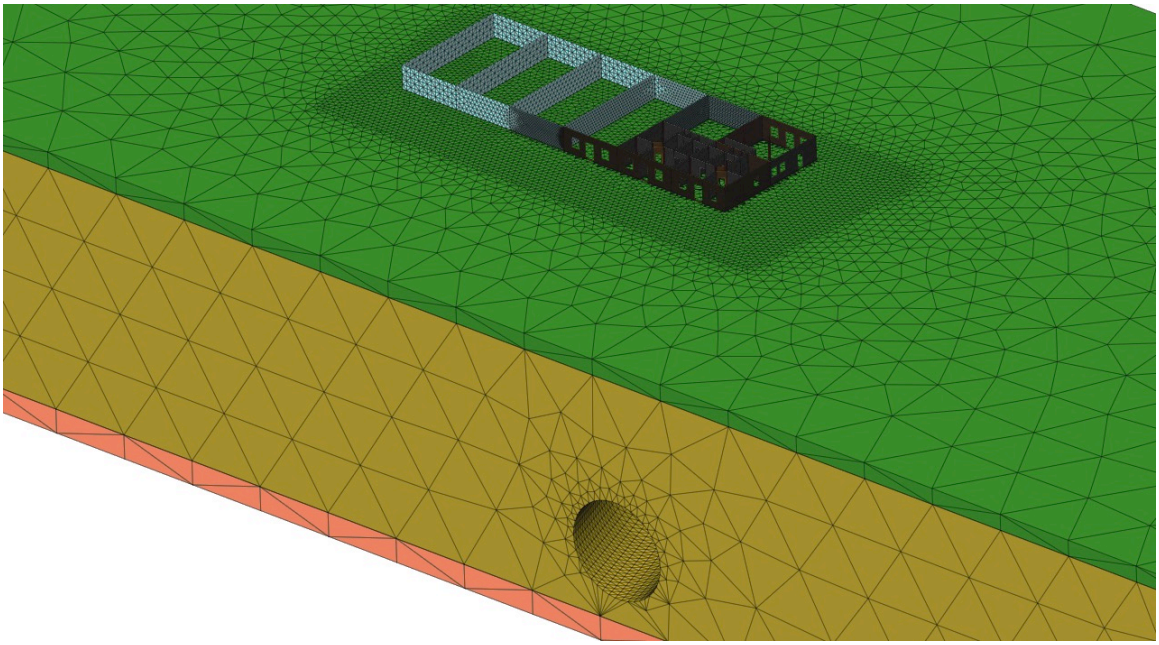

Figure 3.3. Model view of the masonry buildings, the soil and the tunnel lining.

3.3.3 Materials

3.3.3.1 *Masonry*

The non-linear analysis of dwellings DW1 to DW4 is performed using the Total Strain Rotating Crack model (TSRC). This is a fracture model with distribute cracking usually employed to evaluate the non-linear behavior of brittle materials. Masonry is therefore treated assuming isotropic properties. This model is attractive from an engineering point of view, since it suffices to specify non-linear stress-strain curves for the principal directions (Rots, 1989).

According to the data of the material characterization and considering the properties in the weak axis of masonry, the parameters of the walls and the columns are shown in Table 3.1, where E is the Young modulus, G is the shear modulus, ν is the Poisson's ratio, G_{f_t} and G_{f_c} are the tensile and compressive fracture energies respectively, and f_t and f_c are the tensile and compressive strengths of masonry, respectively. The constitutive model of masonry is given by an exponential function to represent the softening of the material after reaching the peak tensile stress. A parabolic model is used instead for the

compressive behavior. Biaxial tests on masonry panels carried out by Ganz (1985) were numerically simulated in Barbosa (2010). The research allowed the realistic assessment of values for the fracture energies of masonry.

*Table 3.1. Material parameters for the Total Strain Rotating Crack model of masonry (*experimental values; ** assumed values). Extracted from Camós et al. (2012).*

Masonry walls	E	G(*)	ν(**)	Density(**)
	2680 MPa	1070 MPa	0.20	1800 kg/m^3
	f_t(**)	f_c (**)	G_{f_t} (**)	G_{f_c} (**)
	0.05 MPa	3.20 MPa	0.02 N·mm/mm^2	10 N·mm/mm^2
Masonry columns	E	G(*)	ν(**)	Density(**)
	6270 MPa	2510 MPa	0.20	1800 kg/m3
	f_t(**)	f_c (**)	G_{f_t} (**)	G_{f_c} (**)
	0.05 MPa	7.60 MPa	0.02 N·mm/mm^2	10 N·mm/mm^2

3.3.3.2 *Soil and tunnel lining*

Ground inspection showed the existence of two different soil layers in the section of study. The first is a thin layer of anthropic deposits, followed by a layer of well-graded (SW) and clayed (SC) sand with presence of well graded gravel (GW) units. Standard Penetration Tests (SPT) carried out in the zone showed mean indexes around values of 7. These typical deltaic materials lay on altered granodiorite (grades IV and V).

The behavior of soil layers is simulated by linear elastic materials in order to reduce the global computational cost of the model. The properties of each layer are considered isotropic (Table 3.2). According to Jiménez Salas (1982), for sand layers with Standard Penetration Tests (SPT) as the present one, the Young modulus E in [MPa] increases linearly with the depth:

$$E(z) = 0.048 \cdot z \tag{3.1}$$

where z is the depth in [cm]. Therefore, the value of E at the surface (z =0cm) should be assumed to be negligible, whereas at tunnel axis (z =2300cm) E would be equal to 110.4MPa. However, such low E values at depths close to the surface imply the generation of unreal high horizontal displacements that are transmitted to the interface elements. This produces the early fracture of the interfaces and thus gives convergence

problems of the model. For this reason, $\partial E/\partial z$ is kept as 0.048, but the initial E value (i.e. E_0) is assumed to be 50MPa. A modulus of 5000MPa is considered for the soil elements directly connected to the columns to simulate the foundations. A high modulus for the granodiorite is considered to simulate the rigid behavior of the layer with respect to the deltaic materials. Tunnel lining is also modeled as a linear elastic material rigidly connected to the soil, with a Poisson coefficient of 0.2 and Young modulus equal to 30.000MPa (Table 3.2).

3.3.3.3 *Interface between walls and soil*

One of the biggest challenges when predicting building damage associated to tunneling is the accurate understanding and simulation of the interaction between the building and the soil. As shown in Chapter 2, empirical approaches for building damage usually assume green-field conditions and hence, they disregard the alteration of ground displacements due to the presence of buildings.

However, in practice, the building self-weight and the foundation stiffness can significantly modify the settlement trough and the transmission of both vertical and horizontal movements to the buildings (Potts and Addenbrooke, 1997). When performing numerical simulation, this contact behavior can be simulated for example by the use of non-linear springs. The correspondent compression stiffness K_s can be estimated according to the subgrade reaction modulus of ground (Camós *et al.*, 2014; Gálvez, 2012). Vertical springs remain inactive when subjected to tensile strains in order to simulate the gapping phenomenon, whereas horizontal springs remain inactive in zones where contact between soil and foundation is lost.

The spring approximation can be improved with the use of non-linear interface elements, which allow incorporating friction criteria. Particularly, line interface elements are used in the present model between the 2D shell elements of walls and the edges of 3D soil elements. Coulomb friction criterion is employed with parameters described in Table 3.3, where k_n and k_t are the linear normal and shear stiffness moduli, C is the cohesion, ϕ the internal frictional angle, ψ the dilatancy angle and f_t is the value of the tensile stress cut-off. The interface bedding k_n and shear k_t stiffness also play crucial roles in the failure mechanism. Lower is k_n, stronger is the redistribution of the displacements on the building base, which implies the generation of lower stresses on the walls. The same

concept applies for k_t: its value will determine the grade of transmission to walls of tangential stresses generated by ground horizontal displacements.

The choice of these parameters has been inspired in the works of Netzel (2009) and Giardina (2013). The difference of one lower order of magnitude of k_t with respect to k_n is justified due to the low monitored horizontal displacements at façade mid-height (see Chapter 2, Figure 2.8). However, a slightly less strict tensile cut-off value has been here assumed (Table 3.3).

Table 3.2. Material parameters for linear elastic soil layers (z in [cm]) and lining.

	E (MPa)	ν	Density (kg/m$^{3)}$
Anthropic deposits	$50+0.048 \cdot z$	0.35	1800
Sand SW-SC		0.3	2000
Granodiorite	10000	0.35	2600
Lining	30000	0.2	2500

Table 3.3. Material parameters for interface elements between walls and soil with Coulomb friction model.

	k_n (N/mm^3)	k_t (N/mm^3)	C (N/mm^2)	ϕ (deg)	ψ (deg)	f_{t_i} (N/mm^2)
Netzel (2009)	0.2	$0.2 \cdot 10^{-4}$	0	30°	0°	0
Giardina (2013)	0.2	0.05	0	30°	0°	0
Present analysis	0.2	0.05	0.05	30°	0°	0.10

3.3.4 Applied loads and modeling of the boring process

3.3.4.1 *Building self-weight and roof load*

The building self-weight is determined according to a typical value of masonry density (1800kg/m^3). The roof load of buildings is estimated in 2.5kN/m^2 according to the Spanish code. The roof load is acting over an area of 7.8m x 7.7m, which gives a total applied load of 150.2kN. This load is distributed among the bearing walls and columns according to the isostatic distribution shown in Figure 3.4. An additional load of 4.0kN/m is applied at facades to simulate the weight of the rake overhang (around 50cm) and the higher width of lintel elements. The applied loads are specified in Table 3.4 for the dwellings located on the corners (DW1 and DW2) and for the rest of the dwellings. The

term 'x-axis' refers to the direction parallel to façades of DW2, DW3 and DW4, whereas 'y-axis' refers to walls perpendicular to them. The roof load is applied at the initial phase, for which the lining elements are deactivated.

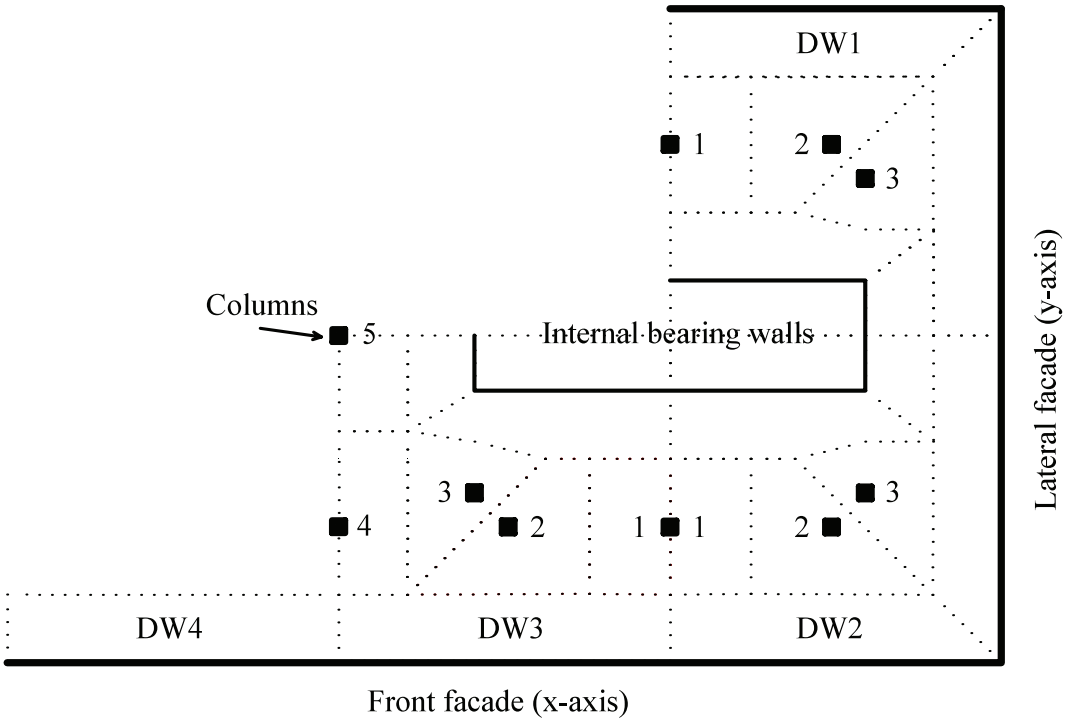

Figure 3.4. Plot of isostatic distribution for the roof load in bearing walls and columns.

Table 3.4. Values of applied loads at bearing walls and columns.

		Dwellings in corners		**Rest of the walls**	
Location	**Length**	**Surface**	**Applied load**	**Surface**	**Applied load**
Facade (x-axis)	7.8m	11.17m^2	3.6kN/m +4.0kN/m	12.54m^2	4.0kN/m+4.0kN/m
Facade (y-axis)	7.7m	11.11m^2	3.6kN/m +4.0kN/m	-	-
Internal wall (x-axis)	4.6m	8.00m^2	4.4kN/m	8.11m^2	4.4kN/m
Internal wall (y-axis)	1.3m	3.01m^2	5.8kN/m	2.80m^2	5.4kN/m
Column 1	0.4m	6.07m^2	37.8kN/m	6.05m^2	37.8kN/m
Column 2	0.4m	8.51m^2	53.2kN/m	8.48m^2	52.9kN/m
Column 3	0.4m	6.23m^2	39.0kN/m	6.24m^2	39.0kN/m
Column 4	0.4m	-	-	6.20m^2	38.8kN/m
Column 5	0.4m	-	-	3.64m^2	22.8kN/m

3.3.4.2 *Generation of ground displacements*

Soil and tunnel elements are directly connected. For this reason, ground displacements are generated by application of radial pressure to the lining in order to produce its shrinkage towards the concentric direction, as shown in Vermeer and Brinkgreve (1993), Augarde (1997) and Liu (1997). As a consequence, the adjacent soil elements will also deform, thus producing a field of ground displacements on the surface.

Analyses show that the generated settlement trough fits well to the classical Gaussian profiles. The volume reduction per unit length of the lining tube ΔV_{tube} will match with the volume of the generated settlement trough V_s per unit length, which is related to the ground volume loss V_L by:

$$V_s = V_L \cdot A_{exc} \tag{3.2}$$

where A_{exc} is the area of excavation per unit length.

A first estimation of the load applicable to the lining can be done with the theory of thin-walled tubes with opened ends. As the lining stiffness tends to be large in comparison to the ground stiffness, the prescribed tunnel contraction imposes a certain prescribed radial displacement towards the center of the tunnel (Möller, 2006). The relation between the radial variation of length δ_R produced and the applied pressure p is given by:

$$\delta_R = \frac{pR^2}{qE}\left(1 - \frac{\nu}{2}\right) \tag{3.3}$$

where R is the cylinder radius, q is the cylinder thickness, E is the Young modulus and ν is the Poisson's modulus. ΔV_{tube} (per unit) can be expressed as:

$$\Delta V_{tube} = \frac{\pi(R + \delta_R)^2 - \pi R^2}{\pi R^2} = \frac{\delta_R^2 + 2R\delta_R}{R^2} \tag{3.4}$$

Note that ΔV_{tube} and δ_R will be negative in case of contraction of the cylinder. The needed radial variation to achieve such ΔV_{tube} is given by:

$$\delta_R = \frac{-2R \pm \sqrt{4R^2 + 4(R^2 \cdot \Delta V_{tube})}}{2} \tag{3.5}$$

One of the solutions of the equation is disregarded due to lack of physical sense. Then if Eq. (3.5) is rearranged, the pressure to be applied on the cylinder is:

$$p = \frac{\delta_R q E}{R^2 \left(1 - \frac{\nu}{2}\right)} \tag{3.6}$$

In this case, R =6m, q =0.35m, E =30.000MPa, ν =0.2, A_{exc} =113.1m^2 and the generated volume loss V_L was around (-)0.7% (see Chapter 2). For these variable values, the required δ_R is (-)21mm, which is achieved by applying a pressure p equal to (-)6.81MPa.

The calculated value of p can be taken as first approximation. Nevertheless, the application of uniform radial pressure in a curved tunnel produces a turning effect of the lining around its longitudinal axis that can generate a field of surface settlements far from the Gaussian-shaped. Fixing the invert and the tunnel portals can be a practical solution for solving this problem, as suggested in the gap method of Rowe *et al*. (1983). Therefore, the value of p has to be then re-adjusted to produce the desired field of settlements. Linear interpolation until reaching the value of maximum settlement above the tunnel crown S_{max} can be applied for this purpose. In the present case, the measured S_{max} was 41mm, which can be generated by applying a pressure value of $p \approx$12MPa. Note the effect of the boundary conditions applied to tunnel invert and portals on the estimated pressure values with respect to the opened thin-wall cylinder approximation.

Applying radial pressure to produce tunnel shrinkage represents a simple way of modeling the generation of surface ground settlements. However, in case of shallow tunnels in soft soils as the present one, the generated surface settlement profiles are usually broader/flatter than the real ones due to the excessive lateral pressure applied to the tunnel, which stretches the corresponding soil elements and generates displacements of ground nodes located notably far from tunnel axis.

A possible solution to address this problem can be the application of a more realistic distribution of pressures to the lining by considering the coefficient of lateral earth pressure K_0. The resultant normal applied pressure p_n to lining elements located at a certain central angle α (Eq. (3.7)) can be then found by simple trigonometry, as shown in Figure 3.5.

$$p_n = p_v(\sin^2 \alpha + K_0 \cos^2 \alpha) \tag{3.7}$$

The value of K_0 can be estimated according to the angle of friction ϕ of soil:

$$K_0 = 1 - \sin\phi \tag{3.8}$$

Typical values of ϕ for sandy soils are around 30° and hence, K_0 equals 0.5. The final applied pressures for adjusting the real ground displacements are thus $p_v = -1.87$MPa and $p_h = -0.94$MPa. The normal load is discretized in arch segments of approximately 9° that match with the size of lining elements (900mm). The effect of tangential loads to the lining is disregarded. The application of pressure to the tunnel is done gradually from one tunnel portal to the other by using a procedure in 8 phases. The pressure to the lining is incrementally applied. The length of the tunnel stretches activated at every stage decreases with the proximity to the building (Figure 3.6). At every stage, soil elements along the tunnel track are removed and lining elements are simultaneously activated.

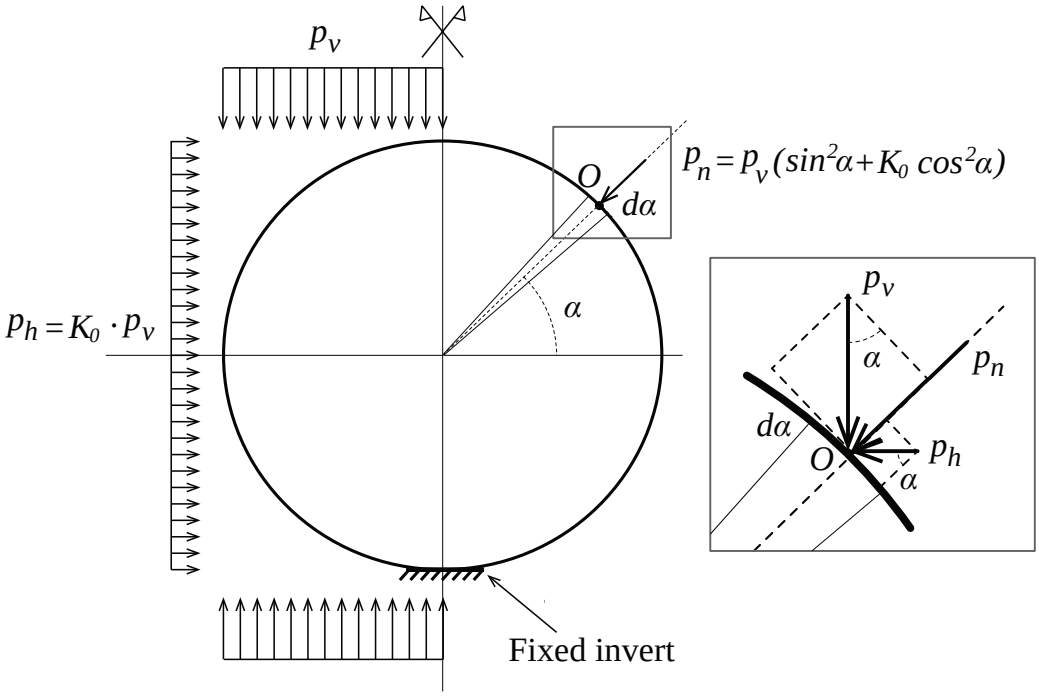

Figure 3.5. Application of pressure to tunnel lining for the simulation of ground volume loss.

Figure 3.7 shows the generated settlement profiles in case of radial uniform pressure (coarse dashed line) and for K_0 =0.5 (thin dashed line). Both curves are compared to the real measurements (small triangles) and to the Gaussian profile that adjusts them (continuous line). As it can be seen, the numerical curves are wider than the real one, although the application of K_0 notably improves the approximation to real measurements. The accuracy of the settlement profiles is discussed in Sec. 3.4.4. For more detailed and

improved simulation of installation procedures for segmental tunnels see Möller (2006), Arnau *et al*. (2011) and Arnau *et al.* (2012).

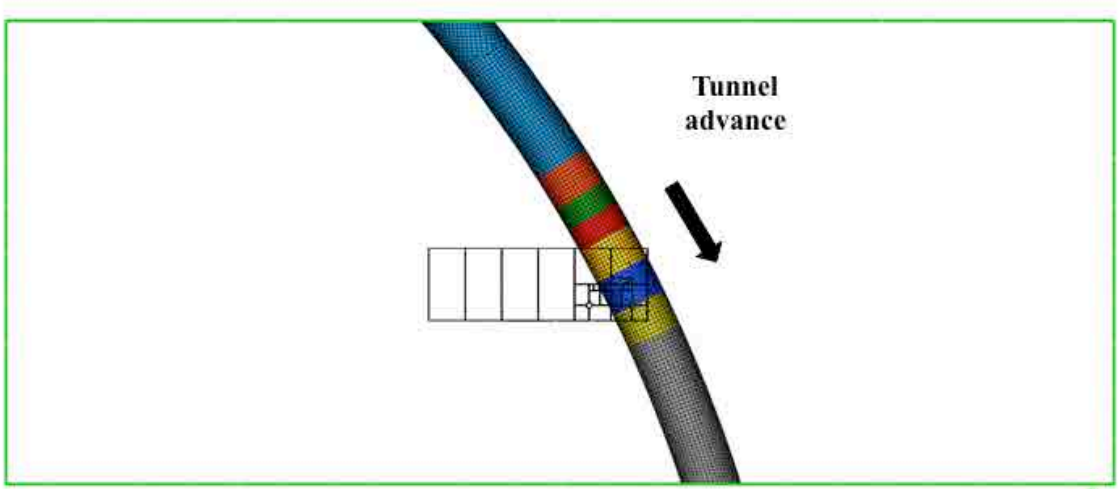

Figure 3.6. Tunnel lining elements activated at each phase of the analysis.

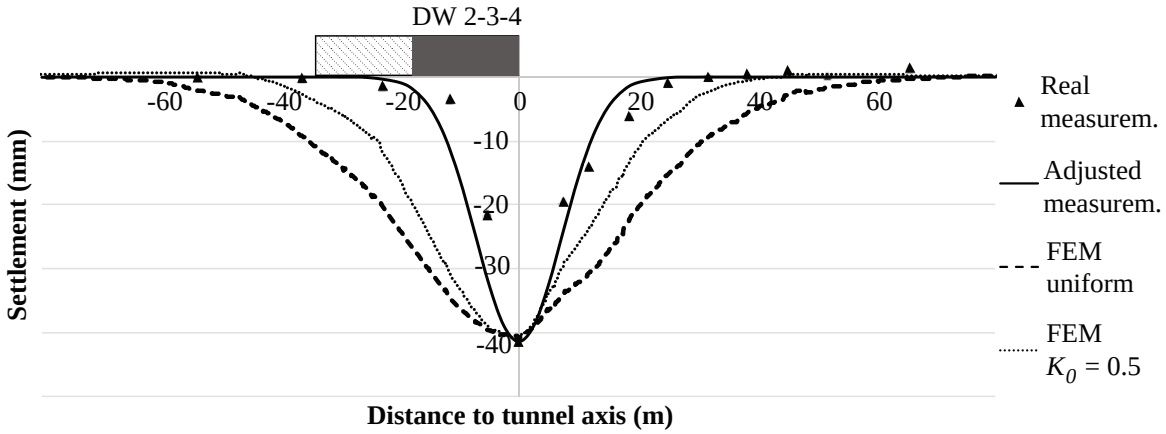

Figure 3.7. Applied settlement curve in the numerical model vs real settlement profile occurred.

3.3.5 Analysis commands and computing time

The energy convergence criterion equals 0.005. The roof load is applied in 5 load steps, whereas the lining pressure is applied in 10 steps at every phase. A maximum of 50 iterations are allowed for every load step. The total computing time for the model of 9 phases (1 for the roof load and 8 for the lining pressure) is around 17 hours. The computer features are: Intel Core i7 930 @ 2.80 GHz processor, 8GB RAM and operating system Windows 7 Professional 64 bits.

3.4 RESULTS OF THE SIMULATION AND COMPARISON TO SURVEY

3.4.1 Introduction

This section shows the results of tensile strains and crack widths that were developed in the buildings during the approach and underpass of the tunnel face. The plots of principal total tensile strains are compared with pictures and illustrations of the damage report. The section also checks the relevance of considering a phased analysis on the predicted damage results.

3.4.2 Cracking patterns (phased analysis)

3.4.2.1 *Damage on the façade of DW1*

Figure 3.8 shows the façade of DW1, where the model predicts a diagonal crack in the zone between the left window and the entrance door. The crack is generated due to the high shearing forces acting in the zone. As it can be seen in the figure, the crack was clearly visible at naked eye. The model also predicts the onset of cracking under the left window, which is confirmed by the damage survey.

3.4.2.2 *Damage on the façade of DW2*

A similar diagonal crack was predicted on the façade of DW2, as shown in Figure 3.9. The cause of this crack is again the important shearing forces induced by the settlement of the building corner. As it can be seen, the crack also was clearly observable.

Another diagonal crack starting at the right bottom corner of the right window was also reported and well predicted by the model, although no pictures of this crack are available.

According to the images of real damages shown in Figure 3.8 and Figure 3.9, the diagonal crack in DW1 seems to be wider than the one in DW2. This difference of width is also well predicted by the numerical model: diagonal crack in DW1 is estimated around 7mm in the center of the crack, and the one in DW2 is around 4mm. Note that these magnitudes are described in the principal direction which is perpendicular to the crack orientation.

3.4.2.3 *Damage on the façade of DW2, DW3 and DW4*

The principal total tensile strains in the façade of DW2, DW3 and DW4 are shown in Figure 3.10. It can be seen that the damage prediction in DW2 shows good agreement with the illustration of the reported cracking patterns. Vertical cracking above the left window of DW4 is also well predicted. Nevertheless, the estimated damages in DW3 are lower respect to the real ones. The reason is that the settlement profile affecting this part

of the façade is flatter than the real one, as it is shown in Figure 3.7 and further discussed in Section 3.4.4.

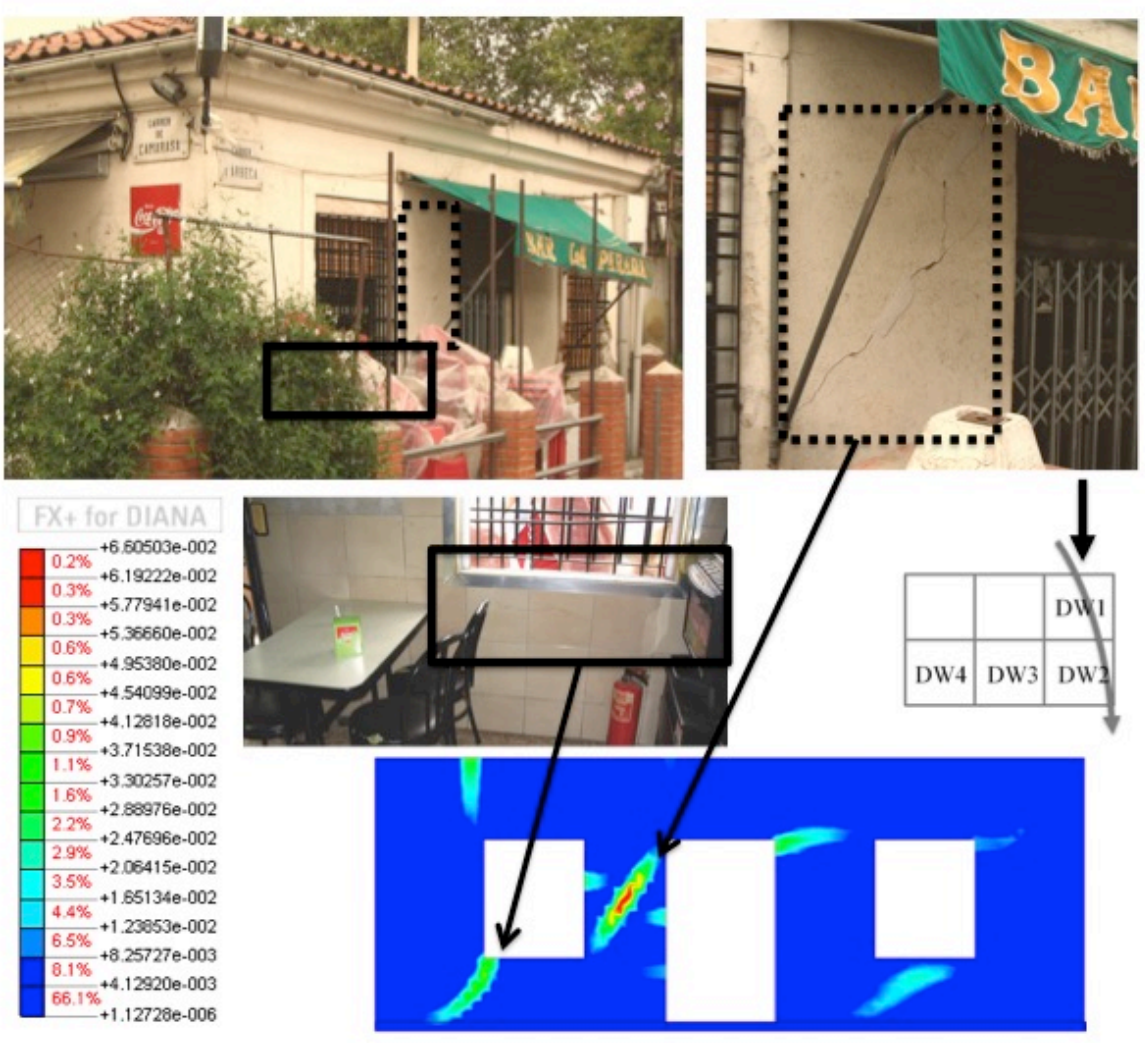

Figure 3.8. Principal total tensile strains at façade of DW1 and comparison to real damage (grey arrow indicates the direction of tunnel advance).

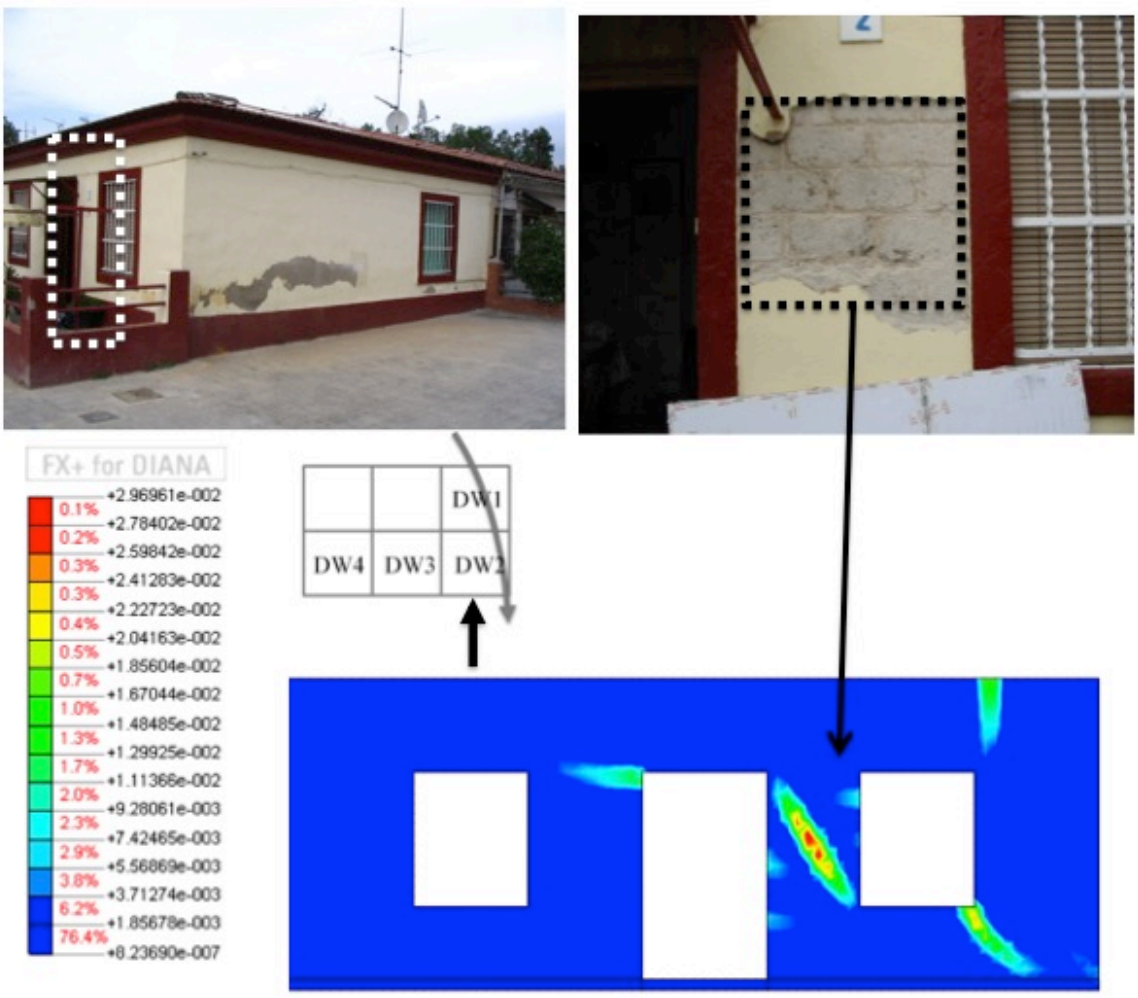

Figure 3.9. Principal total tensile strains at façade of DW2 and comparison to real damage (grey arrow indicates the direction of tunnel advance).

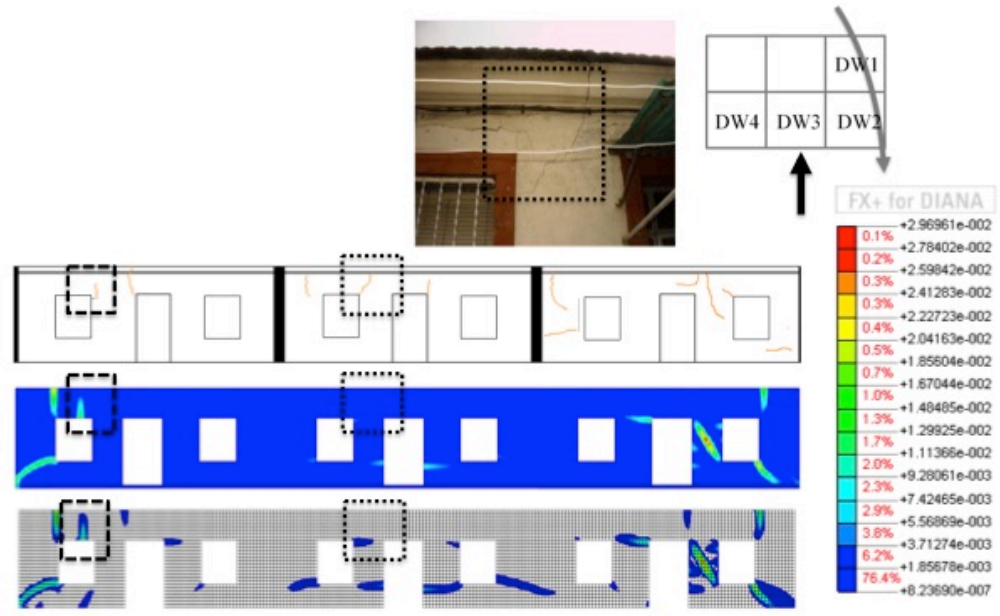

Figure 3.10. Principal total tensile strains at façade of DW2, DW3 and DW4 and comparison to real damage.

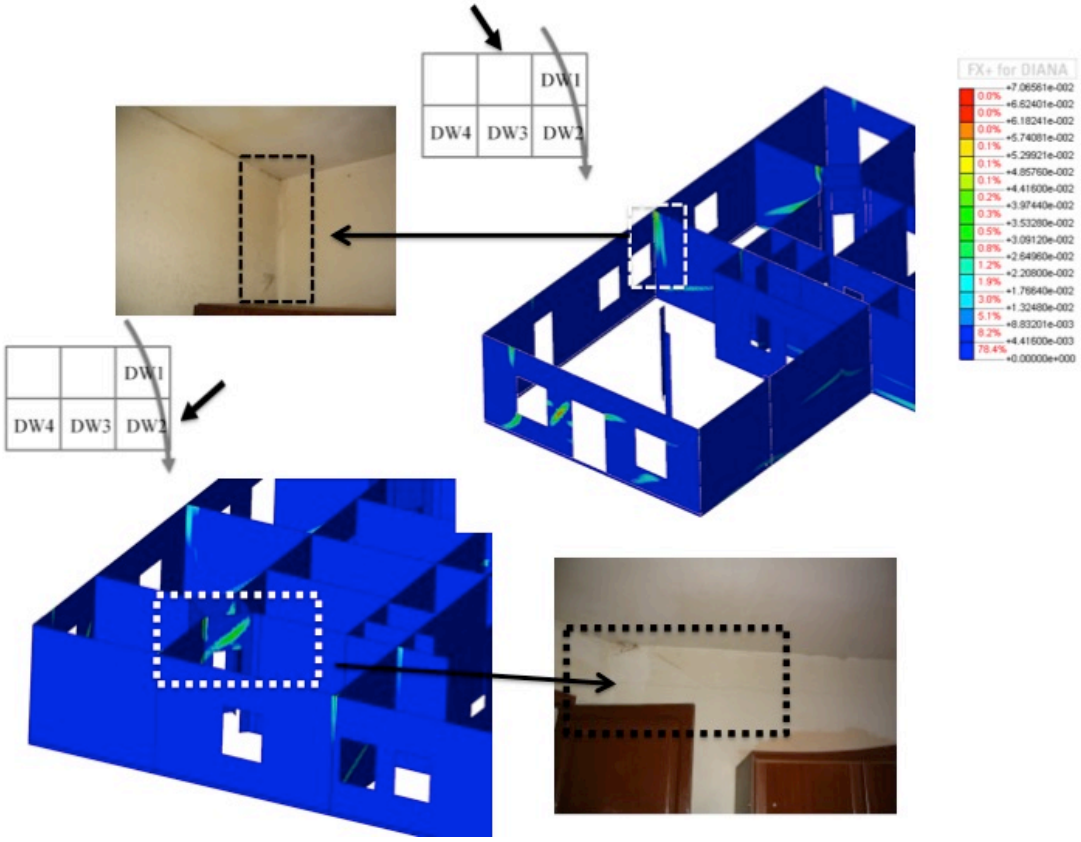

Figure 3.11. Principal total tensile strains in indoor partition walls and comparison to real damage.

3.4.2.4 *Damage on the partition walls*

The comparison of real damage at partition walls with the numerical prediction is more difficult due to the small magnitude of crack widths. Some of the available pictures of occurred cracks agree with predicted tensile strain patterns, as shown in Figure 3.11. For example, a clear vertical crack appeared in the junction of the internal wall that separates DW1 and DW2 and their lateral external walls. This crack is well defined in the model. Other smaller horizontal cracks appeared above the doors close to the center columns. The model reproduces well the start of these patterns in the corners of doors. However, the model predicts other tensile strain patterns where cracks were not reported. A possible reason is that strains didn't result in visible cracking, since the predicted widths in the partition walls are around 1mm or even lower values.

3.4.3 Differences on predicted cracking patterns between the phased and non-phased analyses

The previous section has shown a general good agreement between the real damage in the buildings and the predicted damage by the numerical model when using a phased analysis to simulate the tunnel advance. The phased analysis has however modeling disadvantages in terms of complexity and notable increasing of the computing time. For this reason, a non-phased analysis was also performed in order to check possible differences in the predictions.

The same view of dwellings DW2, DW3 and DW4 as in Figure 3.10 is now shown in Figure 3.12 for a non-phased analysis. No significant differences in the tensile strain patterns are observable, although the predicted crack widths are lower for the non-phased analysis. For example, the predicted diagonal crack in Figure 3.9 would have not been visible for the now reached value of strain.

However, the analysis of the façade of DW1 (Figure 3.13) does show a significant variation of cracking patterns since the diagonal crack in Figure 3.8 does not appear. This shows that the imposed deformation mechanism is slightly different with respect to the phased analysis and hence, the prediction would be here unrealistic. In fact, since the tunnel runs in curve beneath the buildings, the alignments of façades of DW1 and DW2-DW3-DW4 with respect to the tunnel axis differ about 15 degrees. As it will be shown in Chapter 4, small variations of the wall alignment with respect to the tunnel axis can lead

to different estimations of damage due to the effect of the longitudinal component of the settlement field.

3.4.4 Discussion on the applied settlement field

The presented FEM model of a real building includes the modeling of the soil and the tunnel. This allows modeling the tunnel advance and its influence on the final results of damage. Moreover, the application of normal pressure to the lining generates settlement profiles similar to the classical Gaussian curves that are applied for the modeling of tunneling settlement troughs.

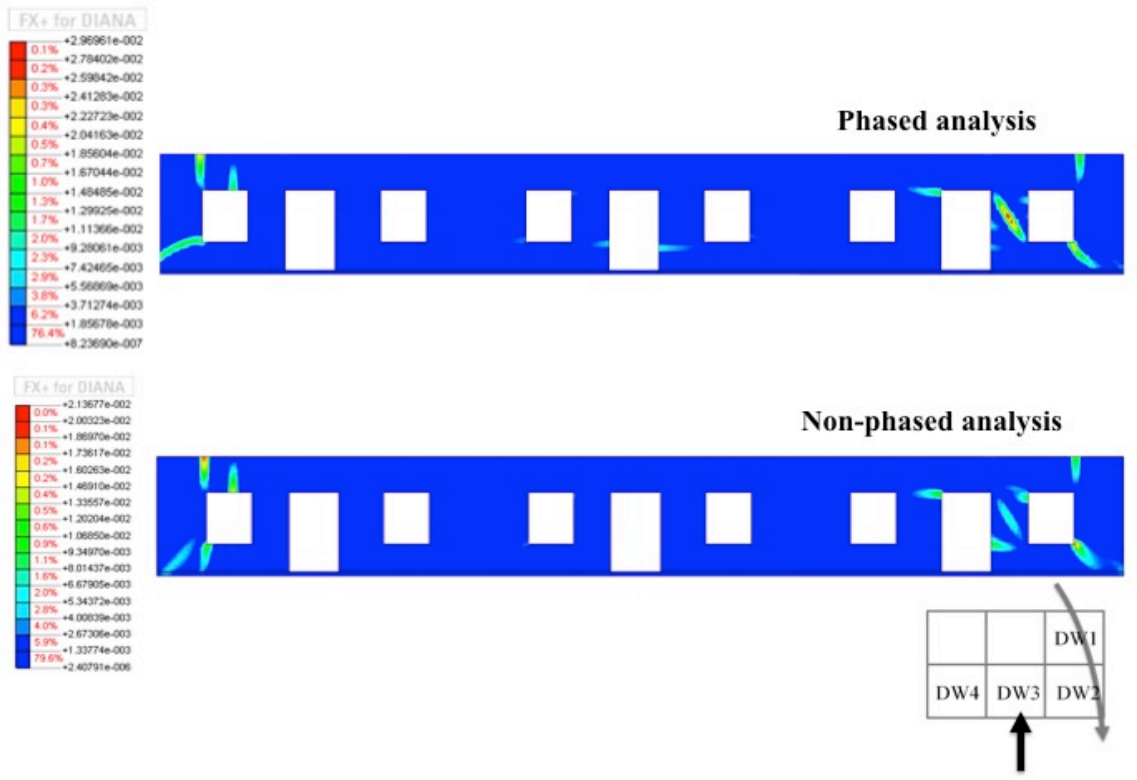

Figure 3.12. Comparison of principal total tensile strains in façade (DW2, DW3, DW4): phased vs. non-phased analysis.

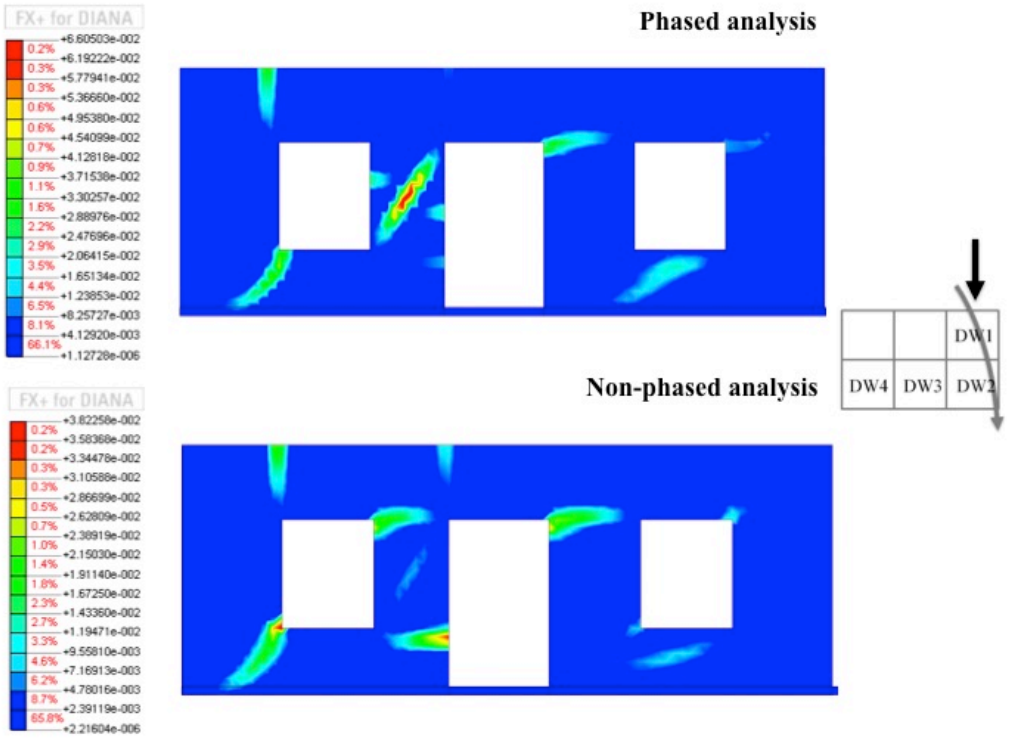

Figure 3.13. Comparison of principal total tensile strains in façade (DW1): phased vs. non-phased analysis.

3.4.5 Conclusions

The present research has shown a numerical model of a set of masonry buildings affected by the construction of the L9 metro line tunnel in Barcelona. The analysis of masonry walls with the Total Strain Rotating Crack model in combination with linear elastic models for the soil and the lining represents a feasible and effective method to predict cracking patterns in the structure. The settlement trough generated by application of normal pressure to the lining can be more realistic with the application of the coefficient of lateral earth pressure, instead of considering uniform radial pressure applied to the tunnel. The real cracking patterns in the building and the results obtained from the non-linear analysis show good agreement. However, the low depth of the presented tunnel, the simplicity of soil models and the uncertainty associated to the interface elements represent modeling challenges when developing this kind of coupled models. The predicted cracking patterns between the phased and non-phased analyses show variations, which demonstrates that the longitudinal component of the settlement trough can have significant influence on the deformation mechanisms of the building and hence, on the damage predictions.

4. 3D Analytical Prediction of Building Damage Produced by Tunneling Subsidence

Abstract: Tunnel construction entails the generation of ground settlements, which can endanger the adjacent buildings. The prediction of damages in buildings is usually based on the classical Gaussian profiles for the approximation of the subsidence trough and the equivalent beam method for modeling the response of building walls. Current available expressions refer to walls aligned transversally with respect to the tunnel axis, which usually represents the worst-case scenario. However, approximations must be done for other building alignments, since no analytical expressions are available for these cases. We propose a novel equation for the determination of the horizontal ground strain, which departs from the equations of the classical Gaussian settlement profiles. The novel formulation allows the application of the equivalent beam method in 3D and the modeling of the tunnel advance. The results show significant variations of the estimated damage depending on the wall position with respect to the tunnel axis. The paper reviews also certain relevant aspects of building damage predictions, such as the influence area of settlements and the possible contribution of ground horizontal strain to damage reduction. A parametric analysis is further performed to create a non-linear regression model that allows direct estimation of the maximum tensile strain in a building wall according to input values of geological conditions and wall and tunnel geometries.

Keywords: Tunnel construction, settlements, subsidence, building damage, equivalent beam, wall alignment, 3D, analytical prediction.

4.1 INTRODUCTION

4.1.1 Background

Design of urban tunnels requires the prediction of possible damages in adjacent buildings produced by tunneling subsidence. The use of Finite Element Models is appropriate for precise evaluations of damages, including the location and width of crack patters (Giardina *et al*. 2013). However, primary assessments of the response of buildings to settlements can be done with the equivalent beam method (Burland and Wroth, 1974; Boscardin and Cording, 1989), which is widely used in tunneling engineering. This method models a building wall as a weightless linear elastic beam subjected to a given ground settlement profile. Strains in the beam are generated (a) due to the deflection when conforming to the settlement profile and (b) due to the ground horizontal strain generated on the base of the beam. The distribution of strains along the beam depends on the mode of deformation, which comprises a combination of bending and shear. For this reason, two extreme modes are typically considered in order to ascertain which is the most critical: pure bending and pure shear. Maximum tensile strains in the beam due to pure bending (ε_{br}) and pure shear (ε_{dr}) deformations are given by the following expressions derived from the elastic beam theory:

$$\varepsilon_{br} = (\varepsilon_{bmax} + \varepsilon_h) \tag{4.1}$$

$$\varepsilon_{dr} = \varepsilon_h \left(1 - \frac{E}{4G}\right) + \sqrt{\frac{\varepsilon_h^2}{16}\left(\frac{E}{G}\right)^2 + \varepsilon_{dmax}^2} \tag{4.2}$$

where E/G is the ratio between the Young and shear moduli of the wall material, ε_{bmax} and ε_{dmax} are the maximum strains due to the deflection of the beam in pure bending and pure shear modes of deformation (Sec. 4.4) and ε_h is the value of horizontal ground strain on the base of the beam, which depends on the shape of the settlement trough and on the location of the wall (Figure 4.1). This location is defined by the proximity and the alignment with respect to the tunnel axis (Sec. 4.2). The maximum tensile strain ε_{max} corresponds to the highest value between ε_{br} and ε_{dr} along the beam. Based on ε_{max}, the approach of Burland *et al*. (1977) is used in this paper for classification of the damage magnitudes (Sec. 4.4).

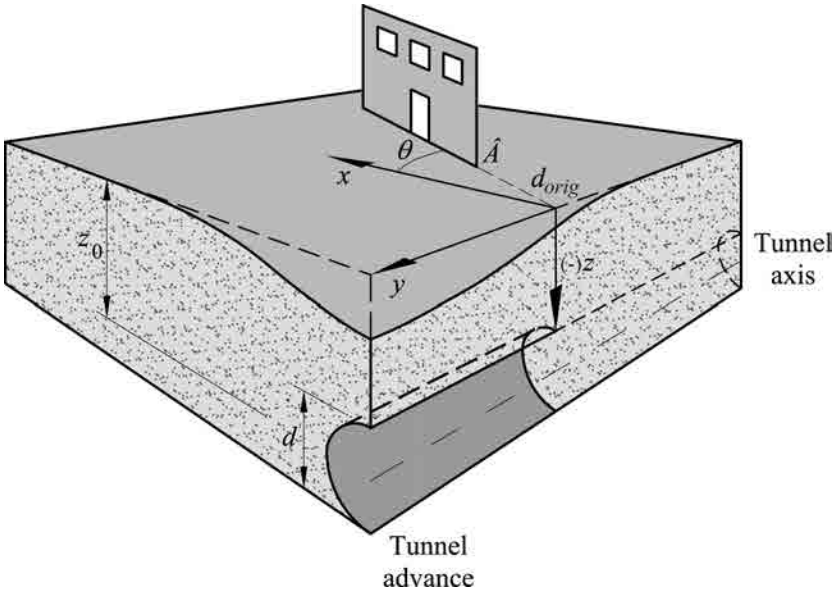

Figure 4.1. 3D settlement trough above an advancing tunnel.

The determination of ε_{max} represents a 3D problem that depends on (a) the ground conditions, (b) the building geometry, (c) the tunnel geometry, (d) the building position with respect to the tunnel axis, (e) the location of the tunnel face and (f) the construction technology. Nevertheless, equivalent beam analyses are usually simplified and performed in 2D. For example, in case of buildings aligned transverse to the tunnel axis (x-direction), data evidence has shown that the shape of the settlement profile S can be closely approximated to a Gaussian probability density distribution (Peck, 1969). The settlement profile in the longitudinal direction (y-direction) is usually described by a Gaussian cumulative distribution function (Attewell and Woodman, 1982). Settlement profiles in both directions are depicted in Figure 4.1.

Expressions of ground horizontal movements in the transverse $U_x(x)$ and longitudinal $U_y(y)$ directions respect to the tunnel axis were given by O'Reilly and New (1982) by assuming that ground particles move towards the tunnel axis. Horizontal ground strain ε_h in the transverse $\varepsilon_{h,xx}(x)$ and longitudinal $\varepsilon_{h,yy}(y)$ directions are directly given by derivation of $U_x(x)$ and $U_y(y)$:

$$\varepsilon_{h,xx}(x) = \frac{dU_x(x)}{dx} \tag{4.3}$$

$$\varepsilon_{h,yy}(y) = \frac{dU_y(y)}{dy} \tag{4.4}$$

Buildings walls aligned transversally and longitudinally with respect to the tunnel axis are statistically representative, since many urban tunnels follow the tracks of avenues or streets. However, there are a significant number of buildings randomly aligned with respect to tunnel axes, in particular when using a Tunnel Boring Machine (TBM). The damage assessment in these cases is usually simplified by projecting the transverse or the longitudinal (whichever is the closest) settlement profile along the axis of the rotated wall, as shown in Figure 4.2 (Kappen J., 2012; Camós, Molins *et al.* 2014). However, this practice can become unrealistic for alignments far from the transverse or longitudinal cases. Therefore, the determination of ε_h and the posterior damage assessments using this practice may be inaccurate.

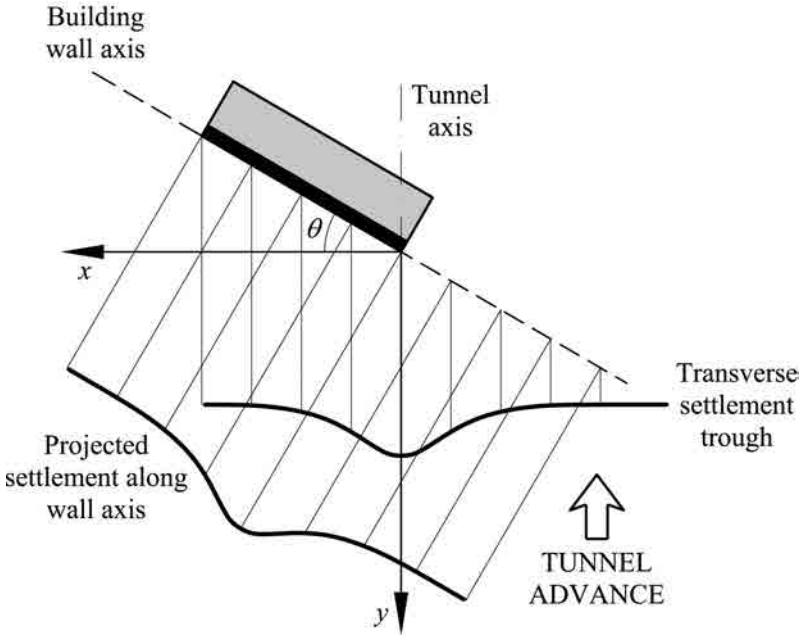

Figure 4.2. Projection of settlement profile in case of a rotated building respect to x-direction.

The models of Peck (1969), Attewell and Woodman (1982) and O'Reilly and New (1982) can be extended to obtain 3D expressions for the settlement trough, $S(x, y, z)$, the ground horizontal displacements, $U_x(x, y, z)$ and $U_y(x, y, z)$ and the ground horizontal strains, $\varepsilon_{h,xx}(x, y, z)$ and $\varepsilon_{h,yy}(x, y, z)$ (see Sec. 4.2). However, no equation has been found in the literature to determine the resultant value of ε_h in a particular wall alignment. Therefore, accurate estimations of ε_h can only be achieved with the use of numerical simulation and hence, the complete analytical assessment of building damage cannot be performed. Moreover, numerical simulation is commonly avoided in practice due to the required computation resources and modeling expertise (Giardina *et al.* 2012).

4.1.2 Content of the paper

The present paper proposes a novel equation for the exact determination of ε_h in a particular wall alignment by applying a change of basis to the infinitesimal ground strain tensor (Sec. 4.2). The new equation departs from the equations of Peck (1969), Attewell and Woodman (1982) and O'Reilly and New (1982), which assume that settlement troughs produced by tunneling construction are Gaussian-shaped. The proposed equation is used to show the influence of the ground conditions and the tunnel geometry in the values of ε_h (Sec. 4.3). The paper furthermore reviews certain relevant aspects of building damage predictions with the equivalent beam method in 3D, such as the influence area of settlements and the possible contribution of ground strain to damage reduction. The influence of the tunnel face location and the position of the building wall in the damage assessment is also shown by means of a parametric analysis (Sec. 4.4). The resulting data is used to create a non-linear regression model that allows the direct estimation of the maximum tensile strain ε_{max} in a building wall according to input parameters of the geological conditions and the wall and tunnel geometries (Sec. 4.5).

4.2 DEVELOPMENT OF A NOVEL EQUATION FOR THE GROUND HORIZONTAL STRAIN ε_h IN 3D

4.2.1 Introduction

The next sections describe the development of a novel equation for the determination of the resultant ground strain ε_h in a particular wall alignment θ with respect to the tunnel axis. For this reason, the notation for the description of the building wall position is given, first for a general case (Sec. 4.2.2.1) and then for the particular case of building walls parallel to tunnel axis (Sec. 4.2.2.2). Sections 4.2.3 and 4.2.4 show the equations in 3D of the settlement profile $S(x,y,z)$ and the ground horizontal displacements, $U_x(x,y,z)$ and $U_y(x,y,z)$ given by Attewell and Woodman (1982) and O'Reilly and New (1982). The development of the new equation for ε_h, which departs from the equations of ground horizontal strains $\varepsilon_{h,xx}(x,y,z)$ and $\varepsilon_{h,yy}(x,y,z)$, is shown at Sec. 4.2.5.

4.2.2 Description of the building wall position

4.2.2.1 *General case*

A typical tunneling situation with a building wall of length l_{build} is depicted in Figure 4.3. The y-axis follows the tunnel longitudinal axis, whereas the x-axis corresponds to a

transverse plane to the tunnel. The origin of the coordinates will be set at the intersection between the wall and the tunnel longitudinal axes. Note that this coordinate system refers to a particular wall and must be changed when other walls are analyzed. The tunnel face is located at coordinate y_s and advances towards $y = -\infty$, following the criteria set by Attewell *et al.* (1986). y_f represents the location of the tunnel portal.

The wall is aligned θ degrees with respect to the tunnel transverse plane. Counterclockwise alignments are considered positive ($\theta > 0$). The distance between the wall reference point $\hat{A}$ and the origin of coordinates is named d_{orig}. For convenience, this distance can also take negative values. Wall positions can be described with this notation within a range of $\theta = [-90°, 90°]$ and $d_{orig} = (-\infty, +\infty)$. However, note that due to symmetry of the settlement trough about the tunnel longitudinal axis, wall positions described by $d_{orig} = d_{orig_1}$, such that $0 > d_{orig_1} \geq -l_{build}$ with $\theta = \theta_1 \epsilon [-90°, 90°]$ are equivalent with the position described by $\theta_2 = -\theta_1$ and $d_{orig_2} = \left|d_{orig_1}\right| - l_{build}$ (see cases d) and e) in Figure 4.4).

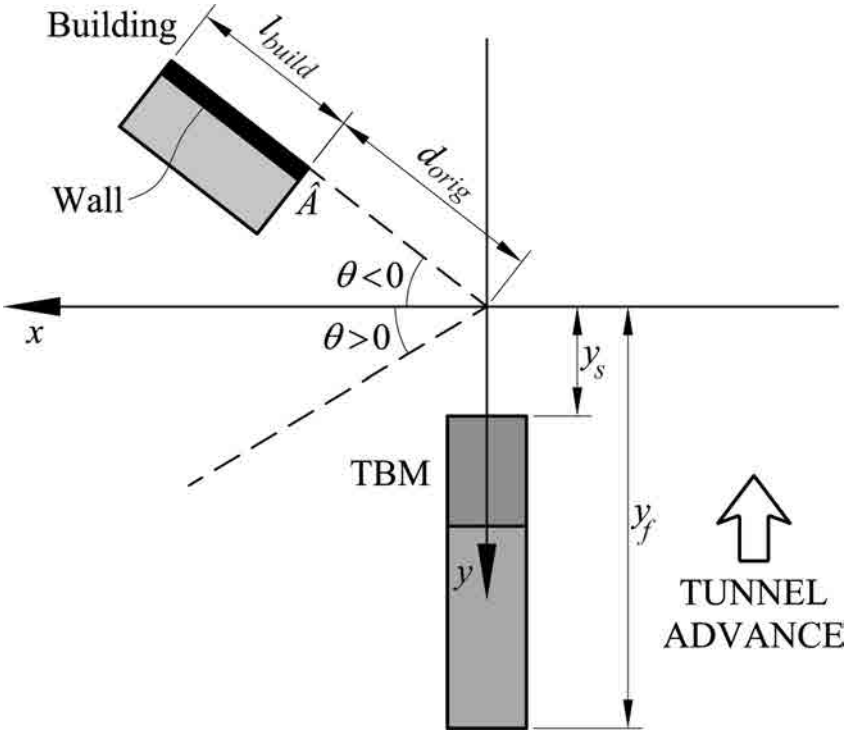

Figure 4.3. Parameters of tunnel and building positions (general case).

4.2.2.2 *Building wall parallel to tunnel axis*

All wall positions can be described with the notation of Sec. 4.2.2.1 except the cases of building walls parallel to the tunnel longitudinal axis. In this case, the x-axis is set at the same coordinate y of the wall reference point $\hat{A}$ (Figure 4.5). The wall is located at a distance d_{axis} from the tunnel axis. This distance is defined in a range $(-\infty, +\infty)$. Due to symmetry, the cases with $d_{axis} < 0$ have the equivalent case on the positive side. Case of $d_{axis} = 0$ can be treated with both notations (the one shown in Sec. 4.2.2.1 and the present one).

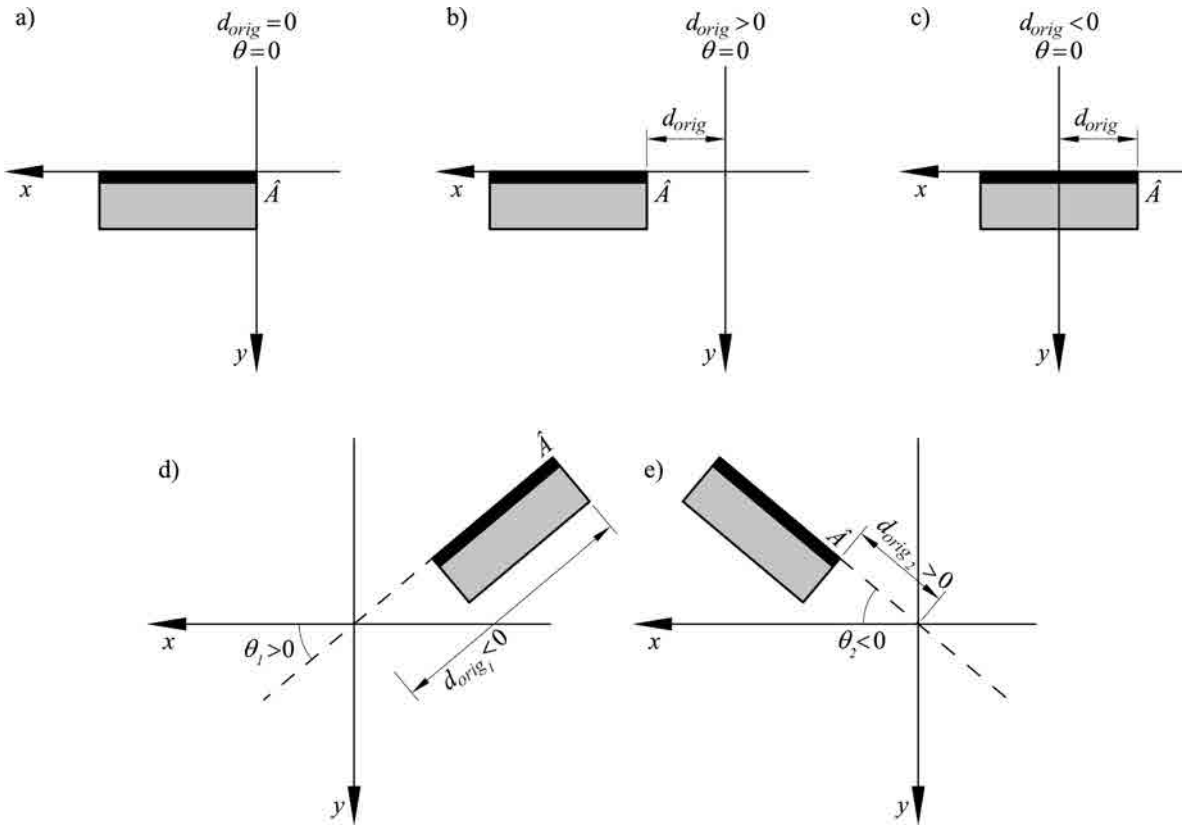

Figure 4.4. Description of building positions according to the values of θ and d_{orig} (general case).

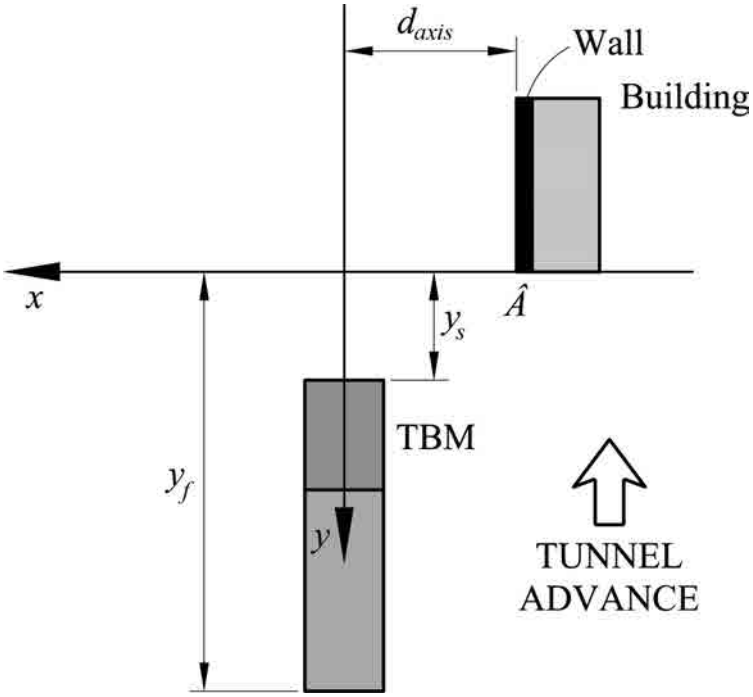

Figure 4.5. Parameters of tunnel and building position (case of parallel walls with respect to the tunnel axis).

4.2.3 Description of 3D settlement Gaussian trough

The settlement in [mm] at a certain position with coordinates x, y, z in [m] is calculated by the expression (Peck, 1969; Attewell and Woodman, 1982; O'Reilly and New, 1982):

$$S = -1000 \cdot S_{max} \cdot exp\left[-\frac{x^2}{2 \cdot K_x^2 \cdot (z_0 - z)^2}\right] \cdot \cdot \left[\Phi\left(\frac{y - (y_s + y_0)}{K_y \cdot (z_0 - z)}\right) - \Phi\left(\frac{y - y_f}{K_y \cdot (z_0 - z)}\right)\right] \quad (4.5)$$

where S_{max} is the absolute value of maximum settlement far behind the tunnel face, where the deformations are fully developed. It is calculated as:

$$S_{max} = \frac{V_L \cdot \pi \cdot d^2}{\sqrt{2\pi} \cdot K_x \cdot (z_0 - z) \cdot 4} \quad (4.6)$$

d and z_0 are the tunnel diameter and depth of the tunnel axis in [m], respectively, with z_0 being a positive magnitude. $\Phi(.)$ is the standard normal cumulative distribution function. Note that term of $\Phi(.)$ that contains y_f becomes 0 if $y_f = +\infty$. V_L is the volume ground loss per unit, K_x and K_y are the non-dimensional shape parameters describing the Gaussian settlement curves in the transverse and longitudinal direction respectively. K_x

and K_y depend on the type of soil: high values of the parameter indicate flat/broad settlement curves (stiff or soft silty clays), whereas low values indicate sharp/narrow settlement curves (granular soils). The products $K_x \cdot z_0$ and $K_y \cdot z_0$ determine the location of the inflection points $i_x = i_y = i$ of the Gaussian curves. Note that settlements S in Eq. (4.5) are considered to be negative along the z-axis. It is important to keep this sign convention for the correct application of related equations of ground horizontal displacements and strain (see Secs. 4.2.4-4.2.5). However, references to settlement magnitudes will be expressed in absolute values throughout the paper.

It is commonly assumed that the settlement above the tunnel face corresponds to half the maximum settlement S_{max}, which occurs at a distance far behind from the tunnel face. However, it has been shown that this value can be lower depending on the type of ground and the construction technology (Nomoto *et al*. 1995, Fargnoli *et al*. 2013). For example, the tunnel pressure of a TBM shield in soft soils restricts the ground movements on the heading, so that the major part of the settlements is related to the tail void. For this reason, a new parameter y_0 has been introduced in the original equation in order to model the shift of the longitudinal settlement profile with respect to the tunnel face position (Figure 4.6). This parameter can be deduced from the equation of Attewell and Woodman (1982) for the surface longitudinal settlement at the tunnel centerline ($x = z = 0$), with the tunnel portal location far from tunnel face ($y_f = +\infty$). This profile is described by a Gaussian cumulative distribution function:

$$|S(x = z = 0, y)| = S_{max} \cdot \Phi\left(\frac{y - y_0}{i_y}\right) \tag{4.7}$$

The settlement above the tunnel face ($y = y_s$) is:

$$|S(x = z = 0, y = y_s)| = S_{max} \cdot \Phi\left(\frac{y_s - y_0}{i_y}\right) \tag{4.8}$$

Rearranging Eq. **Error! Reference source not found.** and setting $i_y = K_y \cdot z_0$, the xpression of the shift of the longitudinal settlement results in:

$$y_0 = -\Phi^{-1}(\delta) \cdot K_y \cdot z_0 \tag{4.9}$$

where δ is the ratio between the surface settlement above the tunnel face and the maximal settlement S_{max} at infinite distance behind of the face:

$$\delta = \frac{|S(x = z = 0, y = y_s)|}{|S(x = z = 0, y = +\infty)|} = \frac{|S(x = z = 0, y = y_s)|}{S_{max}} \tag{4.10}$$

An example of shifted longitudinal settlement profile for a δ ratio equal to 0.2 is also shown in Figure 4.6.

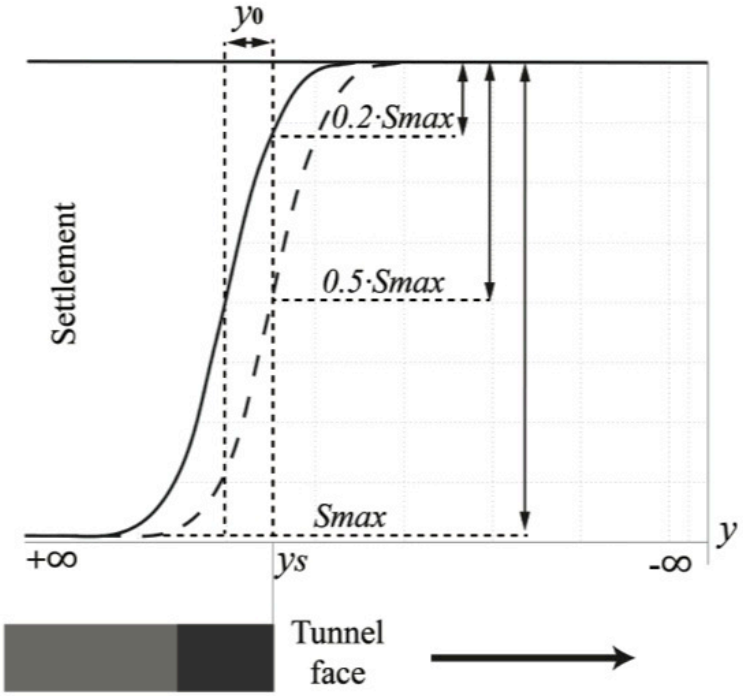

Figure 4.6. Longitudinal settlement profiles for δ =0.2 (solid line) and δ =0.5 (dashed line).

4.2.4 Ground horizontal displacements

Horizontal displacements in [mm] in the transverse (U_x) and longitudinal (U_y) directions with respect to the tunnel axis at a certain position with coordinates x, y, z in [m] are given by (O'Reilly and New,1982):

$$U_x = \frac{x}{z_0 - z} \cdot S \tag{4.11}$$

$$U_y = 1000 \cdot \frac{V_L \cdot d^2}{8 \cdot (z_0 - z)} \cdot \tag{4.12}$$

$$\cdot \left[exp\left(\frac{-(y - (y_s + y_0))^2 - x^2}{2 \cdot K_y^2 \cdot (z_0 - z)^2} \right) - exp\left(\frac{-\left(y - \left(y_f\right)\right)^2 - x^2}{2 \cdot K_y^2 \cdot (z_0 - z)^2} \right) \right]$$

Where S is given by Eq. (4.5).

4.2.5 Ground horizontal strains

4.2.5.1 *Equations for the 3D field*

The fields of strains (per unit) in the transverse ($\varepsilon_{h,xx}$) and longitudinal ($\varepsilon_{h,yy}$) directions respect to the tunnel axis are directly given by derivation of the field of ground displacements:

$$\varepsilon_{h,xx} = \frac{\partial U_x}{\partial x} = \frac{\frac{S}{1000}}{z_0 - z} \cdot \left(1 - \left(\frac{x^2}{K_x^2 \cdot (z_0 - z)^2}\right)\right) \tag{4.13}$$

$$\varepsilon_{h,yy} = \frac{\partial U_y}{\partial y} = \tag{4.14}$$

$$\frac{V_L \cdot d^2}{8 \cdot (z_0 - z)} \cdot \left[\left(\frac{-2y + 2(y_s + y_0)}{2 \cdot K_y^2 \cdot (z_0 - z)^2}\right) \cdot exp\left(\frac{-\left(y - (y_s + y_0)\right)^2 - x^2}{2 \cdot K_y^2 \cdot (z_0 - z)^2}\right) - \left(\frac{-2y + 2(y_f)}{2 \cdot K_y^2 \cdot (z_0 - z)^2}\right) \cdot exp\left(\frac{-\left(y - (y_f)\right)^2 - x^2}{2 \cdot K_y^2 \cdot (z_0 - z)^2}\right)\right]$$

The resultant of ε_h along an alignment θ in the range $(-90°, 0°) \cup (0°, 90°)$ is not directly given with Eqs. (4.13) and (4.14). For this reason, a basis transformation of the infinitesimal strain tensor is used to find the resultant value $\hat{\varepsilon}_{h,\widehat{xx}}$ in a direction $\hat{x}$ that matches with the building wall alignment θ for which ε_h is being determined.

Let $\boldsymbol{\varepsilon}$ be the infinitesimal strain tensor described with the orthonormal basis $\{\boldsymbol{e_1}, \boldsymbol{e_2}, \boldsymbol{e_3}\}$, where $\boldsymbol{e}_1 = (1,0,0)$, $\boldsymbol{e}_2 = (0,1,0)$, $\boldsymbol{e}_3 = (0,0,1)$ represent the directions x, y, z of the reference Cartesian coordinate system (note that $S \equiv U_z$):

$$\boldsymbol{\varepsilon} = \begin{bmatrix} \varepsilon_{h,xx} & \varepsilon_{h,xy} & \varepsilon_{h,xz} \\ \varepsilon_{h,yx} & \varepsilon_{h,yy} & \varepsilon_{h,yz} \\ \varepsilon_{h,zx} & \varepsilon_{h,zy} & \varepsilon_{h,zz} \end{bmatrix} =$$

$$= \begin{bmatrix} \frac{\partial U_x}{\partial x} & \frac{1}{2}\left(\frac{\partial U_x}{\partial y} + \frac{\partial U_y}{\partial x}\right) & \frac{1}{2}\left(\frac{\partial U_x}{\partial z} + \frac{\partial S}{\partial x}\right) \\ \frac{1}{2}\left(\frac{\partial U_y}{\partial x} + \frac{\partial U_x}{\partial y}\right) & \frac{\partial U_y}{\partial y} & \frac{1}{2}\left(\frac{\partial U_y}{\partial z} + \frac{\partial S}{\partial y}\right) \\ \frac{1}{2}\left(\frac{\partial S}{\partial x} + \frac{\partial U_x}{\partial z}\right) & \frac{1}{2}\left(\frac{\partial S}{\partial y} + \frac{\partial U_y}{\partial z}\right) & \frac{\partial S}{\partial z} \end{bmatrix} \tag{4.15}$$

According to the tensor transformation theory, the infinitesimal strain tensor described in a new orthonormal basis $\hat{\boldsymbol{e}}_1, \hat{\boldsymbol{e}}_2, \hat{\boldsymbol{e}}_3$ is given by:

$$\hat{\boldsymbol{\varepsilon}} = \boldsymbol{L}\boldsymbol{\varepsilon}\boldsymbol{L}^T \tag{4.16}$$

And,

$$\hat{\boldsymbol{\varepsilon}} = \begin{bmatrix} \hat{\varepsilon}_{h,\hat{x}\hat{x}} & \hat{\varepsilon}_{h,\hat{x}\hat{y}} & \hat{\varepsilon}_{h,\hat{x}\hat{z}} \\ \hat{\varepsilon}_{h,\hat{y}\hat{x}} & \hat{\varepsilon}_{h,\hat{y}\hat{y}} & \hat{\varepsilon}_{h,\hat{y}\hat{z}} \\ \hat{\varepsilon}_{h,\hat{z}\hat{x}} & \hat{\varepsilon}_{h,\hat{z}\hat{y}} & \hat{\varepsilon}_{h,\hat{z}\hat{z}} \end{bmatrix} \tag{4.17}$$

Where the components of matrix $\boldsymbol{L}$ are defined as:

$$l_{ij} = \hat{e}_i \cdot e_j \tag{4.18}$$

If the vector $\hat{\boldsymbol{e}}_1$ matches the longitudinal direction $\hat{x}$ of a wall with alignment θ, the new orthonormal basis is then given by $\hat{\boldsymbol{e}}_1 = (\cos\theta\,, \sin\theta\,, 0)$, $\hat{\boldsymbol{e}}_2 = (-\sin\theta\,, \cos\theta\,, 0)$, $\hat{\boldsymbol{e}}_3 = \boldsymbol{e}_3 = (0,0,1)$. Then, the components of the tensor transformation matrix $\boldsymbol{L}$ result in: $l_{11} = \cos\theta,\ l_{12} = \sin\theta,\ l_{13} = 0,\ l_{21} = -\sin\theta,\ l_{22} = \cos\theta,\ l_{23} = 0,\ l_{31} = 0,\ l_{32} = 0$ and $l_{33} = 1$. Note that the change of basis represents a rotation of θ degrees counterclockwise about $\boldsymbol{e}_3$.

By multiplying matrices, the resultant horizontal strain along a particular wall alignment θ is given by:

$$\varepsilon_h \equiv \hat{\varepsilon}_{h,\hat{x}\hat{x}} = \cos^2\theta \cdot \varepsilon_{h,xx} + \sin^2\theta \cdot \varepsilon_{h,yy} + 2 \cdot \cos\theta \sin\theta \cdot \varepsilon_{h,xy} \tag{4.19}$$

Note that if the wall is perpendicular to the tunnel axis (i.e. $\theta = 0°$), Eq. (4.19) reduces to $\varepsilon_h = \varepsilon_{h,xx}$, whereas if the wall is aligned with the tunnel longitudinal axis (i.e. $\theta = \pm 90°$), Eq. (4.19) reduces to $\varepsilon_h = \varepsilon_{h,yy}$. By definition of the infinitesimal strain tensor, $\varepsilon_{h,xy}$ is given by:

$$\varepsilon_{h,xy} = \varepsilon_{h,yx} = \frac{1}{2}\left(\frac{\partial U_x}{\partial y} + \frac{\partial U_y}{\partial x}\right) \tag{4.20}$$

Terms $\frac{\partial U_x}{\partial y}$ and $\frac{\partial U_y}{\partial x}$ in Eq.(4.20) are given by derivation of Eqs. (4.11) and (4.12) (check Annex A for further details on the development of Eq. (4.21)):

$$\frac{\partial U_x}{\partial y} = \frac{x}{z_0 - z} \cdot (-S_{max}) \cdot \left(exp\left(-\frac{x^2}{2 \cdot K_x^2 \cdot (z_0 - z)^2} \right) \right) \cdot \tag{4.21}$$

$$\cdot \left(\frac{1}{\sqrt{2\pi}} e^{-\frac{\left(\frac{y-(y_s+y_0)}{K_y \cdot (z_0-z)}\right)^2}{2}} \cdot \left(\frac{1}{K_y \cdot (z_0 - z)} \right) - \frac{1}{\sqrt{2\pi}} e^{-\frac{\left(\frac{y-y_f}{K_y \cdot (z_0-z)}\right)^2}{2}} \cdot \left(\frac{1}{K_y \cdot (z_0 - z)} \right) \right)$$

And,

$$\frac{\partial U_y}{\partial x} = \frac{V_L \cdot d^2}{8 \cdot (z_0 - z)} \cdot \tag{4.22}$$

$$\cdot \frac{(-2x)}{2 \cdot K_y^2 \cdot (z_0 - z)^2} \left[exp\left(\frac{-\left(y - (y_s + y_0)\right)^2 - x^2}{2 \cdot K_y^2 \cdot (z_0 - z)^2} \right) - exp\left(\frac{-\left(y - \left(y_f\right)\right)^2 - x^2}{2 \cdot K_y^2 \cdot (z_0 - z)^2} \right) \right]$$

4.2.5.2 *Equations for building walls parallel to tunnel axis*

If the determination of settlements, ground horizontal displacements and strains is performed for the case of walls parallel to tunnel axis ($S_{par}, U_{y,par}$ and $\varepsilon_{h,par}$, respectively) the latter expressions are reduced to a 2D problem:

$$S_{par} = -1000 \cdot S_{max} \cdot exp\left[-\frac{{d_{axis}}^2}{2 \cdot K_x^2 \cdot (z_0 - z)^2} \right] \cdot \tag{4.23}$$

$$\cdot \left[\Phi\left(\frac{y - (y_s + y_0)}{K_y \cdot (z_0 - z)} \right) - \Phi\left(\frac{y - y_f}{K_y \cdot (z_0 - z)} \right) \right]$$

$$U_{y,par} = 1000 \cdot \frac{V_L \cdot d^2}{8 \cdot (z_0 - z)} \cdot \tag{4.24}$$

$$\cdot \left[exp\left(\frac{-\left(y - (y_s + y_0)\right)^2 - {d_{axis}}^2}{2 \cdot K_y^2 \cdot (z_0 - z)^2} \right) - exp\left(\frac{-\left(y - \left(y_f\right)\right)^2 - {d_{axis}}^2}{2 \cdot K_y^2 \cdot (z_0 - z)^2} \right) \right]$$

$$\varepsilon_{h,par} \equiv \hat{\varepsilon}_{h,\widehat{xx},par} = \frac{\partial U_{y,par}}{\partial y} = \tag{4.25}$$

$$= \frac{V_L \cdot d^2}{8 \cdot (z_0 - z)} \cdot \left[\left(\frac{-2y + 2(y_s + y_0)}{2 \cdot K_y^2 \cdot (z_0 - z)^2} \right) \cdot exp\left(\frac{-\left(y - (y_s + y_0)\right)^2 - {d_{axis}}^2}{2 \cdot K_y^2 \cdot (z_0 - z)^2} \right) \right.$$

$$\left. - \left(\frac{-2y + 2(y_f)}{2 \cdot K_y^2 \cdot (z_0 - z)^2} \right) \cdot exp\left(\frac{-\left(y - (y_f)\right)^2 - {d_{axis}}^2}{2 \cdot K_y^2 \cdot (z_0 - z)^2} \right) \right]$$

where d_{axis} is the horizontal distance between tunnel and wall longitudinal axes shown in section 4.2.2.2. Note that $\hat{\varepsilon}_{h,\widehat{xx},par}$ corresponds to $\varepsilon_{h,yy}$ of Section 4.2.5.1.

4.2.5.3 *Definition of sagging and hogging deflection zones*

The nature of ground horizontal strains ε_h (compressive or tensile) has implications on the damage assessment. This nature is defined by the curvature or concavity of the settlement profile: zones with upwards concavity are known as sagging deflection zones, whereas downwards concavity refers to hogging deflection. The inflection points of the Gaussian settlement profiles delimit these zones. Sagging zones imply the generation of compressive strains ($\varepsilon_h < 0$) and hence, a favorable contribution to damage reduction. Hogging zones imply the generation of tensile strains ($\varepsilon_h > 0$), which will increase damages on the wall (Burland, 2008). In the remainder of the paper, compressive ground strains will be written as ε_{h-} and tensile, ε_{h+}.

4.3 VARIATION OF GROUND HORIZONTAL STRAIN $\boldsymbol{\varepsilon_h}$ WITH THE ALIGNMENT $\boldsymbol{\theta}$

4.3.1 Introduction

Next sections go deeper into the variation of the ground horizontal strain ε_h with the alignment θ, which may play a key role in the building damage assessment. The novel formulation shown in Sec. 4.2.5.1 is used for this purpose. For the ease of illustration, a particular example of the evolution of ε_h with θ during the tunnel face approach is shown in Sec. 4.3.2. ε_h is further calculated for a wide range of ground conditions and tunnel geometries in a parametric analysis. The goal is to determine critical values of θ, regarding the value of ε_h (Sec. 4.3.3). Optimization techniques are used for this objective.

In the following we limit ourselves to the case of $K_x = K_y = K$, as it is often assumed in tunneling design (Attewell *et al.*, 1986). The tunnel portal is considered at infinite distance from the face, i.e. $y_f = +\infty$.

4.3.2 Representation of the field of ground horizontal strain $\boldsymbol{\varepsilon_h}$

Equations (4.13), (4.14) and (4.20)-(4.22) are referred to the Cartesian coordinate system with components x, y and z. However, cylindrical coordinates will be used here instead for making easier the visualization of the next plots. The following transformation is applied:

$$\begin{cases} x = r \cdot cos\,\theta \\ y = r \cdot sin\,\theta \\ z = z \end{cases} \tag{4.26}$$

where r is the horizontal distance between the z-axis and whichever ground point $\hat{P}$ located along the rotated $\hat{x}$-axis. The position of $\hat{P}$ can be described then by the coordinates $(r_{\hat{P}}, \theta_{\hat{P}}, z_{\hat{P}})$. However, the following analysis is only performed at ground surface, i.e. $z = 0$ and hence, coordinates of $\hat{P}$ can be given only by $(r_{\hat{P}}, \theta_{\hat{P}})$ (see Figure 4.7).

An example of settlement profile S and the correspondent ground horizontal strains $\varepsilon_{h,xx}$, $\varepsilon_{h,yy}$, $\varepsilon_{h,xy}$ in the new cylindrical coordinates is shown in Figure 4.8. The resultant strain $\varepsilon_h \equiv \hat{\varepsilon}_{\hat{x}\hat{x}}$ along the considered alignment ($\theta = 60°$) is given by Eq. (4.19). The tunnel face location for this particular case is $y_s = 0$m, the tunnel diameter is d=12m, the tunnel depth is z_0=20m, the trough width parameter is K=0.3, the ground volume loss is V_L=1% and the ratio between the settlement at the face and at the tail is δ=0.3.

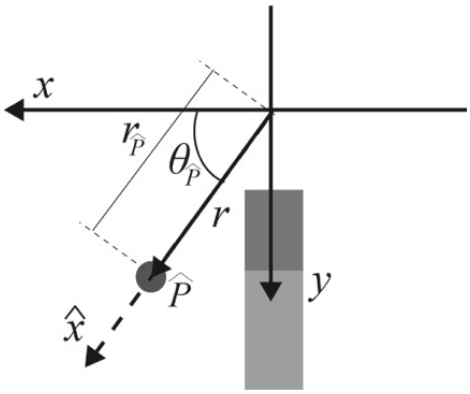

Figure 4.7. Parameters of the change from Cartesian to cylindrical coordinates.

It can be seen that sagging zone extends from $r = 0$m to $r \approx 17$m and that ε_h is there compressive (negative). Hogging deflection and hence, tensile (positive) values of ε_h, start at $r \approx 17$m. The curves of $\varepsilon_{h,xx}$ and ε_h correspond to the profile of ground strain for $\theta = 0°$ and $\theta = 60°$, respectively. Note the substantial difference between the positive peak values of both curves at $r \approx 22$m. This reduction respect to the transverse case may imply notable variations in the estimation of building damage, as it will be shown later in Sec. 4.4.

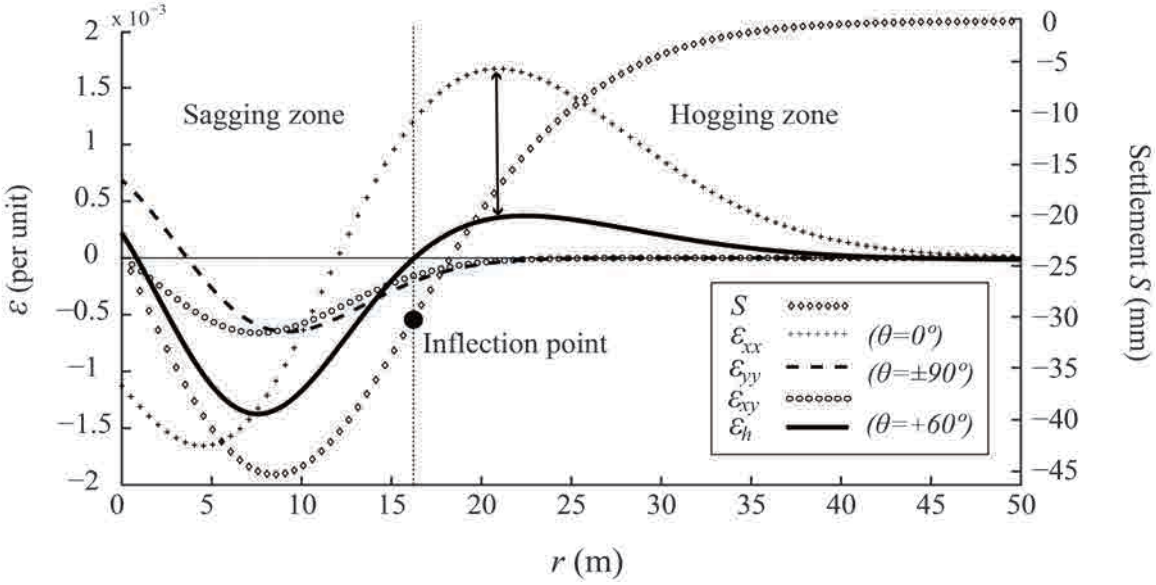

Figure 4.8. Plot of settlement profile S and ground strains $\varepsilon_{h,xx}$, $\varepsilon_{h,yy}$, $\varepsilon_{h,xy}$ and resultant ε_h at θ=60° for y_s=0m (V_L=1%, K=0.3, δ=0.3, z_0=20m, d=12m).

The variation of ε_h with the alignment θ and the position r for different tunnel face locations is depicted in Figure 4.9. Note that this Figure represents the extension of Figure 4.8 for all possible values of θ. It can be seen that the maximum absolute values of ε_{h+} and ε_{h-} are given along $\theta = 90°$ for $r \approx$17m and $r \approx$30m, respectively, when tunnel face is at y_s=+20m (Figure 4.9a). For $90° > \theta > 45°$, ε_{h+} and ε_{h-} tend to decrease, and for $\theta < 45°$, both ε_{h+} and ε_{h-} become negligible. Therefore, the effect of the excavation when y_s=+20m can only be noticed at alignments close to the longitudinal tunnel axis.

If the tunnel face advances till y_s=0m, the maximum absolute value of compressive strain ε_{h-} is then given at $r \approx$7m for $\theta \approx 50°$ (Figure 4.9b). The maximum value of ε_{h+} is given at $\theta \approx$ -90°. The intersection of a vertical plane at θ =60° with the plot of ε_h would result in the curve shown in Figure 4.8. Note also that the less critical θ in terms of ε_{h+} (i.e the range of θ for which ε_{h+} is minimum) is around $\theta \approx$ 60°-70°.

When tunnel face is located at y_s=-20m, both maximum absolute values of ε_{h+} and ε_{h-} occur at $\theta = 0°$ for $r = 0$m and $r \approx 12$m, respectively (Figure 4.9c). It can be seen that ε_h is 0 for all r if $\theta = +90°$. The reason is that the settlement along this alignment is fully developed and hence, the settlement profile curvature is 0.

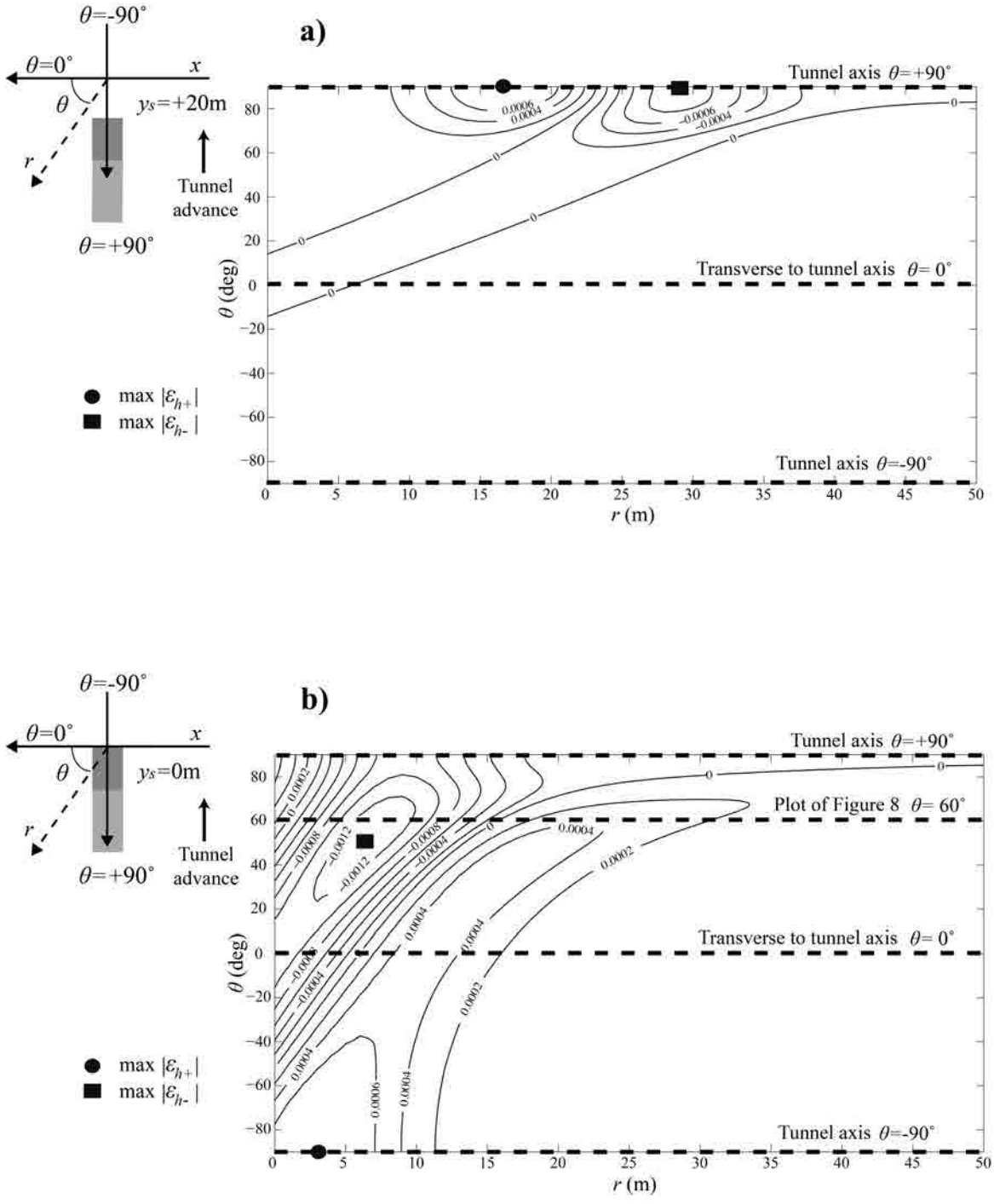

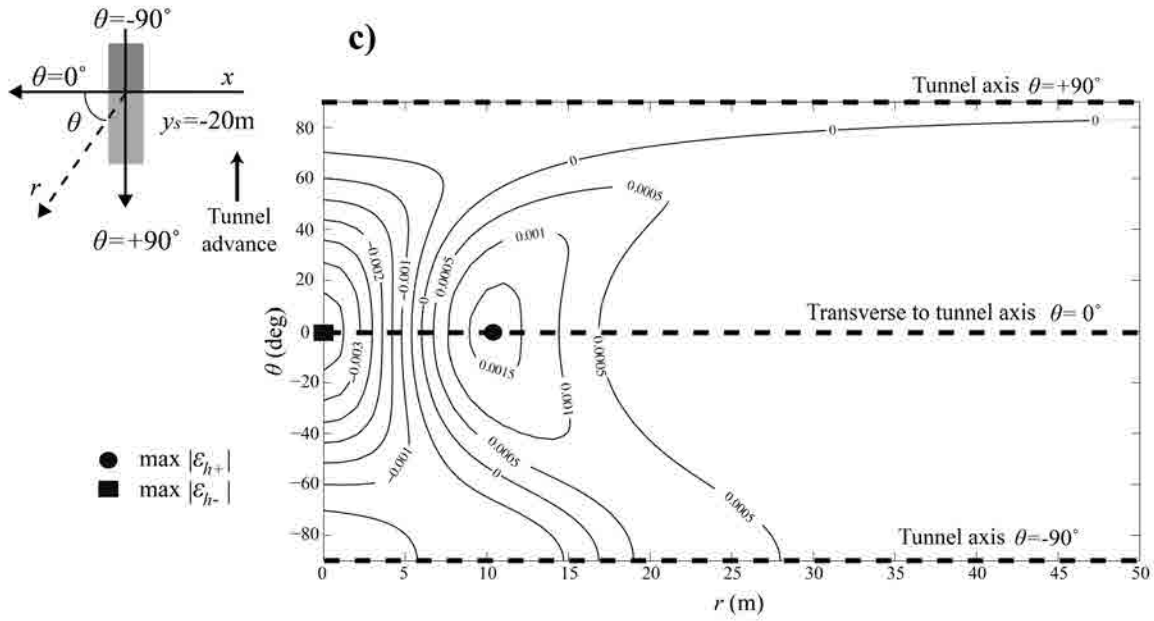

Figure 4.9. Plot of ε_h for all θ and r if tunnel location is at a) y_s=+20m, b) y_s=0m and c) y_s=-20m (V_L=1%, K=0.3, δ=0.3, z_0=20m, d=12m).

4.3.3 Determination of critical values of θ

The generation of the plots shown in Sec. 4.3.2 allows identifying possible critical values of θ concerning the maximum absolute values of ε_{h+} and ε_{h-}. For this purpose, the field of ε_h is generated in a parametric analysis for a wide range of ground conditions and tunnel geometries. For every case, the position (r, θ) of the maximum absolute values of ε_{h+} and ε_{h-} is determined by means of optimization techniques. The analysis includes values of K from 0.2 to 0.7 every 0.05; ground volume losses V_L equal to 0.5%, 1%, 1.5% and 2%, which are typical values considered in tunneling engineering; δ ratios equal to 0.5 (as generally assumed) and δ=0.3 for the case of soft soils; tunnel diameters d equal to 8, 10 and 12m and tunnel axis depths z_0 equal to 20, 30 and 40m. The location of the tunnel face y_s spans from +20m to -20m every 10m to simulate the different phases of approach and underpass of the tunnel face beneath a building wall.

The results show that for tunnel face locations $y_s > 0$ (i.e. tunnel face approaching to the origin of coordinates), the alignment for which ε_{h+} is maximum is $\theta = 90°$, whereas for $y_s < 0$ (i.e tunnel face has underpassed the origin of coordinates), it is $\theta = 0°$. The ratio between the maximum ε_{h+} at $\theta = 0°$ and the maximum ε_{h+} at $\theta = 90°$ is usually

between 1.5 and 2. Then, it is clear that the most critical alignment according to the value of ε_{h+} is the transverse direction with respect to the tunnel axis.

Regarding the compressive strains ε_{h-}, the maximum absolute values are given at $\theta = 0°$ when the tunnel face location is $y_s < 0$. However, the trend is not so clear when the tunnel face location is $y_s > 0$. Highest absolute values of ε_{h-} are found in a range of alignments between $\theta = 50°$ and $\theta = 90°$, depending on the geological conditions and the tunnel geometry. The ratio between the maximum absolute value of ε_{h-} at $\theta = 0°$ and at $\theta \approx 50°$-$90°$ is between 3 and 4. Therefore, the maximum contribution of compressive ground strain ε_{h-} to damage reduction is also at $\theta = 0°$.

4.3.4 Discussion

The presented results show the influence of the alignment θ on the tensile ε_{h+} and compressive ε_{h-} ground horizontal strains. According to the parametric analysis, the maximum absolute values of both ε_{h+} and ε_{h-} are generated for advanced tunnel face locations (i.e. $y_s < 0$) at $\theta = 0°$. Therefore, $\theta = 0°$ is defined as the worst-case scenario regarding ε_{h+}. However, $\theta = 0°$ can give also the maximal contribution of compressive strains ε_{h-} to building damage reduction, but this contribution is generally neglected when using the equivalent beam model, as a conservative practice (see Sec. 4.4). Hence, $\theta = 0°$ is considered to be the most critical alignment regarding ε_h, independently of the contribution of ε_{h-}. Less critical (lower) values of ε_{h+} may be generated at alignments in between $\theta = 0°$ and 90°. This fact can entail a reduction of the estimated damage when analyses are performed along the real wall alignments θ, instead of doing approximations with the transverse case $\theta = 0°$, as it is usually done in tunneling design.

4.4 RELEVANT ASPECTS OF BUILDING RESPONSE MODELING IN 3D

4.4.1 Introduction

Sections 4.2 and 4.3 showed how to deal with the determination of ground horizontal strain ε_h in a particular wall alignment θ. As seen, this represents a 3D problem governed by the ground properties, the construction technology, the tunnel geometry and the tunnel face position. Once the 2D settlement profile and the correspondent ε_h are determined, the building response is modeled with the equivalent beam method from Burland and Wroth (1974) in order to assess the damages that ground subsidence can produce to the

walls. This method is widely used in engineering practice, but however, designers are often not aware of certain aspects that may be critical on the damage predictions.

The present section reviews the application of the equivalent beam method with an advancing tunnel in 3D according to the relative position of the building with respect to the tunnel (Sec. 4.4.2). The delimitation of the influence area of settlements and its effect on the predictions of building damage is analyzed in Sec. 4.4.3. The contribution of the ground horizontal strain in sagging zones to damage reduction is analyzed in Sec. 4.4.4. The influence of the tunnel face location y_s and the building wall alignment θ is studied in Sec. 4.4.5.

4.4.2 Application of the equivalent beam method in 3D

Maximum tensile strains in the beam for pure bending (ε_{br}) and pure shear (ε_{dr}) modes of deformation (Eqs. (4.1)-(4.2)) require the calculation of maximum strains due to the deflection of the beam in pure bending, ε_{bmax}, and pure shear, ε_{dmax}, which are given by the expressions of Burland and Wroth (1974):

$$\varepsilon_{bmax} = \frac{\frac{\Delta}{l}}{\left(\frac{l}{12t} + \frac{3I}{2alH}\frac{E}{G}\right)} \tag{4.27}$$

$$\varepsilon_{dmax} = \frac{\frac{\Delta}{l}}{\left(1 + \frac{Hl^2}{18I}\frac{G}{E}\right)} \tag{4.28}$$

where H is the beam height, I is the inertia per unit length which is equal to $H^3/12$, t is the position of the neutral axis and a is the location of the fiber where strains are calculated. In case of sagging deflection, the neutral axis is assumed to be at middle height ($t = H/2$). In case of hogging deflection, the neutral axis is assumed to be at the top fiber ($t = H$) (Figure 4.10). Strains are calculated in the most critical fiber from the position of the neutral axis, so that $a = t$ in both cases. Δ/l are the maximum deflection ratios for the respective deflection zone: l is the horizontal distance between two reference points and Δ is the relative deflection between these two points. This relative deflection is given by the difference between the settlement profile and the straight lines connecting the settlements at the building extremes and at the inflection points.

The calculation of Eqs. (4.1)-(4.2) and (4.27)-(4.28) is performed separately for the zones of the building undergoing sagging deflection and for those undergoing hogging

deflection (Mair *et al*., 1996). The 3D field of settlements is described by Gaussian curves and therefore, the number of inflection points located along the position of a building can be 0, 1 or 2, depending on its length l_{build}, on the distance from building reference point $\hat{A}$ to the origin of coordinates d_{orig} and on the alignment θ with respect to the tunnel axis. This entails the following cases:

The building is subjected only to sagging (short buildings located above the tunnel axis; no inflection points are located along the building).

The building is subjected only to hogging (buildings located far from the tunnel longitudinal axis; no inflection points are located along the building).

The building is subjected to sagging and hogging (building starts in the zone above the tunnel (sagging) and reaches the hogging deflection zone; 1 inflection point is located along the building).

The central part of the building is subjected to sagging and its laterals to hogging (2 inflection points are located along the building).

Therefore, the total length of the building wall l_{build} can be decomposed in three parts: l_{hog_1}, l_{hog_2} and l_{sag} (Figure 4.10), so that three different deflection ratios can be defined: Δ_{hog_1}/l_{hog_1}, Δ_{hog_2}/l_{hog_2} and Δ_{sag}/l_{sag}. Determination of ε_h in Eqs. (4.1)-(4.2) is also performed separately along the length of building zones undergoing sagging and hogging deflection.

The damage on the building wall is then determined depending on the maximum strain ε_{max}:

$$\varepsilon_{max} = \max\left[\varepsilon_{br}^{sag}, \varepsilon_{dr}^{sag}, \varepsilon_{br}^{hog,1}, \varepsilon_{dr}^{hog,1}, \varepsilon_{br}^{hog,2}, \varepsilon_{dr}^{hog,2}\right] \quad (4.29)$$

where ε_{br}^{sag}, $\varepsilon_{br}^{hog,1}$ and $\varepsilon_{br}^{hog,2}$ are the maximum bending strains in sagging and hogging in the three zones, obtained using Eq. (4.1) and ε_{dr}^{sag}, $\varepsilon_{dr}^{hog,1}$ and $\varepsilon_{dr}^{hog,2}$ are the maximum shear strains in sagging and hogging, obtained using Eq. (4.2).

ε_{max} is further compared with strain thresholds ε_{lim} that define different categories of damage according to the severity of affection and the typical associated damage, as it can be seen in Table 4.1.

Table 4.1. Classification of damage (Burland et al., 1977)

Category of damage	Normal degree of severity	Typical damage	Tensile strain ε_{max} (%)	ε_{lim}(%)
0	Negligible	Hair cracks less than 0.1mm	0 – 0.050	0.050
1	Very slight	Fine cracks up to 1mm	0.050 – 0.075	0.075
2	Slight	Cracks easily filled up to 5mm	0.075 – 0.150	0.150
3	Moderate	Cracks from 5 to 15mm	0.150 – 0.300	0.300
4	Severe	Extensive repair works. Cracks from 15 to 25mm	> 0.300	-
5	Very severe	Partial or complete rebuilding. Cracks > 25mm	-	-

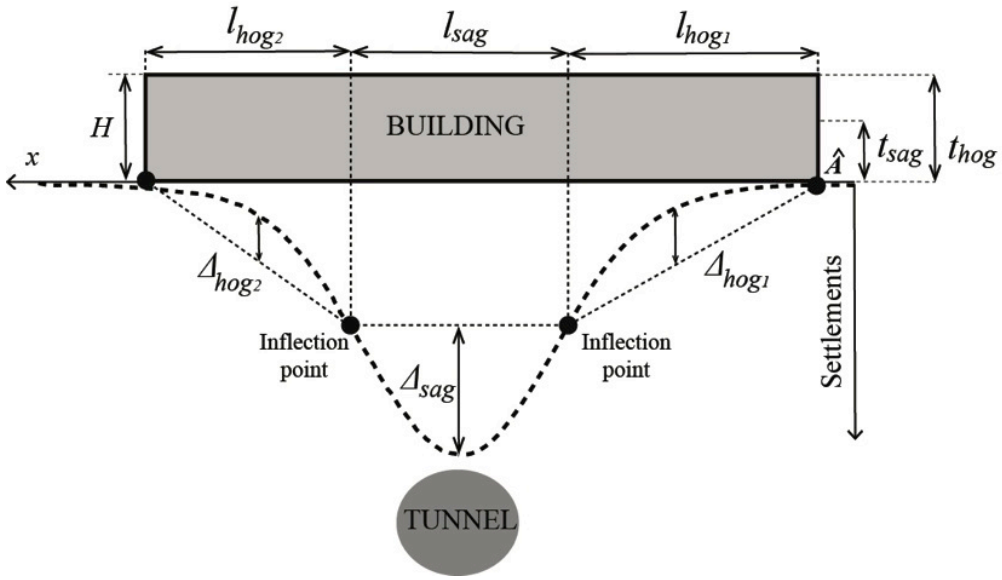

Figure 4.10. Equivalent beam model – Description of building geometry and deflection ratios.

4.4.3 Effect of the influence area of settlements on building damage predictions

4.4.3.1 *Settlement cut-off*

The influence area of a tunnel construction is defined as the zone where ground subsidence can be generated. Therefore, the infrastructures and buildings inside this area may require a damage assessment prior to the tunnel construction. This area is defined in some tunnel projects as a band of 50m of width at every side of the tunnel axis, but however, other criteria can be used. For example, construction projects in the L9 metro tunnel in Barcelona contained damage assessments only for buildings likely to be affected

by settlements higher than 10mm. This limit was reduced to 5mm if the building was of cultural or historical interest.

In Gaussian-shaped settlements troughs, the highest settlements are generated above the tunnel axis and their magnitude decrease exponentially with the distance to tunnel axis. For this reason, buildings can be subjected to high settlements at one side and to negligible at the other. As mentioned in Sec. 4.4.2, the equivalent beam method needs the calculation of deflections, which depend on the value of settlements at the locations of inflection points and building extremes. Considering the whole length of a building could lead to unreliable estimations of damage due to an overestimation of the deflections Δ, usually in the zones of hogging.

To address this, Mair *et al*. (1996) proposed to consider the 1mm settlement line to be the limit of the zone of influence. This value was selected in base of the accuracy of monitoring instruments placed along the tunnel track to control ground movements, which is generally around $\pm$1mm. In cases where the building wall overpasses the 1mm area, only the part of the wall subjected to settlements $|S| \geq$1mm is considered. This hypothesis has implications in the calculation of the maximum tensile strain value ε_{max} due to the possible variation of the considered lengths l_{hog_1}, l_{hog_2}, l_{sag}, deflection ratios Δ_{sag}/l_{sag}, Δ_{hog_1}/l_{hog_1}, Δ_{hog_2}/l_{hog_2} (Figure 4.11) and wall geometry ratios l_{sag}/H, l_{hog_1}/H and l_{hog_2}/H. Moreover, this change of l/H can produce substantial variations on the determination of the most critical mode of deflection, i.e. bending or shear (Burland, 2008). For example, Netzel (2009) show the effect of the influence area in a long structure subjected to subsidence for which the bending strains generated in the beam due to deflection were a 75% higher for the long structure, i.e. considering all the range of settlement, than for the short one, i.e. considering the 1mm settlement line.

However, neglecting a part of the building has also implications on the value of ground horizontal strain ε_h. Its magnitude decays with the distance to tunnel axis and therefore, neglecting the zones where settlements are lower than 1mm will give higher ε_{h+} mean values. This will increase the predicted bending ε_{br} and shear ε_{dr} strains (Eqs. (4.1)-(4.2)) and hence, the estimated damages in the building will also be higher.

The effect of considering the 1mm settlement line is analyzed now by means of a comprehensive parametric study. For notation convenience, disregarding settlements lower than 1mm will be written as cut-off C_1, whereas including all settlements will be

written as cuttoff C_0. A wide range of geological conditions, tunnel geometries, building position and building geometry is analyzed here (Table 4.2) to show the differences when considering each criterion. Crossing all the variable values gives a total number of 1,404,480 analyzed cases. The most critical value of ε_{max} along all the tunnel face positions y_s is calculated using both criteria C_0 and C_1.

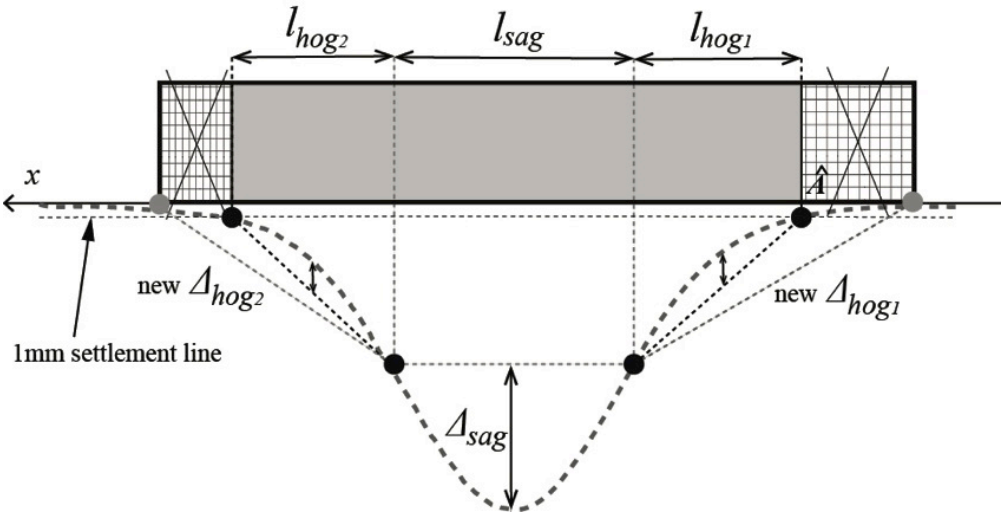

Figure 4.11. Influence area of settlement troughs and disregarded parts of the building.

Table 4.2. Variable values of the parametric analysis showing the influence of the settlement cut-off.

Variable [units]	Description	Analyzed values
K [-]	Trough width parameter	From 0.2 to 0.7, every 0.05
V_L [%]	Ground volume loss	0.05, 1, 1.5, 2
δ [-]	Longitudinal settlement shift ratio	0.3, 0.5
z_0 [m]	Tunnel axis depth	20, 30, 40
d [m]	Tunnel diameter	6, 8, 10, 12
L [m]	Building wall length	10, 20, 30, 40
d_{orig} [m]	Distance from origin of coordinates to wall reference point $\hat{A}$	6, 8, 10, 12
H [m]	Building wall height	3, 6, 9, 12, 15
θ [deg]	Building wall alignment	From 90° to -90°, every 10°
y_s [m]	Tunnel face location	From 60m to -60m, every 5m

The results show a 49% of cases where the estimated ε_{max} is the same using both C_0 or C_1, whereas ε_{max} is lower using C_1 in a 37% of cases and higher in the resting 14%. However, the resulting categories of damage are the same in the 94% of cases, showing

that differences of ε_{max} do not generally give significant variations on the damage category estimation. The other 6% of cases give higher or lower categories depending on the values of l_{build}, d_{origin} and l_{build}/H. Table 4.3 summarizes the differences in the categories and the most relevant parameters of the corresponding buildings. Note that these are the most significant observable parameters of the buildings and do not exclude other possible values to produce the same differences on the damage category estimation.

Cases of more than one category of difference represent only the 0.6% of cases. However, the analysis show extreme cases with substantial different estimation of the damage. Cases of +4 categories of difference using C_1 refer to long one-floor buildings starting at tunnel axis. Note also that C_0 could give higher categories in cases of buildings with low l_{build}/H ratios.

Table 4.3. Differences of the estimated category of damage according to the considered settlement cut-off

Difference of estimated category of damage (C_1- C_0)	**Percentage of total number of cases**	**Relevant characteristics of buildings**
+4	0.001%	l_{build}/H = 13; d_{orig} =10m; l_{build} =40m
+3	0.032%	l_{build}/H = 10,13; d_{orig} =20m; l_{build} =40m
+2	0.423%	l_{build}/H = 6,10,13; d_{orig} =20m; l_{build} =40m
+1	2.668%	l_{build}/H = 4,6,10 and 13; d_{orig} =15m; l_{build} =30 and 40m
0	94.279%	All types
-1	2.578%	l_{build}/H = from 1 to 3; l_{build} =20, 30 and 40m
-2	0.017%	l_{build}/H = from 1 to 3; l_{build} =20 and 30m

The criteria C_1 of Mair *et al*. (1986) avoids the underestimation of the ground horizontal strain ε_h and thus, it would be more appropriate for the majority of cases. In the remainder of the paper, the analyses will be performed following this criterion.

4.4.4 Considering the contribution of ground horizontal strain in sagging zones

The nature of strain in sagging zones is compressive and therefore, it can contribute to damage reduction. For conservativeness, this contribution is usually neglected and thus the value of ε_{h-} is considered to be equal to 0. This section analyzes which is the effect of considering the mean value of ε_{h-} along the sagging zone.

The values of ε_{max} for the cases of the parametric study shown in Sec. 4.4.3 are recalculated with this new assumption and further compared. The results show that considering the mean value of ε_{h-} (instead of neglecting it) give the same value of ε_{max} in the 78.6% of cases, a lower value in a 14.3% and a higher value in the resting 7.1%. This increase of ε_{max} is given in some cases where ε_{dr} is higher than ε_{br}. This is so, because considering the mean value of ε_{h-} will always give lower values of ε_{br} (Eq. (4.1)), but not of ε_{dr} (Eq. (4.2)). Indeed, low values of ε_{dmax} in sagging (named ε_{dmax}^{sag}) and high mean values of ε_{h-} can lead in higher values of ε_{dr} in sagging (named ε_{dr}^{sag}), with respect to the case of neglecting ε_{h-}. This is shown in Figure 4.12, where the difference of ε_{dr}^{sag} considering one or the other criteria is depicted. Negative differences of ε_{dr}^{sag} indicate that ε_{dr}^{sag} is higher in the case of neglecting the contribution of ε_{h-} (i.e. the same behavior as in ε_{br}). Contrarily, positive differences indicate that ε_{dr}^{sag} is higher in the case of considering the contribution of ε_{h-}. This can occur for example in long buildings subjected to very sharp profiles for which the generated ground strain ε_{h-} is high and ε_{dmax}^{sag} is low. Note that the plot in Figure 4.12 does not refer to any particular ground and tunnel parameters, but to a general range of values of ε_{dmax}^{sag} and ε_{h-} introduced in Eq. (4.2).

The variations of ε_{max} considering one or the other criteria keep however the estimated category of damage in the 97.63% of the total cases. Again, the most significant characteristics of buildings that give differences in the estimated categories of damage are described in Table 4.4.

Table 4.4. Difference of estimated category of damage according the value of ε_h in sagging zones.

Difference of estimated category of damage (ε_{h-} = mean) - ($\varepsilon_{h-} = 0$)	**Percentage of total number of cases**	**Relevant characteristics of buildings**
+2	0.004%	l_{build}/H = 0.7, 1; d_{orig} =0m, -10m; l_{build} =10m
+1	0.065%	l_{build}/H = 1; d_{orig} =-10m, 0m, 5m; l_{build} =10m
0	97.631%	All types
-1	1.948%	l_{build}/H = 1 to 3; d_{orig} =-10m, 0m, 5m; l_{build} =20m, 30m
-2	0.352%	l_{build}/H = 1 to 3 ; d_{orig} =-10m, 0m, 5m; l_{build} =20m

Note that neglecting the contribution of the ground strain in sagging will be generally conservative, although in some cases it could lead to an underestimation of the damage.

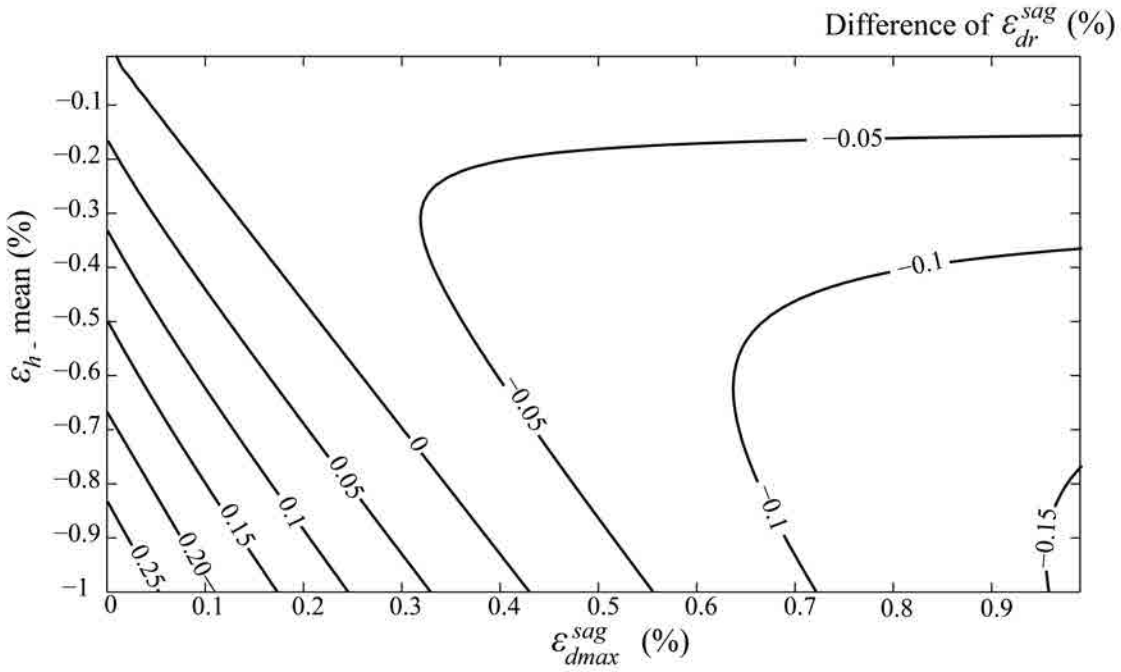

Figure 4.12. Difference of predicted ε_{dr}^{sag} when the contribution of ε_{h-} is considered or neglected.

4.4.5 Influence of the tunnel face location y_s and alignment θ on ε_{max}

The novel equation proposed in this paper (Eq. (4.19)) in combination with the Gaussian approximations of the settlement trough and the equivalent beam model allow the determination of ε_{max} in walls located in whichever position with respect to the tunnel axis. The present section analyzes particularly the influence of the alignment θ and the tunnel face location y_s in the assessment of ε_{max}.

Figure 4.13a) shows an example of the evolution of ε_{max} when the tunnel face advances to $y \to -\infty$ for different wall alignments θ. The ground parameters and the tunnel geometry are the same as in the example shown in Sec. 4.3. The building length is L=30m and the height is H=3m. The building corner is located in the origin of coordinates, so that d_{orig} =0m. The material ratio E/G is 2.6, as it is usually assumed for masonry buildings (Burland, 2008).

It can be seen that at θ=+90°, the value of ε_{max} starts to increase for earlier tunnel face locations (approx. at y_s ≈55m). The maximum value of ε_{max} is reached when y_s is in the

range of [+25m,+50m] and then it decreases again till zero. This behavior is explained by the fact that after the tunnel underpass, the longitudinal settlement is fully developed and hence the curvature is zero, so that both Δ and ε_h become zero. Obviously, the plot of ε_{max} for θ=-90° at Figure 4.13b) is identical with a shift in the y^- direction.

For θ=+60°, +30° and 0°, the maximum value of ε_{max} is given after the tunnel face underpass beneath the building. However, note that ε_{max} and the associated categories of damage will be substantially different for the three alignments: category 2 for θ=+60°, category 3 for θ=+30° and category 4 for θ=0°. For θ=-60° and θ=-30°, ε_{max} tends to the same values as for the corresponding positive alignments. However, the peak values that are achieved during the tunnel face underpass are different, which make pictures non identical. This variation is more significant in the case of θ=-60°: the peak value of ε_{max} is given at earlier y_s than for θ=+60°.

It is also of interest to observe the variation of ε_{max} with θ for fixed tunnel face locations y_s. For this purpose, the plot of ε_{max} for a range of θ between [+90°,-90°] and y_s=+30, +10, 0 and -30m is depicted in dashed lines in Figure 4.14. It can be seen that the most critical alignment is θ =90° when tunnel face is approaching to the building (y_s=+30) and θ =0° for the rest of y_s.

The envelope of the maximum value of ε_{max} for each position of tunnel face y_s is depicted in the same figure with a solid line. As it could be expected, the peak value of ε_{max} is given at θ =0°. This agrees with the alignment for which the tensile ground horizontal strain ε_{h+} was maximal (shown in Sec. 4.3). Moreover, it is evident that the maximum deflections Δ will also be given along θ =0°. The interesting point here is to see the notably reduction of damage that can be given for θ ≠0°. Minimum damages are achieved for wall alignments close to θ ≈+65°, which matches with the direction of minimum ε_{h+} that was shown in Sec. 4.3.2. The reduction of ε_{max} in this case is about the 70%, which implies a difference of 2 categories of damage with respect to the transverse case.

Note that all the presented results refer to a particular example that was chosen for illustrations purposes. The value of θ plays here a key role in the assessment of damage but however, the influence of θ may not be so critical for other combination of ground parameters, building locations and tunnel and building geometries. It is also important to note that the present novel formulation does not conflict with the typical analyses that

assume the building located transverse to the tunnel axis. As it has been shown, this represents the worst-case scenario but however, significant reductions of estimated damage may be achieved if the real wall alignment θ is considered, thus avoiding possible overestimation of predicted damages.

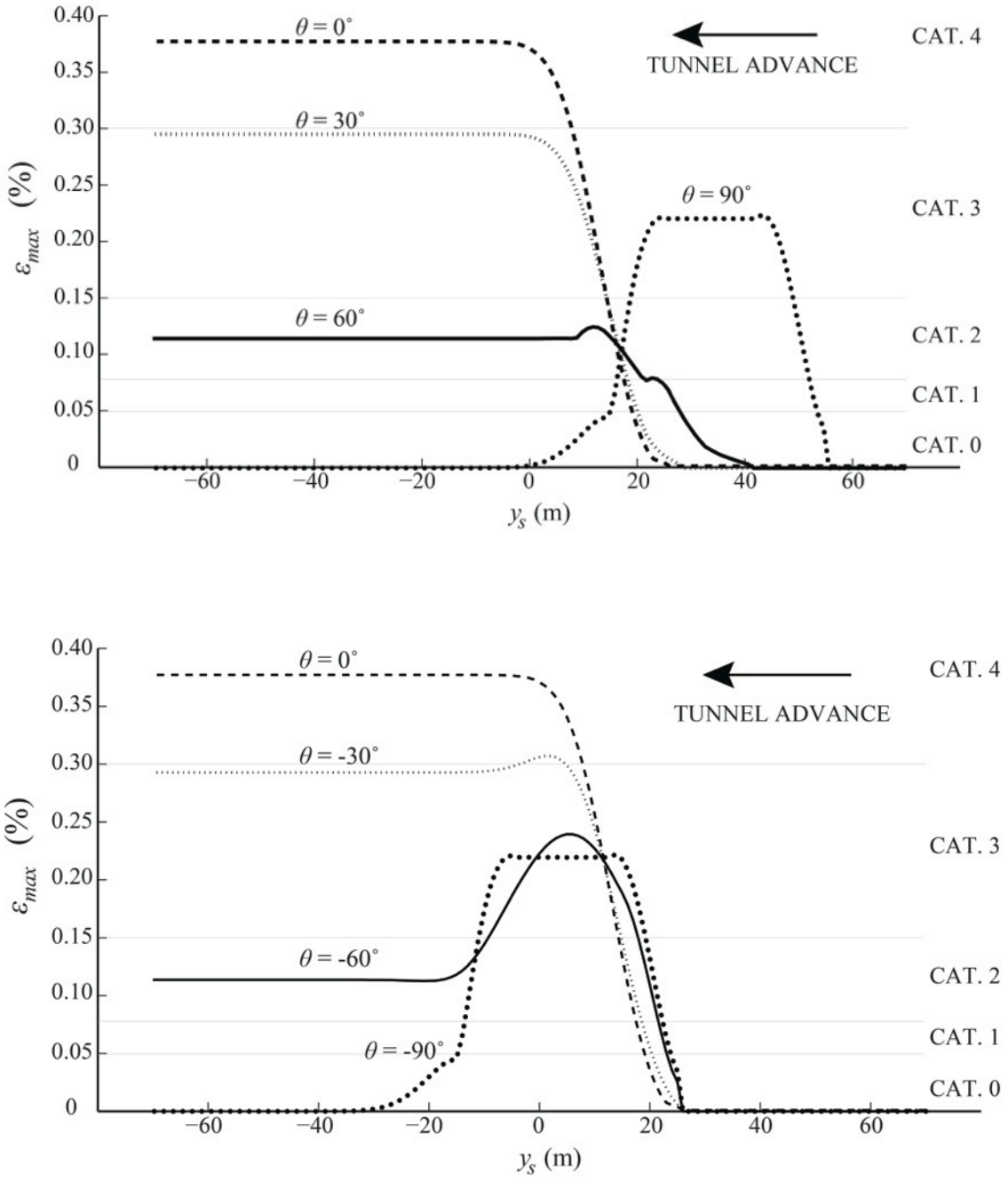

Figure 4.13. Evolution of ε_{max} for an advancing tunnel face from y_s =70m to $y_s = -70$m for a) θ =+90°, +60°, +30°, 0° and b) θ =-90°, -60°, -30°, 0° (L =30m, d_{orig} =0m, H =3m, E/G =2.6, z_0 =20m, d =12m, K =0.3, V_L =1%, δ =0.3).

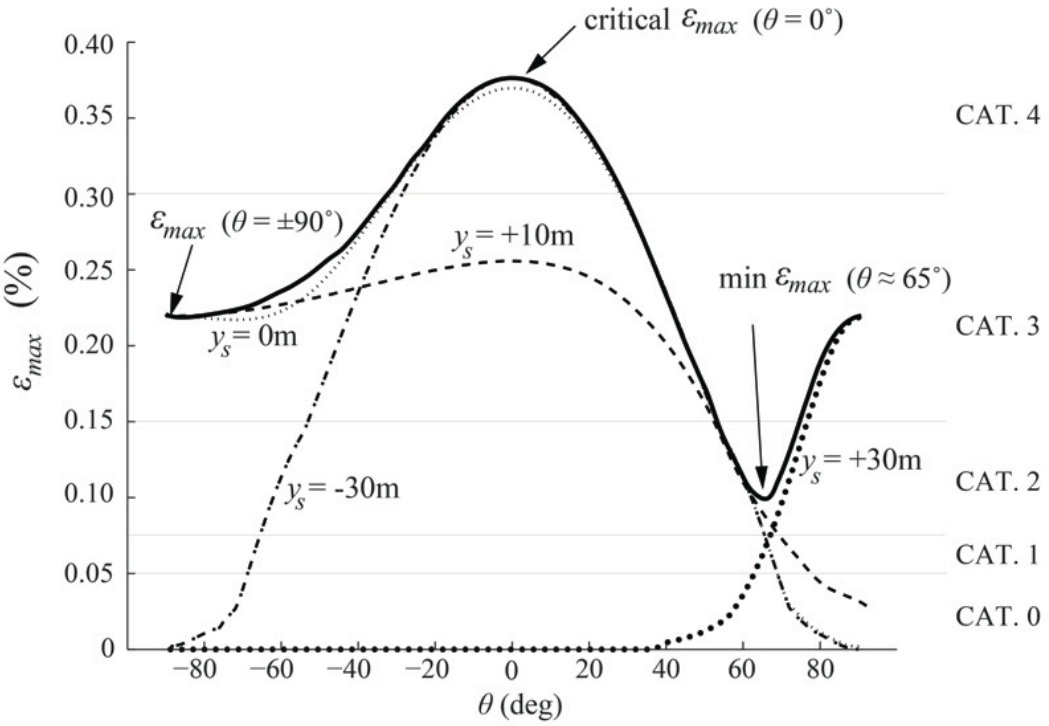

Figure 4.14. Envelope of ε_{max} for an advancing tunnel face from θ =90° to -90° for y_s =+30m, +10m, 0m and -30m (L =30m, d_{orig} =0m, H =3m, E/G =2.6, z_0 =20m, d =12m, K =0.3, V_L =1%, δ =0.3).

The consideration of the wall alignment θ has practical implications in tunneling design, for example in the choice of the tunnel depth. For this particular example, if the damage assessment is done for θ =0°, the minimum tunnel depth z_0 for which ε_{max} does not cross the threshold of category 0 of damage (ε_{lim} =0.050%) is 50m (see Figure 4.15). On the contrary, if the wall alignment is for example θ =60°, the minimum depth that fulfills damage requirements is 30m (consider that neither the diameter d nor the expected volume loss V_L can be decreased). The difference of 20m of depth may have important economical implications, since construction costs of tunnels increase with the depth. Obviously, other less drastic measures could be implemented to avoid this large increase of depth, such as the construction of retaining walls or the stabilization of ground with grout injection. Nevertheless, their effect cannot be taken into account with the presented methodology.

All the proposed models in Sections 4.2, 4.3 and 4.4 can be used in combination with reliability techniques to take into account the uncertainty regarding the settlement trough models and the building response, as shown in Camós, Špačková *et al*. (2014).

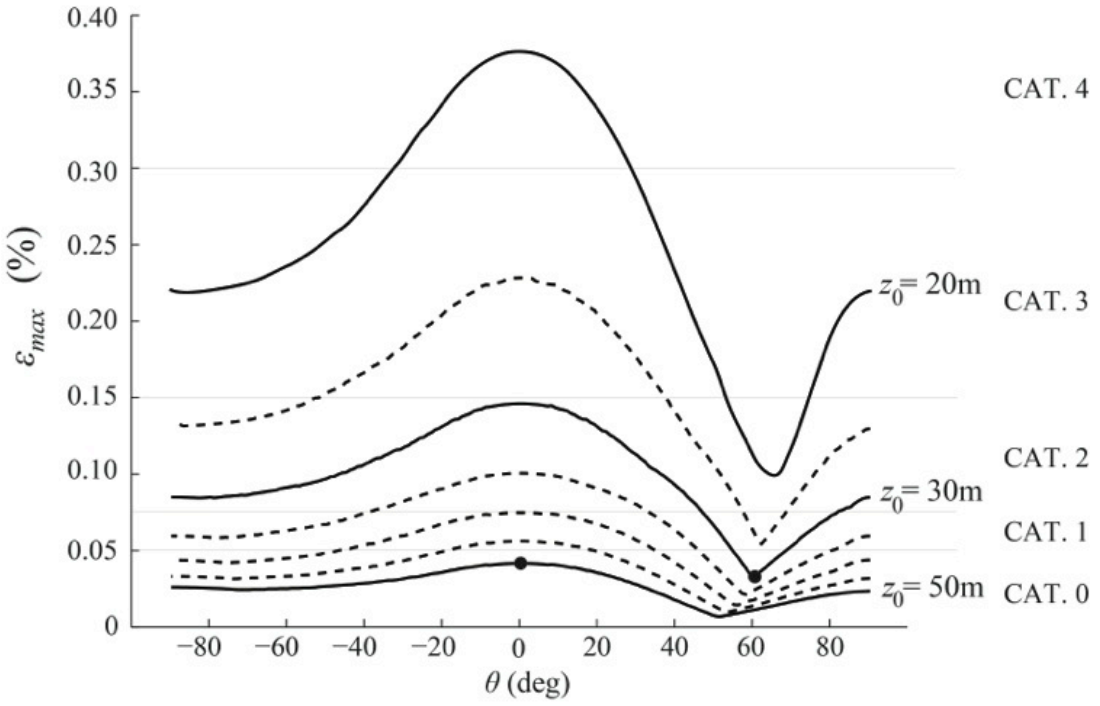

Figure 4.15. Evolution of ε_{max} for an advancing tunnel face from θ =90° to -90° at different z_0 for the most critical tunnel face location y_s (L =30m, d_{orig} =0m, H =3m, E/G =2.6, d =12m, K =0.3, V_L =1%, δ =0.3).

4.5 NON-LINEAR PARAMETRIC REGRESSION MODEL FOR DIRECT ESTIMATION OF ε_{max}

The process of determining ε_{max} comprises several steps including (1) the determination of the settlement trough according to tunnel geometry and ground conditions, (2) the determination of the influence area where $|S| \geq$1mm, (3) the delimitation of zones subjected to sagging and hogging deflection, (4) the determination of the profile of ε_h and (5) the calculation of deflection ratios Δ/L. No expression has been found in the literature to directly estimate the value of ε_{max} for given input parameters V_L, K, z_0, d, L, H and d_{orig}. For this reason, the results generated in the parametric analysis of Sec. 4.4 are used to adjust a non-linear parametric regression model (named $\varepsilon_{max,fit}$) that fits the output values of ε_{max} for every combination of ground, tunnel and building wall. The proposed model has been inspired in the equations for describing the Gaussian settlement profile in the transverse direction with respect to the tunnel axis and applies only for the case $\theta = 0°$. Therefore, only the value of ε_{max} at $y_s = -\infty$ (i.e. the most critical) is considered:

$$\varepsilon_{max,fit} = A \cdot exp(B) \tag{4.30}$$

where,

$$A = \frac{V_L \cdot d^2}{K^2 \cdot z_0^2} \cdot H^{\alpha_1} \tag{4.31}$$

And,

$$B = \alpha_2 + \alpha_3 \frac{L}{H} + \alpha_4 d_{orig} + \alpha_5 \left(\frac{L}{H}\right)^2 + \alpha_6 d_{orig} \frac{L}{H} + \alpha_7 d_{orig}^2 + \alpha_8 L^2 d_{orig} + \alpha_9 d_{orig} L + \alpha_{10} d_{orig}^2 L + \alpha_{11} K z_0 + \alpha_{12} (K z_0)^2 + \alpha_{13} K z_0 d_{orig} + \alpha_{14} H \tag{4.32}$$

where L, H, z_0, d and d_{orig} are given in [m], V_L is introduced per unit value and K is non-dimensional. The output value of $\varepsilon_{max,fit}$ is directly given in [%]. The regression coefficients α_i obtained by least squares estimation (Smyth, 2006) are summarized in Table 4.5 for cases of $d_{orig} \geq 0$ and $d_{orig} < 0$. The purpose of this separation is the improvement the adjustment. The range of variable values for which the model is applicable is: V_L from 0.5% to 2%, K from 0.25 to 0.7, z_0 from 20m to 40m, d from 8m to 12m, L from 10m to 40m, H from 3m to 15m and d_{orig} from -40m to 20m.

The case of $d_{orig} \geq 0$ has been adjusted with 28800 observations and shows a coefficient of determination R^2=0.91. The case of $d_{orig} < 0$ is adjusted with 38400 observations with R^2=0.92. The predicted values of $\varepsilon_{max,fit}$ match in category of damage in the 81% of cases with the categories given by the exact results of ε_{max}. Differences of 1 category of damage are given in the 16% of cases and differences of 2 categories or more in about the 3%.

In general terms, the proposed equation represents well the variation of ε_{max} with the input parameters in the majority of cases. However, the value of $\varepsilon_{max,fit}$ may be overestimated if ε_{max} is expected to be very low. This can occur for example with walls positioned far from the tunnel axis (i.e. with high positive values of d_{orig}). For this reason, the use of this expression should be limited to cases of preliminary assessments of damage.

Table 4.5. Regression coefficients for the determination of ε_{max} with Eq. (4.30)-(4.32) ($\theta = 0°$).

	α_1	α_2	α_3	α_4	α_5	α_6	α_7
$d_{orig} \geq 0$	0.75188	-0.65019	0.24838	-0.049307	-0.011983	-0.0011347	-0.0065007
$d_{orig} < 0$	0.95388	-0.17492	0.20823	-0.020049	-0.0078135	0.00094454	-0.0031526
	α_8	α_9	α_{10}	α_{11}	α_{12}	α_{13}	α_{14}
$d_{orig} \geq 0$	$-3.0141 \cdot 10^{-6}$	-0.0013133	$4.0938 \cdot 10^{-5}$	0.27747	-0.017491	0.016701	-0.052683
$d_{orig} < 0$	$6.1548 \cdot 10^{-5}$	-0.002026	$6.7886 \cdot 10^{-5}$	0.061016	-0.0073386	-0.0037471	-0.0796

4.6 CONCLUSION

The paper proposes a novel equation for the determination of the ground horizontal strain along an alignment θ with respect to the tunnel axis. This equation comes from the application of the strain tensor theory to the classical Gaussian models that describe the settlement troughs generated by tunnel constructions. The proposed methodology allows the modeling of the effect of the tunnel face advance on the settlement profiles, as well as applying the equivalent beam method for whichever position of the building walls in 3D.

Building damage predictions usually assume that walls are located transverse to the tunnel axis (θ =0°). This represents the worst-case scenario and a conservative practice. The reason is that ground horizontal strain and deflections are maximal along this alignment. The novel formulation allows considering the real building wall alignment θ and hence, the possibility of reducing the estimated damage on buildings, which can be significant for some cases. An example was shown where the reduction of ε_{max} was about the 70%.

The presented formulation allows also determining the position of the tunnel face y_s along the tunnel track for which damages in walls are maximal. In cases of θ =0°, the most critical position y_s is always at $y_s \to -\infty$, i.e. after the tunnel face underpass

beneath the building. However, in cases where $\theta \neq 0°$, the value of y_s that maximizes ε_{max} can be given during the tunnel approach and hence, an iterative analysis should be performed to determine it. A general procedure is developed to calculate the most critical tunnel face location. For example, in case of longitudinal buildings with respect to the tunnel axis, the most critical situation tends to be when the tunnel face reaches the building corner.

Furthermore, a comprehensive parametric analysis has been performed for a wide range of geological conditions, walls and tunnel geometries in order to review relevant aspects of building damage predictions in 3D. The importance of delimiting the influence area of settlements has been shown. Overestimation of deflections Δ and underestimation of tensile ground strain ε_{h+} may occur in case of long buildings subjected to a high variation of differential settlements along its length. To avoid this, the part of the buildings subjected to settlements lower than 1mm should be disregarded.

The data generated in the parametric analysis is used to create a non-linear regression model for making preliminary damage assessments. The model allows direct estimation of the maximum tensile strain ε_{max} in building walls aligned $\theta = 0°$ for given input values of geological conditions and wall and tunnel geometries. The presented model shows a good fit of the data and foresees the category of damage correctly in more than 80% of the cases.

Acknowledgements

The Spanish Ministry of Economy and Competitiveness (MINECO) and the ERDF (European Regional Development Funds) have funded this research in the framework of the SUBTIS project (‘Study of the Sensitivity of Urban Tunnels to Tunneling Induced Settlements’ – BIA-2009-13233) by means of a pre-doctoral scholarship (FPI – BES-2010-030132).

5. Probabilistic Approach to Assessing and Monitoring Settlements Caused by Tunneling

Abstract: Tunnel construction commonly causes deformations of the surrounding ground, which can endanger buildings and other structures located in the vicinity of the tunnel. The prediction of these deformations and damages to buildings is difficult, due to limited knowledge of geotechnical conditions and due to uncertainty in predicting the response of the structures to the settlements. This motivates the development of a probabilistic model for the prediction of tunneling-induced damage to buildings. We propose such a model, based on the classical Gaussian profiles for the approximation of the subsidence trough and the equivalent beam method for modeling the response of the building walls. In practice, settlements are commonly monitored through deformation measurements. To account for this, we present a Bayesian method for updating the predicted settlements when measurements are available. Finally, we show how maximum allowable settlements, which are used as threshold values for monitoring the construction process, can be determined based on reliability-based criteria in combination with measurements. The proposed methodology is applied to a group of masonry buildings affected by the construction of the L9 metro line tunnel in Barcelona.

Keywords: Tunneling, tunnel construction, allowable settlement, building damage, equivalent beam, reliability, Bayesian updating.

5.1 INTRODUCTION

Tunneling construction leads to ground subsidence, which can endanger buildings and infrastructure in the vicinity of the tunnel. Settlements caused by tunneling can be modeled using Gaussian profiles (Peck, 1969; Attewell and Woodman, 1982; Attewell *et al*., 1986). This simple model describes the geotechnical conditions by two parameters: the volume loss V_L and the trough width parameter K of the settlement trough. Once the settlement profile is determined, the resulting damages in buildings are commonly modeled by applying the equivalent beam method (Burland and Wroth, 1974; Boscardin and Cording, 1989). This method determines the maximum tensile strain in a particular building wall by modeling it as a linear elastic beam subjected to a given deflection ratio. This strain value is then compared with limiting strain values, which define different categories of damage to buildings, from negligible to very severe.

Prediction of damages is important as a basis for tunnel design, selection of the construction technology and for setting allowable limits on settlements. These allowable values of settlement are used in the construction phase for control purposes: if the measured settlement exceeds the allowable values, the construction is stopped and/or additional safety measures are taken. However, the prediction of damages to buildings caused by tunnel construction entails uncertainty due to (a) our limited knowledge of geotechnical conditions and simplified geotechnical models and (b) uncertainty on the response of structures subjected to differential settlements. This motivates the use of probabilistic approaches for the prediction of settlements and for determining allowable settlement values (Gong *et al*., 2014).

First attempts to the determination of allowable settlements for buildings were made by Skempton and McDonald (1959), who defined allowable settlements according to evidence of existing data surveys of buildings. Settlement limits were determined for cases of panels in frame buildings and walls in load-bearing wall buildings. At present, the limits on allowable settlements are usually determined on a deterministic basis without consideration of uncertainty in the ground and building parameters. For example, Yoo and Kim (2003) proposed an approach for the determination of the maximum allowable volume loss in the construction of the Metro Subway Line 2 in Daegu (South Korea). The approach was based on a Gaussian profile of the settlement trough and the equivalent beam model. An iteration procedure was applied to identify the value of

volume loss (and hence the allowable value of settlement) that would lead to damages below an acceptable level.

We propose a probabilistic model for the estimation of building damage due to tunneling, which is based on the Gaussian profile for the approximation of the subsidence trough and the equivalent beam method for modeling the response of the building walls (Sec. 5.2). The proposed methodology allows taking into account the uncertainties associated with the main model parameters, namely the volume loss V_L, the trough width parameter of the settlement profile K, the ratio of the Young's modulus to the shear modulus of the building and the model errors.

Based on the probabilistic model, we propose a novel approach for determining the allowable settlement on a reliability basis (Sec. 5.3). We demonstrate how the probabilistic model can be updated based on measurements using Bayesian analysis. This technique is used in a wide range of engineering fields (see for example an application in aircraft engineering in Cottone *et al*., 2013). It allows here the computation of the conditional probability of damages given settlement measurements. The allowable settlement is then defined as the maximum measured settlement, for which the conditional probability of damage to a building wall is acceptably low. The approach was first introduced in Camós *et al*. (2013), here it is extended to account for the fact that the settlement depends on the actual phase of construction, i.e. on the distance of the tunnel heading from the point of measurement.

The proposed methodology is applied to a case study of masonry buildings affected by the construction of the L9 metro line in Barcelona (Sec. 5.4). A parametric study is included to analyze the influence of the different model parameters on the estimation of allowable settlements.

5.2 PROBABILISTIC MODEL OF BUILDING DAMAGE DUE TO TUNNELING

A typical tunneling situation is depicted in Figure 5.1 and Figure 5.2, with a building wall of length l_{build}, with its reference point $\hat{A}$ located at a distance d_{orig} from the origin of coordinates and aligned θ degrees with respect to the tunnel transverse plane (Camós and Molins, 2014). Note that the analysis of an entire building should include all exterior walls. However, from now on we will refer to *building damage* as the damage occurring only in a particular wall, without considering the contribution of the other walls.

Alignments counterclockwise with respect to the x-axis are positive ($\theta > 0$). The y axis follows the tunnel longitudinal axis, whereas the x axis corresponds to a transverse plane to the tunnel. The origin of coordinates is set to the intersection of the longitudinal axes of the tunnel and of the building wall. This implies that the coordinate system is a different one for each considered building (wall). The tunnel face is located at coordinate y_s and it advances towards $y = -\infty$, following the criteria set by Attewell *et al.* (1986).

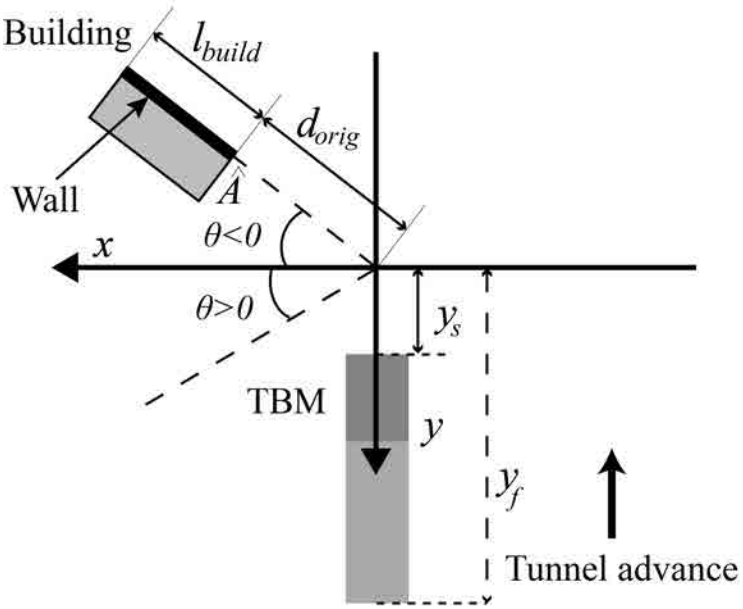

Figure 5.1. Tunnel and building positions (from Camós and Molins, 2014).

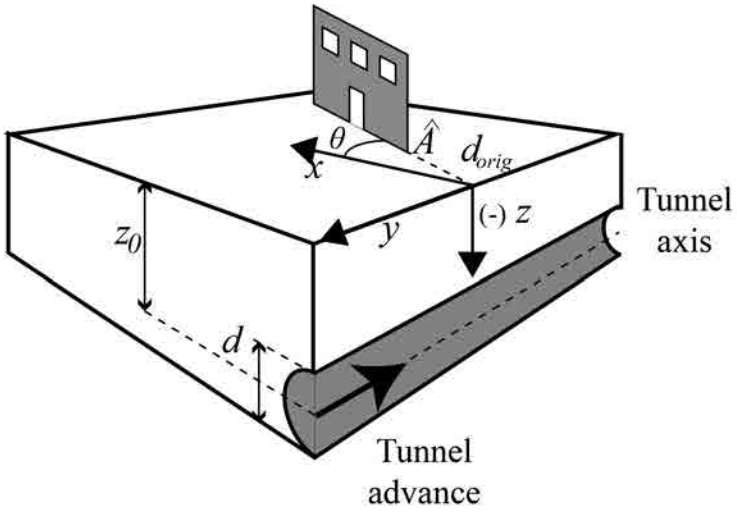

Figure 5.2. 3D view of tunnel and building wall positions.

5.2.1 Modeling of ground settlement – Gaussian profiles

Gaussian profiles of tunneling-induced settlements consist of a Gaussian probability density function describing the shape of settlements in the transverse direction (x-axis) and a Gaussian cumulative distribution function describing it in the longitudinal direction (y-axis). An example of a Gaussian profile is shown in Figure 5.3.

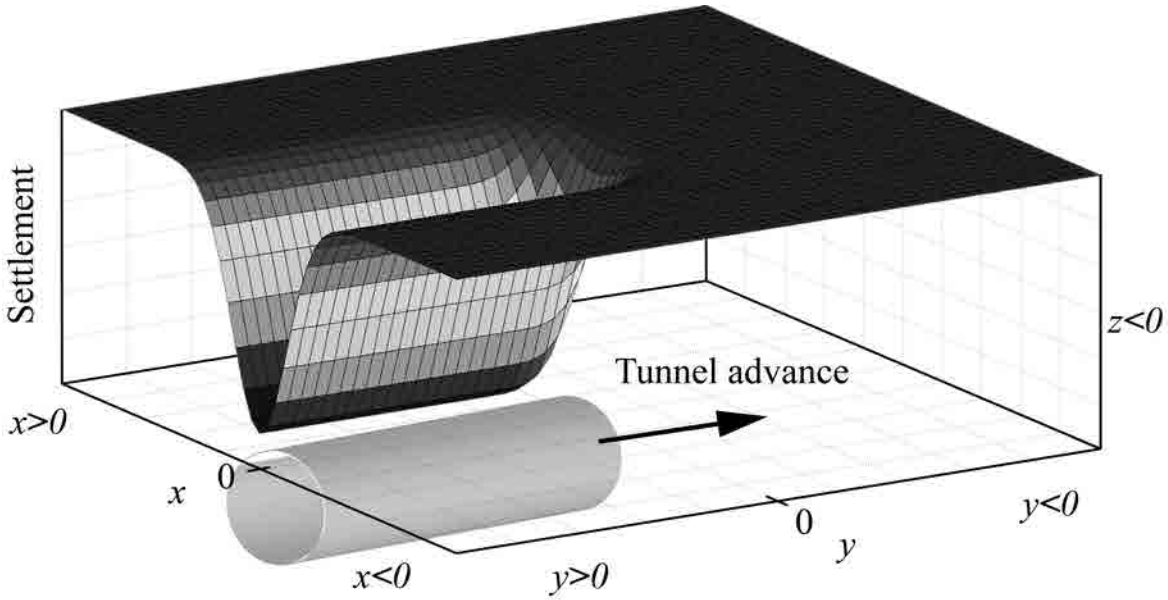

Figure 5.3. Settlement trough produced by tunnel excavation in the transverse (x) and longitudinal (y) directions. The origin of the coordinate system is set relative to the position of the analyzed building wall.

The settlement in [mm] at a certain position with coordinates x, y, z in [m] is calculated by (Peck, 1969; Attewell and Woodman, 1982; O'Reilly and New, 1982):

$$S(x, y, z, d, y_s, y_0, y_f, z_0, V_L, K_x, K_y) = -1000 \cdot S_{max} \cdot exp\left[-\frac{x^2}{2 \cdot K_x^2 \cdot (z_0 - z)^2}\right] \cdot \cdot \left[\Phi\left(\frac{y - (y_s + y_0)}{K_y \cdot (z_0 - z)}\right) - \Phi\left(\frac{y - y_f}{K_y \cdot (z_0 - z)}\right)\right] \quad (5.1)$$

where S_{max} is the absolute value of maximum settlement far behind the tunnel face, where the deformations are fully developed. It is calculated as:

$$S_{max} = \frac{V_L \cdot \pi \cdot d^2}{\sqrt{2\pi} \cdot K_x \cdot (z_0 - z) \cdot 4} \quad (5.2)$$

d and z_0 are the tunnel diameter and depth of the tunnel axis (in meters), respectively. z_0 is a positive magnitude. y_s represents the position of the tunnel face as shown in Figure

5.1. y_0 is the horizontal shift of the longitudinal settlement profile with respect to the tunnel face. y_f is the distance of the tunnel portal. In the remainder of this paper we consider a situation when the tunnel heading is far from the tunnel portal, i.e. we set $y_f = +\infty$. $\Phi(.)$ is the standard normal cumulative distribution function. Note that term of $\Phi(.)$ in Eq. (5.1) that contains y_f becomes 0 if $y_f = +\infty$. V_L is the volume ground loss per unit, K_x and K_y are non-dimensional trough width parameters describing the Gaussian settlement profiles in the transverse and longitudinal direction. K_x and K_y depend on the type of soil: high values of the parameter indicate flat/broad settlement curves (stiff or soft silty clays), low values indicate sharp/narrow settlement curves (granular soils). In this paper we limit ourselves to the case of $K_x = K_y = K$, as it is often assumed in tunneling design (Attewell *et al.*, 1986). The product $K \cdot z_0$ determines the location of the inflection points $i_x = i_y = i$ of the Gaussian profiles. V_L and K are modeled as random variables (RVs). Note that settlements S in Eq. (5.1) are considered to be negative along the z-axis. It is important to keep this sign convention for the correct application of related equations of ground horizontal displacements and strain (see Secs. 4.2.4 and 4.2.5). However, references to settlement magnitudes will be expressed in absolute values throughout the paper.

It is usually assumed that the settlement above the tunnel face corresponds to half the maximum settlement S_{max}, which occurs at a distance far behind from the tunnel face. However, it has been shown that this value can be lower, depending on the type of ground and the construction technology (Nomoto *et al*. 1995, Fargnoli *et al*. 2013). Field observations for shield tunneling in sands or silts indicate that a major part of the settlements is related to the tail void, since tunnel pressure tends to restrict ground movements on the heading. Therefore, the surface settlement above the tunnel face is expected to be lower than $0.5 \cdot S_{max}$ for these soil types. To address this, the parameter y_0 is introduced in Eq. (5.1) to model the shift of the longitudinal Gaussian settlement profile with respect to the tunnel face – see Figure 5.4. The horizontal shift y_0 is given by:

$$y_0 = -\Phi^{-1}(\delta) \cdot K \cdot z_0 \tag{5.3}$$

where δ is the ratio between the surface settlement above the tunnel face and the maximal settlement S_{max} at infinite distance of the face:

$$\delta = \frac{|S(x = z = 0, y = y_s)|}{|S(x = 0, y = +\infty, z = 0)|} = \frac{|S(x = z = 0, y = y_s)|}{S_{max}} \tag{5.4}$$

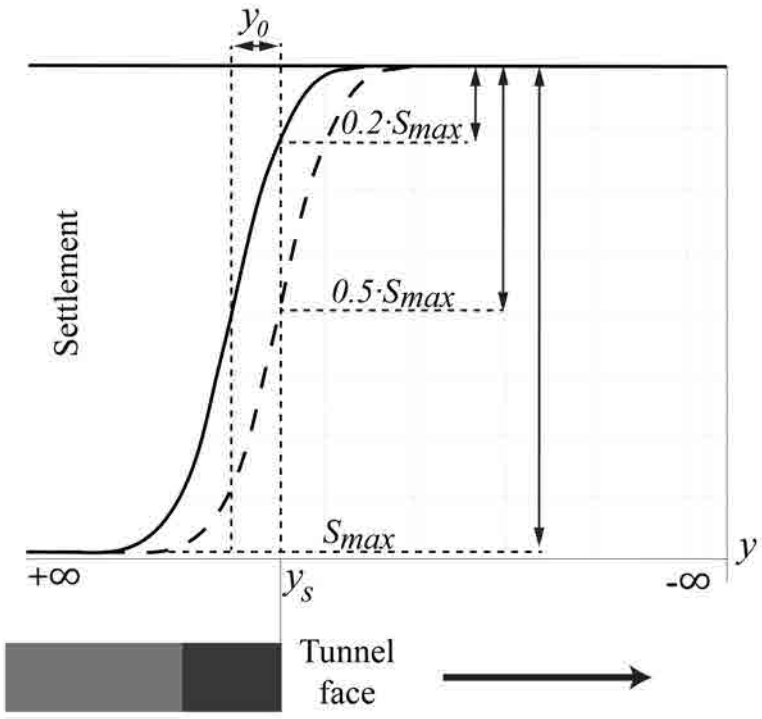

Figure 5.4. Longitudinal settlement profile for $\delta = 0.2$ (solid line) and for $\delta = 0.5$ (dashed line) (from Camós and Molins, 2014).

5.2.2 Modeling of the building response: the equivalent beam method

The response of the building to the settlement is modeled using the equivalent beam method, which represents a building wall by means of a weightless linear elastic rectangular beam. The extreme tensile strains in the beam are calculated for a given shape of the deflection. The distribution of strains in the beam depends on the mode of deformation. Therefore, extreme modes of bending and shear are analyzed separately. The extreme fiber strains in bending, ε_{br}, and in shear, ε_{dr}, are given by the following equations:

$$\varepsilon_{br}\left(V_L, K, \frac{E}{G}\right) = (\varepsilon_{bmax} + \varepsilon_h) \cdot E_{\varepsilon_{br}} \tag{5.5}$$

$$\varepsilon_{dr}\left(V_L, K, \frac{E}{G}\right) = \left[\varepsilon_h\left(1 - \frac{E}{4G}\right) + \sqrt{\frac{\varepsilon_h^2}{16}\left(\frac{E}{G}\right)^2 + \varepsilon_{dmax}^2}\right] \cdot E_{\varepsilon_{dr}} \tag{5.6}$$

where $\frac{E}{G}$ is the ratio between the Young's modulus and the shear modulus of the building material; $\frac{E}{G}$ is modeled as a RV. $E_{\varepsilon_{br}}$ and $E_{\varepsilon_{dr}}$ are multiplicative model errors, they are lognormal RVs with mean value equal to 1.

ε_{bmax} and ε_{dmax} are the maximum bending and shear strains due to deflection. Their calculation is described in Sec. 4.4.2. ε_h is the resultant horizontal strain in the ground surface along the base of the beam. It is calculated based on the field of ground horizontal displacements as (Camós and Molins, 2014):

$$\varepsilon_h(x, y, z, V_L, K) \equiv \cos^2\theta \cdot \varepsilon_{h,xx} + \sin^2\theta \cdot \varepsilon_{h,yy} + 2 \cdot \cos\theta \sin\theta \cdot \varepsilon_{h,xy} \quad (5.7)$$

where θ is the angle between the axes of the wall and of the tunnel, as shown in Figure 5.1 and $\varepsilon_{h,xx}$, $\varepsilon_{h,yy}$ and $\varepsilon_{h,xy}$ are the fields of strain in the ground that are calculated as shown in Sec. 4.2.5. Note that Eq. (5.7) is an extension of the typically used model that assumes that one of the building axes is perpendicular to the tunnel axis. The proposed extension allows modeling an arbitrary position of the building wall with respect to the tunnel. If the wall is perpendicular to the tunnel axis (i.e. $\theta = 0$), Eq. (5.7) reduces to $\varepsilon_h = \varepsilon_{h,xx}$. If the wall is aligned with the tunnel longitudinal axis (i.e. $\theta = 90$), Eq. (5.7) reduces to $\varepsilon_h = \varepsilon_{h,yy}$.

The calculation of extreme fiber strains according to Eqs. (5.5)-(5.6) is performed separately for the zone of the building undergoing sagging deflection and for the zones undergoing hogging deflection, as explained in Sec. 4.4.2. The building can be divided into up to 3 zones: one sagging zone and two hogging zones (case *d* in Sec. 4.4.2). For each zone, the maximum strains in bending and in shear are calculated. The damage on the buildings is then determined depending on the maximum strain ε_{max}:

$$\varepsilon_{max} = \max\left[\varepsilon_{br}^{sag}, \varepsilon_{dr}^{sag}, \varepsilon_{br}^{hog,1}, \varepsilon_{dr}^{hog,1}, \varepsilon_{br}^{hog,2}, \varepsilon_{dr}^{hog,2}\right] \quad (5.8)$$

where ε_{br}^{sag}, $\varepsilon_{br}^{hog,1}$ and $\varepsilon_{br}^{hog,2}$ are the maximum bending strains in sagging and hogging in the three zones, obtained with Eq. (5.5), and ε_{dr}^{sag}, $\varepsilon_{dr}^{hog,1}$ and $\varepsilon_{dr}^{hog,2}$ are the maximum shear strains in sagging and hogging obtained with Eq. (5.6). ε_{max} is a function of the random variables $\mathbf{X} = [V_L; K; \frac{E}{G}; E_{\varepsilon_{br}}^{sag}; E_{\varepsilon_{br}}^{hog,1}; E_{\varepsilon_{br}}^{hog,2}; E_{\varepsilon_{dr}}^{sag}; E_{\varepsilon_{dr}}^{hog,1}; E_{\varepsilon_{dr}}^{hog,2}]$. The last six random variables in **X** are the errors of the equivalent beam model in individual zones of sagging and hogging. All these errors are assumed to be statistically independent.

Based on ε_{max}, one can estimate the size of the cracks in the building. The approach of Burland *et al*. (1977) is used in this paper for classification of the damage magnitudes as shown in Table 5.1.

Table 5.1. Classification of damage (Burland et al., 1977)

Category of damage	**Normal degree of severity**	**Typical damage**	**Tensile strain $\boldsymbol{\varepsilon_{max}}$(%)**	$\boldsymbol{\varepsilon_{lim}}$(%)
0	Negligible	Hair cracks less than 0.1mm	0 – 0.050	0.050
1	Very slight	Fine cracks up to 1mm	0.050 – 0.075	0.075
2	Slight	Cracks easily filled up to 5mm	0.075 – 0.150	0.150
3	Moderate	Cracks from 5 to 15mm	0.150 – 0.300	0.300
4	Severe	Extensive repair works. Cracks from 15 to 25mm	> 0.300	-
5	Very severe	Partial or complete rebuilding. Cracks > 25mm	-	-

5.2.3 Definition of intolerable damage

The failure of the construction process F is here defined as a situation when the tunneling causes an intolerable damage to the building.

The interest is in calculating the probability of an intolerable damage in the building due to the tunneling-induced settlements. It is assumed that intolerable damage F occurs if the maximum strain (ε_{max}) according to Eq. (5.8) exceeds the limiting tensile strain value ε_{lim} for a target category of damage (Table 5.1). In the following, we consider cracks with a width larger than 0.1mm to be not tolerable; hence the limiting strain defining the intolerable damage is taken as $\varepsilon_{lim} = 0.05\%$.

To describe failure, the limit state function (LSF) is defined as

$$g(\mathbf{X}) = \varepsilon_{lim} - \varepsilon_{max}(\mathbf{X}) \tag{5.9}$$

By definition, failure F occurs when the LSF takes values smaller or equal to zero (Melchers, 1999). In the outcome space of the random variables $\mathbf{X}$, we can identify the failure domain $\Omega_F = \{g(\mathbf{x}) \leq 0\}$. The probability of intolerable damage hence equals the probability of $\mathbf{X}$ taking a value within the failure domain:

$$\Pr(F) = \Pr(\mathbf{X} \in \Omega_F) \tag{5.10}$$

Note that this definition of LSF is suitable when applying sampling methods for the computation of probabilities. If methods such as First-Order Reliability Method (FORM) were used, separate LSFs for $E_{\varepsilon_{br}}^{sag}$, $E_{\varepsilon_{br}}^{hog,1}$, $E_{\varepsilon_{br}}^{hog,2}$, $E_{\varepsilon_{dr}}^{sag}$, $E_{\varepsilon_{dr}}^{hog,1}$ and $E_{\varepsilon_{dr}}^{hog,2}$ should be defined and the failure event should be described as a series system (Der Kiureghian, 2005). For a different definition of failure related to building damage produced by tunneling, see Huber et al. (2010).

5.3 RELIABILITY-BASED CRITERIA FOR SETTLEMENT MONITORING

During the construction, measurements of the surface settlement are performed. These measurements are used to decide if the settlements are acceptable or if additional mitigation measures must be taken.

We denote by S_m a settlement measurement that is used for the control of ground behavior in the vicinity of a building. It is taken at the position (x_m, y_m, z_m), at the time when the tunnel face is located at y_{s_m} as shown Figure 5.5. It is here assumed that the position of the measurement is so close to the analyzed building wall that the same ground behavior can be expected at the point of measurement and under the building. For this analysis it will be considered that $z_m = 0$.

The quantity used for deciding if additional measures are necessary is the probability of failure Pr (F), i.e. the probability of intolerable damage. If this probability exceeds the target probability p_T, then measures must be taken. When a measurement S_m is available, the relevant quantity becomes the conditional probability of failure given the measurement, Pr $(F|S_m = s_m)$.

To facilitate application of this criterion in practice, one can determine a corresponding allowable settlement s_{lim} from the following condition:

$$\Pr(F|S_m = s_{lim}) = p_T \tag{5.11}$$

Any measurement $s_m > s_{lim}$ implies that Pr $(F|S_m = s_{lim}) > p_T$ and triggers further actions.

In Sec. 5.3.1, the computation of the allowable settlement s_{lim} is presented. Sec. 5.3.2 describes the calculation of s_{lim} when additional observations of settlement gathered during the tunnel construction (denoted as s_i) are taken into account.

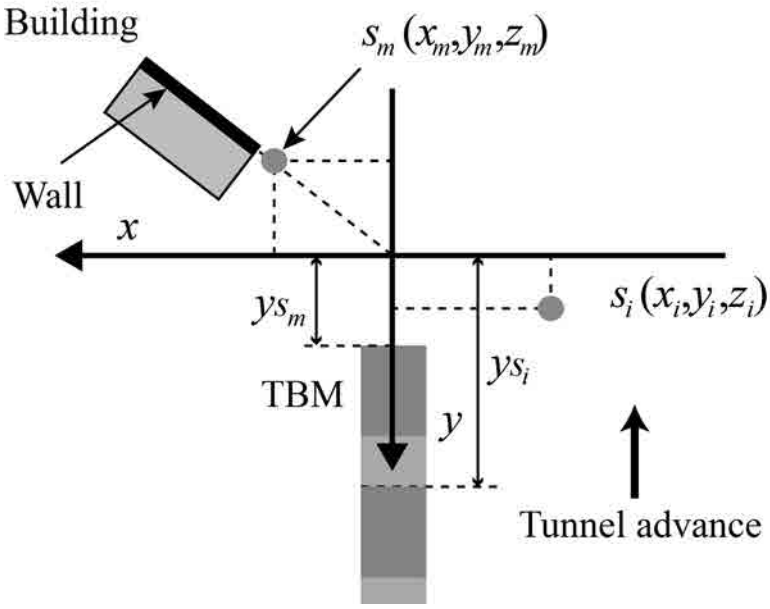

Figure 5.5. Position of the analyzed building, tunnel face, and measurements.

5.3.1 Determination of the allowable settlement and effect of the measurement on the reliability

The conditional probability of Eq. (5.11) can be determined by means of Bayesian updating techniques following Straub (2011). The approach was applied to geotechnical reliability with deformation measurements in Papaioannou and Straub (2012).

The relationship between the measured settlement S_m and the settlement S calculated according to Eq. (5.1) is:

$$S_m = S(x_m, y_m, z_m, V_L, K) + E_f + E_m = S(x_m, y_m, z_m, V_L, K) + E_E \tag{5.12}$$

where E_f is the model error representing the deviation of the real settlement from the idealized Gaussian shape, and E_m is the error of measurement on the site, which reflects imprecision of the instruments, human errors, effect of temperature changes. It is $E_E = E_f + E_m$.

The measurement S_m is used to update the random variables volume loss V_L and trough width parameter K at the location of the measurement. The relation between the measurement S_m and V_L and K can be described by a likelihood function. The likelihood function is the conditional probability density function (PDF) of the measurement outcome given particular values $V_L = v_L$ and $K = k$. By rearranging Eq.(5.12) we obtain

$E_E = S_m - S(x_m, y_m, z_m, V_L, K)$. The PDF of the error E_E is f_E. The likelihood function is therefore:

$$L(v_L, k) = f_E\big(s_m - S(x_m, y_m, z_m, v_L, k)\big) \tag{5.13}$$

Following Straub (2011), this likelihood function can be expressed by a LSF:

$$h(v_L, k, u) = u - \Phi^{-1}[cL(v_L, k)] \tag{5.14}$$

where u is the realization of a standard normal RV, Φ^{-1} is the inverse standard normal CDF and $c = \sigma_{E_E} \cdot \sqrt{2\pi}$ is a scaling constant chosen to ensure that $cL\big((v_L, k)\big) \leq 1$ for all v_L, k. This LSF defines the observation domain $\Omega_0 = \{h(v_L, k, u) \leq 0\}$ in the outcome space of the RVs **X** and the standard normal variable U. The conditional probability of failure for a given settlement measurement s_m is then computed as:

$$\Pr\,(F|S_m = s_m) = \frac{\Pr(F \cap\ S_m = s_m)}{\Pr(\ S_m = s_m)} = \frac{\Pr([\mathbf{x}, u] \epsilon \{\ \Omega_0 \cap\ \Omega_F\})}{\Pr([\mathbf{x}, u] \epsilon\ \Omega_0)} \tag{5.15}$$

where Ω_F is the failure domain defined by the LSF given in Eq. (5.9).

This conditional probability is evaluated with Monte Carlo Simulation(MCS) for different values of s_m. The allowable settlement value s_{lim} ensuring Eq. (5.11) is then found iteratively.

5.3.2 Including additional measurements at earlier locations

Measurements of surface settlement are made during the whole construction process, not only in the vicinity of the analyzed building. All measurements that are taken in the quasi-homogeneous geotechnical section of the tunnel in which the analyzed building is located may be used to infer the behavior of the ground at the building. N measurements $\mathbf{s} = (\mathrm{s}_1, \mathrm{s}_2, \ldots, \mathrm{s}_\mathrm{i}, \ldots \mathrm{s}_\mathrm{N})$ are obtained along the tunnel. The i-th measurement is made at position $x_i, y_{i,} z_i$, when the tunnel face is located at y_{s_i} (see Figure 5.5).

As above, the uncertain geotechnical conditions in the quasi-homogeneous section are characterized by volume loss V_L and trough width parameter K. The values of these parameters vary even within a quasi-homogeneous section, due to random fluctuations. This variability of V_L and K is here described by stationary stochastic processes with constant autocorrelation functions $R_K(b) = \rho_K$ and $R_{VL}(b) = \rho_{V_L}$, where $b > 0$ is the distance between two locations within the section. In other words, it is assumed that

trough width parameter K has the same marginal distribution at any location within the section and that the values of K at two locations are correlated with correlation coefficients ρ_K, independent of the distance between them. The same holds for V_L. This simple correlation model was selected based on analysis of a small dataset from a constructed tunnel; it should be enhanced in the future based on the analysis of a larger amount of data.

The new measurements $s_1, \dots s_N$ can be expressed by separate likelihood functions $L_1, \dots, L_N$, following Eq. (5.13). For each likelihood function L_i, one can find the corresponding observation domain Ω_i defined by means of a LSF $h_i(v_{L_i}, k_i, u_i)$ as described in Eq. (5.14). Here, v_{L_i} and k_i are the realizations of the random processes K and V_L at the location x_i, y_i, z_i of the measurement.

To update the maximum allowable settlement measurement at the position (x_m, y_m, z_m) conditional on the existing measurements **s**, the failure probability conditional on s_m and **s** is computed (compare with Eq. (5.15)):

$$\Pr(F|S_m = s_m, \mathbf{S} = \mathbf{s}) = \frac{\Pr(F \cap S_m = s_m \cap \mathbf{S} = \mathbf{s})}{\Pr(S_m = s_m \cap \mathbf{S} = \mathbf{s})} = \frac{\Pr([\mathbf{x}, u, u_1, \dots u_N] \in \Omega_F \cap \Omega_0 \cap \Omega_1 \cap \dots \cap \Omega_N)}{\Pr([\mathbf{x}, u, u_1, \dots u_N] \in \Omega_0 \cap \Omega_1 \cap \dots \cap \Omega_N)} \tag{5.16}$$

Analogous to the procedure in Sec. 5.3.1, this conditional probability is evaluated for different values of s_m. The updated allowable settlement s^*_{lim} ensuring Eq. (5.11) is found iteratively.

It is important to remark that the uncertainty of errors has computational implications. The calculation of $\Pr(F_{\varepsilon_{lim}}|s_m)$ is performed by using Eqs. (5.15) and (5.16): the total number of samples being in the failure and observation domains ($\Omega_F \cap \Omega_0$) is divided by the total number of samples in the observation domain Ω_0. The acceptance of samples being in the observation domain Ω_0 depends on the likelihood of the observations (Eq. (5.14)). Therefore, the higher the standard deviation of the errors, the higher is the number of samples included in Ω_0. Low standard deviations of E_f and E_m will reduce substantially the number of samples fulfilling the condition to be in the observation domain Ω_0 and thus, the accuracy of the determination of the probability of failure will be rather low. If computational efficiency were desirable, advanced sampling methods could

be used instead of MCS for solving Eq. (5.15), see Straub (2011), Papaioannou and Straub (2012), Straub and Papaioannou (2014), Mollon et al. (2013).

5.4 CASE STUDY

The proposed method is applied to a case study of the L9 metro line construction in Barcelona. The damage produced to a complex of attached masonry buildings from the late 1920's located in the Bon Pastor area is studied. Buildings were affected by the construction of a precast segment tunnel lining with an Earth Pressure Balance - Tunnel Boring Machine (EPB-TBM). An equivalent beam analysis of the buildings was performed in Camós, Molins and Arnau (2014), showing the validity of this model. The location of the buildings and the tunnel is shown in Figure 5.6. The curvature of the tunnel axis is neglected in the following calculations. The analysis will be performed on the façade of 6 attached dwellings. The soil in the zone of study is characterized by the interbedding of sediment layers with a high variety of grain particle distributions such as grained sands, gravels, blocks in sandy matrix, clay and silts and coarse sands and gravels (Deulofeu *et al*. 2007).

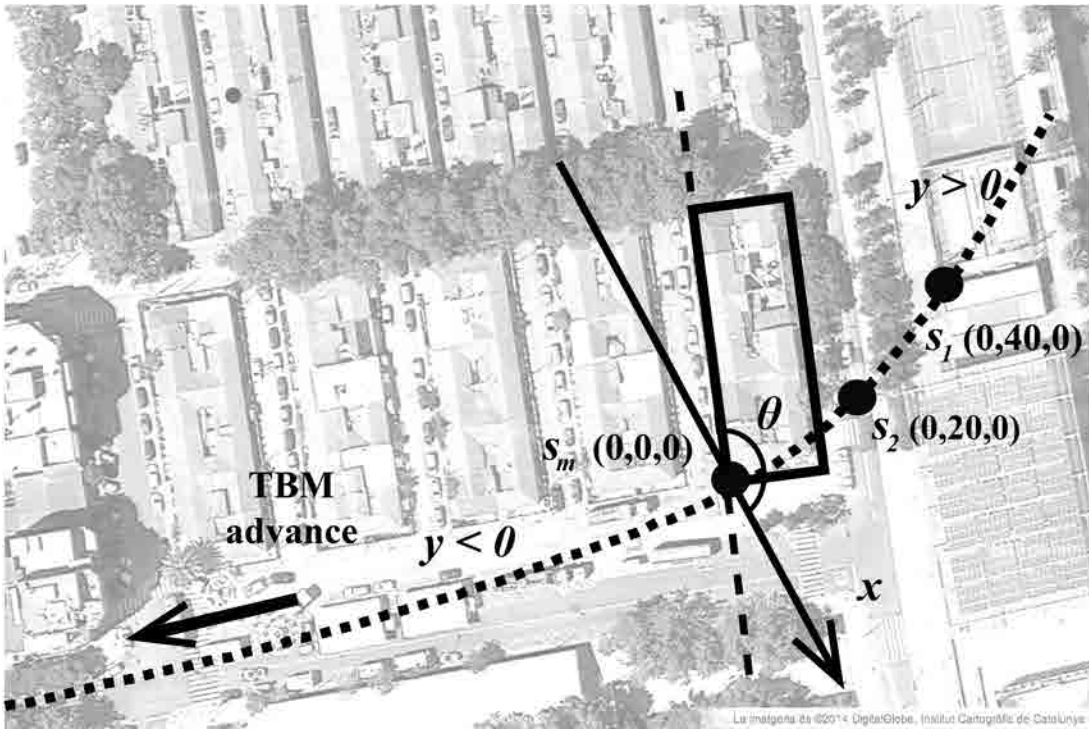

Figure 5.6. Location of attached buildings, tunnel track and position of measurements (dataset DS1) in Bon Pastor - Barcelona (source of the aerial map: DigitalGlobe®2014 – Institut Cartogràfic de Catalunya).

5.4.1 Model parameters

The tunnel diameter d in the studied section is 12m, the depth of the tunnel is $z_0 = 23$m. The length of the building façade complex is 46m, the angle between the axes of the building and the tunnel is $\theta = 154^o$. Note that due to symmetry about the y-axis, both alignments $\theta = 154^o$ and $\theta = 26^o$ are equivalent. The wall height is H =3m and it follows that the inertia per unit length of the cross-section of the wall is equal to I =2.25m^4/m. The parameter t equals 1.5m in the sagging zone and 3m in the hogging zone and it is $a = t$ for both zones. The ratio between the surface settlement above the tunnel face and the maximal settlement is selected as δ=0.3, which is a realistic value for the type of ground considered here (Nomoto *et al*. 1995, Fargnoli *et al*. 2013).

The parameters of the random variables considered in the model are summarized in Table 5.2. The trough width parameter of the settlement profile K usually varies in the range from 0.2 to 0.3 in case of granular soils, from 0.4 to 0.5 in case of stiff clays and it can reach a value of 0.7 in soft silty clays (Burland, 2008). The mean value of the trough width parameter K is set at 0.3 and the coefficient of variation (C.V.) is assumed equal to 0.2. K is non-negative and the lognormal distribution is thus used. A high spatial correlation of K is assumed within the quasi-homogeneous geotechnical section and the correlation coefficient of the underlying normal RV is thus set to $\rho_K = 0.7$.

Experience from tunneling constructions in similar conditions (TYPSA, 2003) shows that the volume loss V_L typically takes values in the range from 0.1% to 0.6%. The uncertainty on these values is high due to many unpredictable factors that influence ground losses, including unexpected geological strata, technical problems of the TBM and human errors. V_L is modeled by a lognormal distribution with mean 0.4% and C.V. 0.4. V_L is primarily influenced by the construction process and it is typically highly variable within one quasi-homogeneous section. For this reason, the spatial correlation of the volume loss is assumed to be zero, $\rho_{V_L} = 0$.

A value equal to 2.5 is typically assumed for the ratio E/G of masonry buildings. Uncertainty is also present in this parameter due to the variety of orthotropic materials composing a building, yet this uncertainty is relatively small. Therefore, E/G is here modeled by a beta distribution defined on the interval 2.4 to 2.6, which is a typical range of this ratio for masonry (Burland, 2008). Ideally, an unbounded distribution should be

chosen, since the bounds imposed by the beta distribution are not physically justified. However, the effect of this modeling choice here is small.

The building is divided to one sagging and one hogging zone. Two values of extreme fiber strain in shear ε_{dr}^{sag} and ε_{dr}^{hog} and two values of extreme fiber strain in bending ε_{br}^{sag} and ε_{br}^{hog} are thus computed using the equivalent beams model following Eqs.(5.5)-(5.7). The multiplicative model errors of the model $E_{\varepsilon_{br}}^{sag}$, $E_{\varepsilon_{dr}}^{sag}$, $E_{\varepsilon_{br}}^{hog}$, $E_{\varepsilon_{dr}}^{hog}$, are described by lognormal distributions with mean equal to 1 and st.dev. 0.05. The errors are assumed to be independent.

Table 5.2. Random parameters of the model.

Parameter [units]	Description	Distribution	Mean	St. dev.
$\boldsymbol{K}$ [-]	Trough width parameter	lognormal (-1.22, 0.20)	0.3	0.06
$\boldsymbol{V_L}$ [%]	Volume loss	lognormal (-0.99,0.39)	0.4	0.16
$\boldsymbol{E/G}$ [-]	Material ratio	beta (2,2,[2.4,2.6])	2.5	0.045
$\boldsymbol{E_m}$ [mm]	Measurement error	normal (0.0,1)	0.0	1
$\boldsymbol{E_f}$ [mm]	Settlement model error	normal (0.0,2)	0.0	2
$\boldsymbol{E_{\varepsilon_{br}}^{sag}}$, $\boldsymbol{E_{\varepsilon_{dr}}^{sag}}$, $\boldsymbol{E_{\varepsilon_{br}}^{hog}}$, $\boldsymbol{E_{\varepsilon_{dr}}^{hog}}$ [-]	Eq. beam model errors	lognormal (0.0,0.05)	1.0	0.05

The results of the analyses performed in the following paper are achieved with $5 \cdot 10^6$ simulations. The building is discretized in 50 calculation points. The computing time is about one hour by using a computer with Intel Core i7 930 @ 2.80 GHz processor, 8GB RAM and operating system Windows 7 Professional 64 bits.

For simplicity, the following calculations take into account the whole length of the building. However, in case of long buildings as the analyzed one, the part of the building subjected to settlements lower than 1mm should be disregarded in order to avoid the possible overestimation of ε_{bmax} and ε_{dmax} and the underestimation of ε_h (see Camós and Molins, 2014).

5.4.2 Probabilistic prediction of settlement and building damage

A probabilistic prediction of settlement at the location of the building $(x, y, z) = (0,0,0)$ is performed by using the Eq. (5.1). Figure 5.7 shows the cumulative distribution functions of the predicted settlement $S_{(0,0,0)}$ for different positions of the tunnel face y_s,

Table 5.3 summarizes its mean and standard deviation. The predicted mean values of settlement vary from 0.6mm for the case when the tunnel face is 10 meters before the building (y_s=+10) to 27mm for the case when the tunnel face passed under the building and it is 50 meters behind (y_s=-50m). The difference of the settlement for y_s=-20m and y_s=-50m is very low, which indicates that at these distances, the maximal settlement S_{max} is reached.

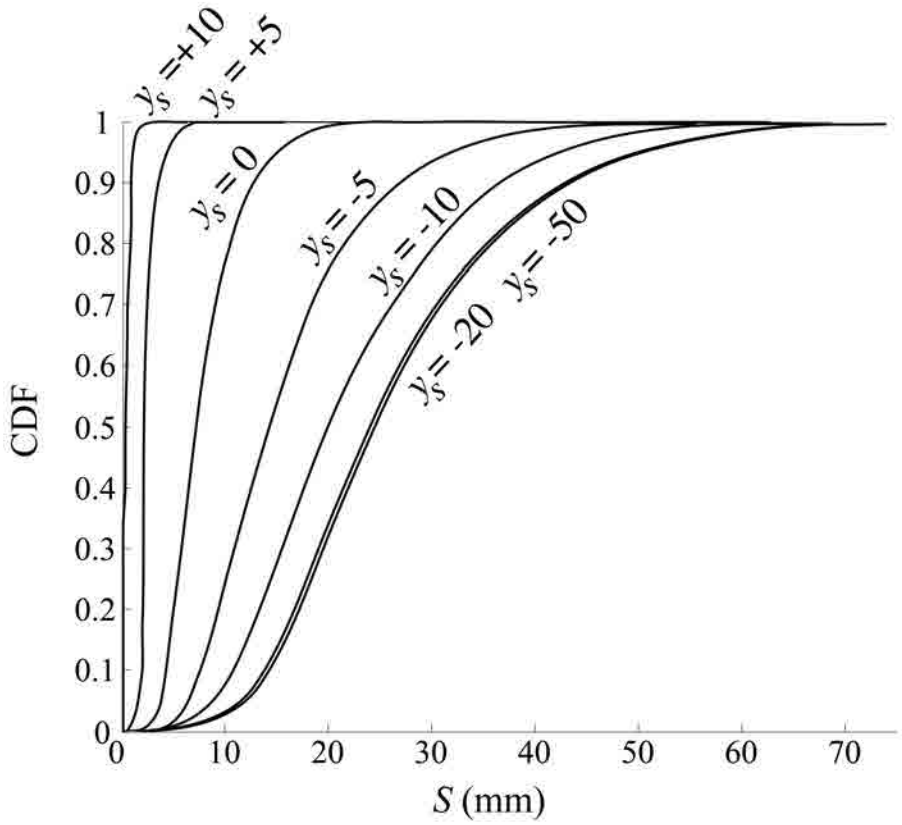

Figure 5.7. Cumulative distribution function of settlement $S_{(0,0,0)}$ for different positions of the tunnel face y_s. Means and standard deviations of the settlements are summarized in Table 5.3.

Only a negligible damage (Category 0) is considered as acceptable, as is usual in tunneling construction. More severe damages to buildings are considered as intolerable, therefore the limiting tensile strain is set to $\varepsilon_{lim} = 0.05\%$ following Table 5.1.

The prior probabilities of intolerable damage calculated using Eq. (5.10) are shown in Table 5.4. It can be seen that for positions of the tunnel face $y_s < 0$, the probability of damage is in the order of 25%. This high probability of damage is due to the large uncertainties of the ground behavior and of the measurement and model errors as well as due to the strict definition of intolerable damage (category 1 or higher of Table 5.1). Note

that the probability of intolerable damage is slightly higher if tunnel face is located at y_s =-10m than at y_s =-20m. This difference is due to the alignment of the building with respect to the tunnel axis ($\theta = 26°$). The combination of deflection ratios and ground horizontal strain ε_h at the wall results to be more critical when tunnel face is at y_s =-10m than when it is at y_s =-20m.

Table 5.3. Mean and standard deviation of settlement $S_{(0,0,0)}$ for different positions of the tunnel face y_s.

Position of tunnel face y_s (m)	**Mean (mm)**	**St. dev. (mm)**
+10	0.6	0.4
+5	2.7	1.1
0	8.2	3.7
-5	16.3	8.6
-10	22.8	11.6
-20	26.9	12.6
-50	27.2	12.5

Table 5.4. Unconditional probabilities of intolerable damage for different positions of the tunnel face.

Position of tunnel face	y_s =+10m	y_s =+5m	y_s =0m	y_s =-5m	y_s =-10m	y_s =-20m
Probability of damage $\mathbf{Pr}(F)$	0%	0.01%	8%	23%	28%	25%

5.4.3 A-priori determination of the allowable settlement

We are looking for allowable settlement s_{lim} at the position $(x_m, y_m, z_m) = (0,0,0)$ that satisfies Eq. (5.11). The target probability for intolerable damage is set to p_T =5%.

The allowable settlement is determined using the approach described in Sec. 5.3.1. The probability of damage conditional on measured settlements s_m is calculated following Eq. (5.15), the results for s_m in the interval from 0 to 40mm are displayed in Figure 5.8 for different positions of the tunnel face.

The allowable settlement s_{lim} for each location of the tunnel face y_s can be determined from the intersection of the relevant probability curve with the p_T line. The results are summarized in Table 5.5. For example, for y_s =-20m, i.e. for the case when the tunnel face is 20m behind the building and the settlement is almost fully developed, the

allowable settlement s_{lim} is 25mm. On the contrary, for y_s =0m, i.e. for the case when the tunnel face is beneath the building, the allowable settlement s_{lim} is 10mm. The generated settlements in the zone of analysis when the tunnel face is still far are generally small due to the shift of the longitudinal profile ($\delta = 0.3$). Hence, the measurements will have limited expressiveness with the presented model. For this reason, the measurement error will dominate at these locations and no measurement will sufficiently reduce the probability of intolerable damage. Therefore, the analysis at tunnel face locations y_s =+5m and y_s =+10m is not performed in the following.

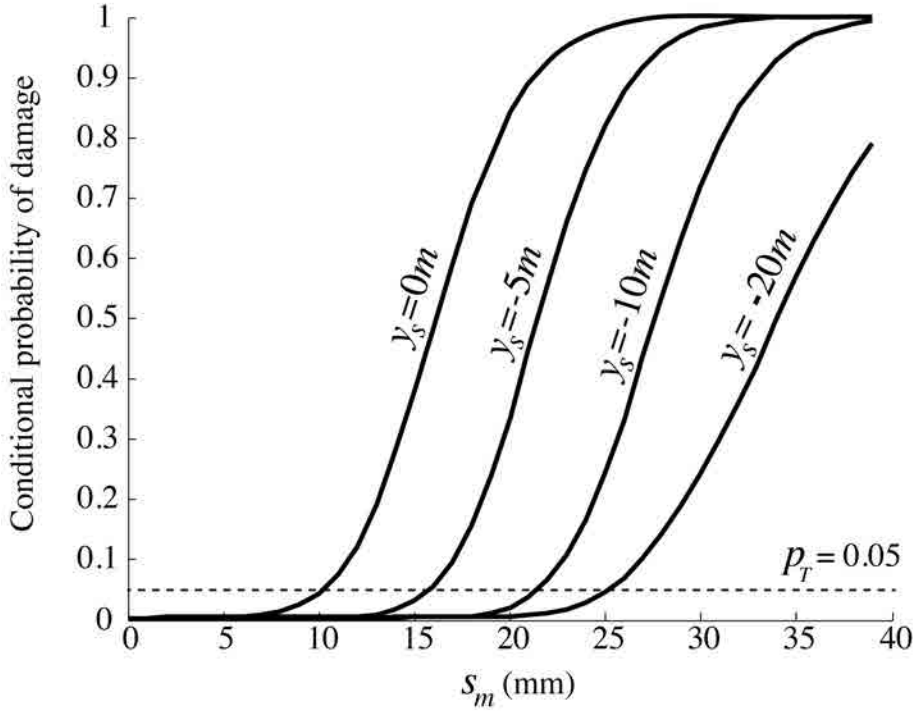

Figure 5.8. Conditional probability of intolerable damage Pr ($F_{\varepsilon_{lim}=0.050\%}|s_m$) *as a function of measured settlement* s_m *for different positions of tunnel face* y_s.

Table 5.5. Prior values of allowable settlement for different locations of tunnel face.

Position of tunnel face	y_s =0m	y_s =-5m	y_s =-10m	y_s =-20m
Prior allowable settlement, s_{lim}	10mm	15mm	21mm	25mm

5.4.4 Updating with observations from monitoring instruments

The prior estimation of the allowable settlement is updated with earlier measurements made in other locations within the same quasi-homogeneous section of the tunnel,

following the procedure described in Sec. 5.3.2. For the numerical investigation, two different data sets denoted as DS1 and DS2 are used.

DS1 consists of two real measurements of the settlement performed in the same quasi-homogeneous section (Figure 5.6): measurement s_1 =11mm was taken at position $(x_1, y_1, z_1) = (0,40,0)$ and measurement s_2=19mm was taken at $(x_2, y_2, z_2) = (0,20,0)$, as shown in Figure 5.6. Both measurements were made at the moment when the tunnel face was under the location of the measurement, therefore y_{s_1}=+40m and y_{s_2}=+20m.

DS2 is a hypothetical data set, introduced for illustration purposes. The measured settlement values are: s_1 =19mm taken at position $(x_1, y_1, z_1) = (7,20,0)$, s_2 =18mm taken at position $(x_2, y_2, z_2) = (0,40,0)$ and s_3 =19mm taken at position $(x_3, y_3, z_3) = (-8,20,0)$. Measurements s_1 and s_3 are taken close to the inflection point of the transverse Gaussian settlement profile, whereas s_2 is taken at tunnel centerline. All three measurements are taken at the moment when the tunnel face is underneath the building, so that $y_{s_1} = y_{s_2} = y_{s_3} = 0$m. DS2 indicates a higher volume loss and a flatter settlement profile than DS1.

Table 5.6 shows the updated values of allowable settlement with the two datasets. Accounting for the measurements DS1 slightly reduces the allowable values of settlement compared to the prior values shown in Table 5.5. Accounting for the measurements DS2 slightly increases these values. The reason for these opposite trends is the posterior distribution of the trough width parameter K at the location of the building, conditional on DS1 or DS2; its CDF is presented in Figure 5.9. It can be observed that the measurements DS1 lead to a lower posterior estimate of K indicating a sharper profile, whereas DS2 lead to a higher posterior estimate of K indicating a flatter profile. The sharper profile is more critical for the buildings since it produces higher deflection ratios and thus more severe damages. Because the volume loss V_L is not correlated from one location to another, only the trough width parameter K can be learned. Overall it can be observed that with the assumed correlation model, the overall effect of the additional measurements is relatively small.

Table 5.6. Values of allowable settlement s_{lim} for different locations of tunnel face updated with the two datasets.

Position of tunnel face	y_s =0m	y_s =-5m	y_s =-10m	y_s =-20m
s_{lim} updated with DS1	8mm	14mm	20mm	23mm
s_{lim} updated with DS2	11mm	16mm	22mm	26mm

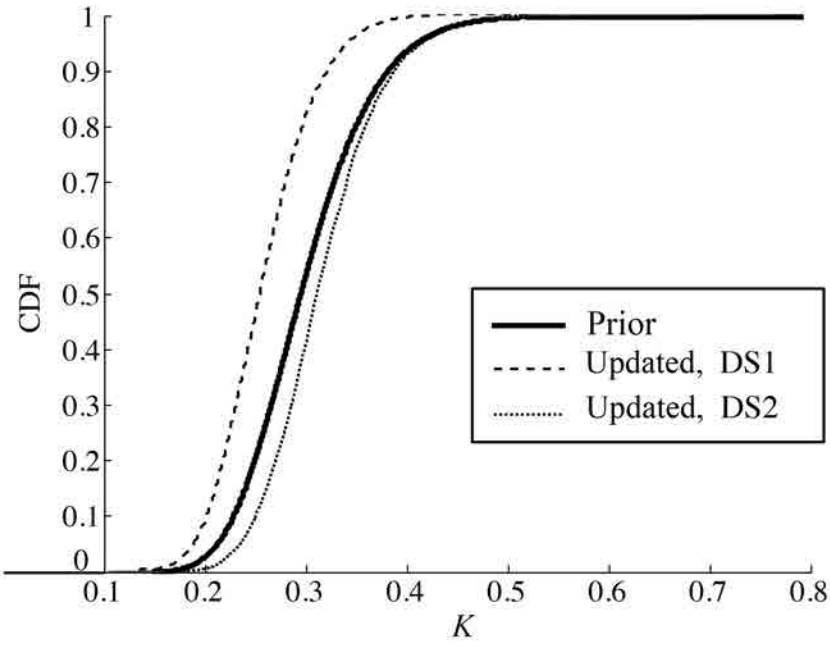

Figure 5.9. Prior and updated cumulative density function of trough width parameter K.

5.5 PARAMETRIC STUDY

In this section, the influence of selected model parameters on the allowable settlement is examined.

5.5.1 Influence of the shift of the longitudinal Gaussian settlement profile characterized by parameter δ

Following Eq. (5.4), the parameter δ defines the ratio between the immediate surface settlement above the tunnel face and the maximal settlement S_{max} at a location far from the face. In Sections 5.4.1-5.4.4 it was assumed that $\delta = 0.3$, i.e. that at the moment when the tunnel face is under the location of interest, the settlement at this location corresponds to 30% of the final/maximal settlement S_{max}. The longitudinal Gaussian settlement profile is thus shifted in the horizontal direction as illustrated in Figure 5.4. In the

practice, however, it is common to assume $\delta = 0.5$. The influence of this assumption is tested here.

Table 5.7 shows the a-priori allowable settlement s_{lim} for both δ=0.3 and δ=0.5. The allowable settlement for δ=0.5 for positions of tunnel face close to the analyzed building, i.e. for y_s being in the interval from $y_s = +0$m to $y_s = -10$m, are higher than for δ=0.3. The reason for the higher allowable values in case of δ=0.5 is that we assume an earlier development of the settlement (50% of the final settlement at the moment when the face undergoes the building) and thus a smaller increase of the settlement after the tunnel face passes the building. A higher settlement is thus acceptable.

Table 5.7. Prior values of allowable settlement for different locations of tunnel face for different values of δ.

Ratio $\boldsymbol{\delta}$ \ Position of tunnel face	$\boldsymbol{y_s}$ =0m	$\boldsymbol{y_s}$ =-5m	$\boldsymbol{y_s}$ =-10m	$\boldsymbol{y_s}$ =-20m
$\boldsymbol{\delta}$=0.3	10mm	15mm	21mm	25mm
$\boldsymbol{\delta}$=0.5	13mm	19mm	23mm	25mm

5.5.2 Influence of the uncertainty of ground parameters V_L and K

In the Gaussian profile model of tunneling induced settlement, the ground is described by volume loss V_L and trough width parameter K, as discussed in Section 5.2.1, which are here modeled probabilistically, following Table 5.2. To assess the influence of the assumptions on the uncertainty in V_L and K, the computations are repeated with the standard deviations of these variables doubled, from σ_K =0.06 to σ_K =0.12, and from σ_{V_L} =0.16 to σ_{V_L} =0.32. (The parameters of the corresponding lognormal distributions are μ'_K =-1.28, σ'_K =0.39, and μ'_{V_L} =-1.16, σ'_{V_L} =0.7.)

A comparison of the resulting allowable settlements obtained with the original model to those from the modified model is shown in Table 5.9. It can be seen that increasing the standard deviation of the RVs leads to stricter (lower) limits on the allowable settlement, because a higher uncertainty on the ground behavior causes a higher probability of intolerable damage. Increasing the standard deviation of both V_L and K by a factor of two leads to a reduction of the allowable settlement by 10% - 30%.

Table 5.8. Prior values of allowable settlement for different positions of tunnel face for different standard deviations of the ground parameters V_L and K.

Uncertainty on ground parameters \ Position of tunnel face	y_s =0m	y_s =-5m	y_s =-10m	y_s =-20m
σ_K =0.06 σ_{V_L} =0.16	10mm	15mm	21mm	25mm
σ_K =0.12 σ_{V_L} =0.32	7mm	13mm	18mm	19mm

5.5.3 Influence of the correlation coefficients ρ_{V_L} and ρ_K

The spatial correlation of the geotechnical parameters volume loss V_L and trough width parameter K is modeled by means of a constant autocorrelation function as described in Section 5.3.2. The spatial correlation determines the effect of measurements made at other locations of the quasi-homogeneous section on the probabilistic model, and consequently the allowable settlement, at the location of interest. Earlier it was assumed that the trough width parameter K is correlated with correlation coefficient $\rho_K = 0.7$ and the volume loss V_L is uncorrelated, therefore ρ_{V_L} =0. This implies that learning of V_L based on measurements from other locations was not possible.

To assess the effect of the correlation, the correlation coefficient of V_L is modified to 0.7, whereas the one for K is kept, i.e. $\rho_K = \rho_{V_L} = 0.7$. The resulting allowable settlements are summarized in Table 5.9. It can be observed that the higher correlation leads to a slight increase in the allowable settlements. With the higher correlation, the uncertainty in V_L at the location of interest is reduced, as evident from Figure 5.10.

Table 5.9. Updated values of allowable settlement for different positions of tunnel face for different correlation coefficients ρ_{V_L} and ρ_K.

	Position of tunnel face	y_s =0m	y_s =-5m	y_s =-10m	y_s =-20m
$\rho_K = 0.7$, $\rho_{V_L} = 0$	s_{lim} updated with DS1	8mm	14mm	20mm	23mm
	s_{lim} updated with DS2	11mm	16mm	22mm	26mm
$\rho_K = 0.7$, $\rho_{V_L} = 0.7$	s_{lim} updated with DS1	8mm	15mm	21mm	24mm
	s_{lim} updated with DS2	12mm	18mm	24mm	29mm

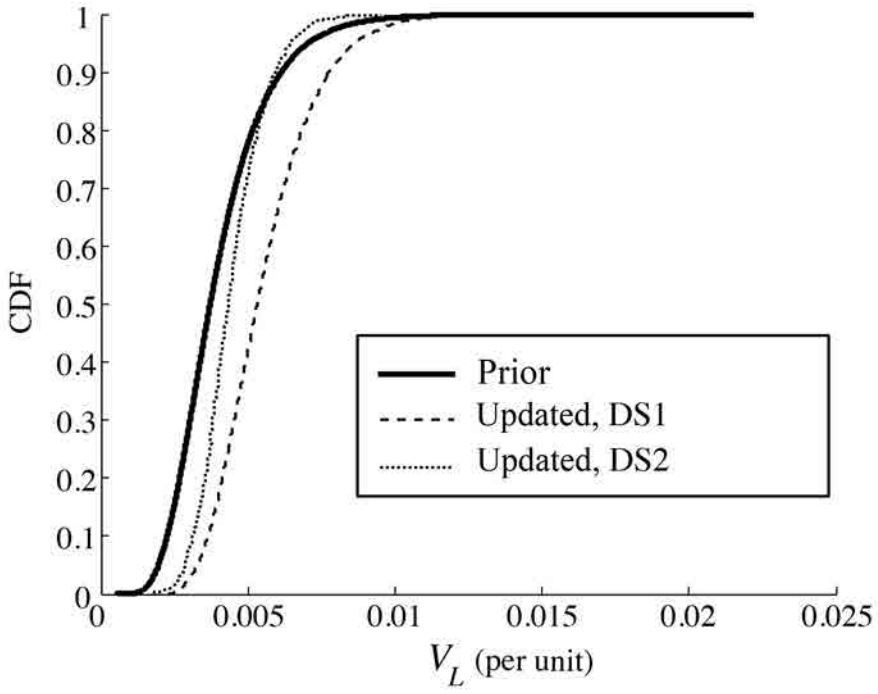

Figure 5.10. Prior and updated cumulative density function of V_L with ρ_{V_L} =0.7.

5.5.4 Influence of the uncertainty of the model error E_f and measurements error E_m

The determination of allowable settlements is based on the probability of damage conditional on measured settlements s_m, Eq. (5.11). This probability can be determined by reliability updating techniques based on the likelihood of a certain observation s_m, Eq. (5.13). This likelihood is defined as the probability of having a certain error between the measured settlement s_m and the settlement S given by the Gaussian profile model. Therefore, the PDF of the total error E_E depends on the distribution parameters of the ground model error E_f and the measurement error E_m. These errors are considered as random with normal distribution and mean and standard deviation according to Table 5.2: the measurement error E_m was assumed to have a standard deviation of 1 mm while the model error E_f a standard deviation of 2mm.

To investigate the effect of the distribution of these errors, computations are repeated with reduced standard deviations of the errors. Table 5.10 compares the allowable values for the original assumption with the case in which the standard deviations of both errors are decreased to 50% of the original value. As can be observed, the higher the uncertainty on

the model errors, the lower the allowable values of settlements s_{lim}, but the difference among the two investigated cases is low.

Table 5.10. Prior values of allowable settlement s_{lim} for different positions of tunnel face for different standard deviations of the measurement error E_m and of the ground model error E_f.

Position of tunnel face	y_s =0m	y_s =-5m	y_s =-10m	y_s =-20m
σ_{E_f} =2mm σ_{E_m} =1mm	10mm	15mm	21mm	25mm
σ_{E_f} =1mm σ_{E_m} =0.5mm	10mm	16mm	22mm	26mm

5.6 DISCUSSION

In the case study, the allowable value of settlement is determined as 25mm for positions where the settlement is fully developed (far from the tunnel heading). This value corresponds well with the allowable settlement that was used during the construction (24mm) if the type of foundation and the initial state of the buildings are not considered in the analysis. For buildings with shallow foundations and deteriorated initial states as the studied one, constructors employed a more restrictive allowable settlement value of 8mm. However, the proposed methodology does not allow taking into account these two factors and hence, engineering judgment should be used in these cases to decrease the allowable settlement to more reasonable values. The actually observed maximal settlement in the zone reached 41mm and the damages in the building were described as "slight" (Category 2). The volume loss was abnormally large because of an unexpected deterioration of the TBM cutting tools due to the presence of coarse gravel.

The parametric analysis in Sec. 5.5 has shown the influence of the model parameters on the determination of allowable settlements. Variations of the δ ratio, the measurement error E_m and the ground model error E_f have little effect on the allowable settlements, whereas the uncertainty of ground parameters (K, V_L) and the correlation coefficients (ρ_K, ρ_{V_L}) show a more significant influence. However, the changes in the results with the different assumptions are generally limited, which indicates that the method is applicable even when limited information about the site is available.

It was shown in Table 5.4 that a-priori, i.e. before the measurements, the probability of intolerable damage is higher than the selected value of p_T (5%). For this reason, the resulting allowable settlement values s_{lim} are always stricter (lower) than the expected settlement values S shown in Table 5.3. Therefore, the selected value of p_T could be seen as too strict. An improved choice of the target probability for intolerable damage p_T could be obtained by means of a risk-based approach. Expected monetary damages and consequences should be considered in a decision analysis for evaluating the optimality of decision alternatives. Mitigation measures could be implemented, such as the stabilization of ground with retaining walls or grout injection, and the cost of such measures should be compared against the risks incurred by continuing the construction process without them. The probability of intolerable damage could then be substituted by a threshold value for the acceptable risk. Such an approach could be implemented into practice by means of specific software used at tunnel construction control. This software would contain information about the probabilistic model shown throughout this paper and a database of those buildings that are potentially subjected to ground subsidence. Monitoring data gathered during the excavation would be used for updating of the probabilistic model. The existing risk at every location of tunnel face would be quantified and compared with the threshold value to decide whether the excavation should continue or mitigation measures should be implemented.

5.7 CONCLUSION

The paper presented a model for probabilistic prediction of building damage due to tunneling that is applicable in engineering practice (Sec. 5.2). A Gaussian profile model was used to simulate the settlement trough produced by tunneling. The equivalent beam method was then applied to determine the damage on buildings. The parameters describing the ground behavior and the building response were considered as uncertain. Additionally, the measurement and model errors were taken into account. An extension of the equivalent beam method was used to analyze buildings, which are not transverse to the tunnel axis.

A novel method for determining allowable settlements was presented (Sec. 5.3), which is a more systematic reliability-based approach with an explicit rationale than the deterministic methodology typically used in practice. Allowable settlements were defined as a settlement for which the probability of damage to the building is acceptably low. The

allowable settlement differs for different positions of the tunnel heading: they are stricter if the TBM is approaching the building and the settlement is not fully developed and they increase after the tunnel face passes the location of the building. The proposed reliability-based approach additionally allows incorporating measurements made during the construction for updating the prediction of ground behavior and for updating the allowable settlements.

The proposed procedure was demonstrated on a case study of a tunnel construction in Barcelona (Sec. 5.4). The input values were selected based on the real documentation of the project and the results show a good agreement with the observed settlements and damages during the construction. A parametric study has shown the influence of the different model parameters on the resulting predictions. It was shown that the effect of the assumptions made in the probabilistic model have limited effect on the resulting allowable settlements.

Acknowledgements

The Spanish Ministry of Economy and Competitiveness (MINECO) and the ERDF (European Regional Development Funds) have funded this research in the framework of the SUBTIS project ('Study of the Sensitivity of Urban Tunnels to Tunneling Induced Settlements' – BIA-2009-13233) by means of a pre-doctoral scholarship (FPI – BES-2010-030132). The authors want to thank the cooperation of *Infrastructures.cat* (before *Gestió d'Infraestructures S.A.* - GISA), the public company responsible for the design and construction of the L9 Metro Line in Barcelona.

6. Conclusions

The present research has allowed achieving several innovative contributions to the field of building damage produced by tunneling subsidence. General conclusions are outlined in the following, whereas specific conclusions are given at the end of each chapter.

6.1 GENERAL CONCLUSIONS

- Nowadays, several analytical and numerical techniques allow the assessment of building damage produced during the construction of tunnels. The literature in this field and the use of these techniques in the engineering practice are extensive. However, the existence of back analyses for checking the reliability of these approaches is rather scarce. For this reason, the presented study of a real building affected by tunneling subsidence represents a notable contribution to the field.

- The numerical simulation of the studied building has shown that Finite Element Models can be a powerful tool for the assessment of cracking patterns generated in buildings in case of tunneling subsidence.

- The Rankine-Hill macro-model in 2D, which uses two yield surfaces and allows considering cracking and crushing effects, has predicted a crack pattern in accordance with the damage survey. The distribution of plastic strains has clearly shown that the presence of openings in the façade has a notable importance in the onset of cracking.

- The Total Strain Rotating Crack model has been used for the 3D analysis of the studied building. The simulation of the construction process was here included, which allowed considering the effect of the longitudinal component of the

settlement. This may influence the deformation mechanism of the building and hence, the prediction of damage. The real cracking patterns in the building and the results obtained from the non-linear analyses have shown good agreement.

- The settlement trough generated in the 3D model by application of normal pressure to the lining can be more realistic when considering the coefficient of lateral earth pressure. However, the low depth of the presented tunnel, the simplicity of the soil models and the uncertainty associated to the interface elements still represent modeling challenges when developing this kind of coupled models.

- The predictions of damage done with the equivalent beam method showed good agreement with the real damage occurred. The application of this method revealed in turn certain factors that might be critical in assessment of damage. For example, it is usually assumed that walls are located transversally to the tunnel axis. This represents a conservative practice, but however, it can induce to high overestimations of the damages.

- A novel analytical formulation has been presented, which allows considering the real building wall alignment and hence, the possibility of reducing the estimated damage on buildings, which can be significant for some cases. An example was shown where the reduction of the maximum tensile strain in walls was about the 70%.

- The maximal damage in walls that are located perpendicular to the tunnel axis is produced once the tunnel face has passed under the building. However, in cases of walls not transversal to the tunnel track, the position of the tunnel heading that maximizes the damage can be given during the approach to the building. An iterative procedure has been developed in the thesis to determine the most critical tunnel face position.

- A comprehensive parametric analysis has been performed for a wide range of geological conditions and wall and tunnel geometries. The generated data was further used to create a non-linear regression model for making preliminary damage assessments. The model allows direct estimation of the maximum tensile strain in walls aligned transversally to tunnel axis. The presented model showed

good fit of the data and foresaw the category of damage correctly in more than 80% of the cases.

- The research also revealed the high sensitivity of predictions to the governing parameters regarding the characterization of ground. To the best author's understanding, predictions with a deterministic basis are barely reliable. The reason derives from the uncertainties surrounding the models used for the description of settlement trough and for the structural response of the building to such ground displacements. Examples of these uncertainties are the limited knowledge of the geotechnical conditions, the effect of the foundations in the transmission of ground movements to the buildings and the influence of the openings in walls when cracks are generated.

- The thesis has presented a model for the probabilistic prediction of building damage due to tunneling that is applicable in engineering practice. Gaussian profiles were used to model the settlement trough, whereas a novel analytical formulation was then applied to determine the damage on the buildings. The parameters describing the ground behavior and the building response were considered as uncertain. The measurement and model errors were also taken into account.

- A novel method for determining allowable settlements was also presented, which is a more systematic reliability-based approach with an explicit rationale than the deterministic methodology typically used in practice. Allowable settlements were defined as a settlement for which the probability of damage to the building is acceptably low. The allowable settlement differs for different positions of the tunnel heading: they are stricter if the tunnel face is approaching the building and the settlement is not fully developed and they increase after the tunnel face passes the location of the building. The proposed reliability-based approach additionally allows incorporating measurements made during the construction for updating the prediction of ground behavior and for updating the allowable settlements.

6.2 FUTURE RESEARCH

The present research has provided significant knowledge in the prediction of building damage due to tunneling subsidence. However, the analysis of the presented results

arouses other interesting topics to study. Therefore, the following research works are proposed:

- Development of strategies for improving the modeling of settlement troughs in Finite Element models that combine buildings, the tunnel and the soil, while keeping computational effort at feasible limits.

- Development of analytical expressions for the modeling of settlement troughs in case of curved tunnel tracks. Current available expressions apply only for straight tracks. This involves also the extension of the presented equation for ground horizontal strain to the curved case. With this, analytical predictions of damage done by the equivalent beam method could be performed for all possible shapes of the tunnel track.

- Development of the presented probabilistic model for setting limits on existing risk, not only on allowable settlements. This would allow considering for example the costs of mitigation measures and reparation of buildings.

- The achievement of the previous two points would allow the development of software to be implemented during tunnel construction. The existing risk of damage in the surrounding buildings would be known for every tunnel face position. Hence, decisions could be taken on whether the tunnel construction should be stopped or not.

- Improvement of the non-linear regression model for making preliminary damage assessments by direct estimation of the maximum tensile strain in building walls.

References

Abramowitz, M. and Stegun, I. A. (1972). Handbook of Mathematical Functions with Formulas, Graphs and Mathematical Tables, 9th printing. New York: Dover, p.11.

Arnau, O. and Molins, C. (2011). Experimental and Analytical Study of the Structural Response of Segmental Tunnel Linings Based on an in situ Loading Test. Part 2: Numerical simulation. Tunnelling and Underground Space Technology n. 26, p.778-788, 2011.

Arnau, O., Molins, C., Blom, C.B.M. and Walraven, J.C. (2012). Longitudinal Time-Dependent Response of Segmental Tunnel Linings. Tunnelling and Underground Space Technology n. 28, p.98-108, 2012.

ASTM International (2010). ASTM C803 / C803M-03(2010) Standard Test Method for Penetration Resistance of Hardened Concrete. ASTM INTERNATIONAL, West Conshohocken, PA (USA).

Attewell, P. B. and Woodman, J. P. (1982). Predicting the Dynamics of Ground Settlement and its Derivatives Caused by Tunnelling in Soil. Ground Engineering, 15 (7), p.13-22 and 36.

Attewell, P.B., Yeates, J. and Selby, A.R. (1986). Soil Movements Induced by Tunneling and Their Effects on Pipelines and Structures. Blackie Academic and Professional, Glasgow.

Augarde, C.E. (1997). Numerical Modelling of Tunnelling Processes for the Assessment of Damage to Buildings. PhD Thesis. University of Oxford.

Barbosa, B. (2010). Análisis del comportamiento de un edificio de obra de fábrica sometido a asentamientos inducidos por la perforación de túneles. Master Thesis. Universitat Politècnica de Catalunya.

Boscardin, M.D. and Cording, E.J. (1989). Building Response to Excavation-Induced Settlement. Journal of Geotechnical Engineering, ASCE , 115(1), p.1-21.

Burd, H.J., Houlsby, G.T., Augarde, C.L. and Liu, G. (2000). Modeling Tunneling-Induced Settlement of Masonry Buildings, 143 (Paper 11831), p. 17-29.

Burland, J.B., Standing, J.R. and Jardine, F.M. (2001). Building Response to Tunnelling: Case Studies from Construction of the Jubilee Line Extension, London. Thomas Telford.

Burland. J.B. (2008). The Assessment of the Risk of Damage to Buildings due to Tunnelling and Excavations. Jornada Técnica Payma Cotas: Movimiento de edificios inducidos por excavaciones. p. 3.

Burland, J.B., Broms, B. and De Mello,V.F.B. (1977). Behaviour of Foundations and Structures. Proc. 9th International Conference on Soil Mechanics and Foundations Eng., 2, p.495-546.

Burland, J.B. and Wroth, C.P. (1974). Settlement of Buildings and Associated Damage. London: Pentech Press.

Camós, C., (2011). A Case Study of Damage on Masonry Buildings Produced by Tunneling Induced Settlements. Master Thesis. Universitat Politècnica de Catalunya.

Camós, C., Molins, Arnau, O. and Gálvez, J. (2012). Numerical Simulation of the Structural Behaviour of Buildings Under Tunneling Induced Settlements. Proc. 8th Int. Conf. on Structural Analysis of Historical Constructions (Wrocklaw, Poland).

Camós, C. and Molins, C. (2013). A 3D Temporal Evolutionary Numerical Model of a Masonry Building in Barcelona Subjected to Tunnelling Subsidence. Proc. 3rd Int. Conf. on Computational Methods in Tunnelling and Subsurface Engineering (Ruhr University Bochum, Germany).

Camós, C., Molins, C. and Arnau, O. (2014). A Case Study of Damage on Masonry Buildings Produced by Tunneling Induced Settlements. International Journal of Architectural Heritage, 8, p.602-625.

Camós, C. and Molins, C. (2014) 3D Analytical Prediction of Building Damage Produced by Tunneling Subsidence. (Submitted to Tunnelling and Underground Space Technology).

Camós, C., Molins, C., Arnau, O. and Alegre V. (2011). Estudio de las cubetas de asientos producidas por la tunelación y simulación de la respuesta estructural de edificios afectados. V Congreso de ACHE, 2011, Barcelona.

Camós, C., Serrà, I., Molins, C. and Chirino, M. (2011). Clasifcación de los tipos constructivos y estructurales de los edificios para el estudio de su sensibilidad frente a los efectos de la tunelación. V Congreso de ACHE, 2011, Barcelona.

Camós, C., Špačková, O., Straub, D. and Molins, C. (2014). Probabilistic Approach to Assessing and Monitoring Settlements Caused by Tunneling. (Submitted to the Tunnelling and Underground Space Technology journal).

Camós, C., Špačková, O., Straub, D. and Molins, C. (2013). Development of a Probabilistic Model for the Prediction of Building Damage due to Tunneling Induced Settlements. 4th International Symposium on Geotechnical Safety and Risk. The Hong Kong University of Science and Technology, Hong Kong (China). Eds. L.M. Zhang, Y. Wang, G. Wang and D.Q. Li, Taylor and Francis Group.

Cottone, G., Gollwitzer, S. and Heckenberger, U. (2013). Reliability-Oriented Optimization of Replacement Strategies for Monitored Composite Panels for Aircraft Structures. Structural Health Monitoring 2013, Vols. 1 and 2, p. 2728-2735.

Der Kiureghian, A. (2005). First- and Second-Order Reliability Methods. Engineering design reliability handbook. E. Nikolaidis, D. M. Ghiocel and S. Singhal. Boca Raton, FL., CRC Press.

Deulofeu, C., Schwarz, H., Maidl, U., and Comulada, M. (2007). Data Management for Highly Mechanized Shield Tunneling in the Construction of the L9 Metro BCN. In Underground space—the 4th dimension of metropolises, eds. Barták, Hrdina, Romancov and Zlámal. London, UK: Taylor and Francis Group.

Devriendt, M. (2003). Assessing Building Response at King's X. Tunnels & Tunnelling International 2003 (July): 24.

Dimmock, P.S. (2008). Effect of Building Stiffness on Tunnelling-Induced Ground Movement. Tunnelling and Underground Space Technology, 23(4), p. 438-450.

Eisenstein, Z., Heinz, H. and Negro, A. (1994). On Three-Dimensional Ground Response to Tunnelling. In: Tunnelling in Soil and Rock, Proc. GEOTECH '84, Atlanta, May. New York: ASCE, 107-127.

EN 772-1 (2002). Methods of Test for Masonry Units. Part 1: Determination of the Compressive Strength. European Committe for Standardization, Brussels, Belgium.

Fargnoli, V., Boldini, D., Amorosi, A. (2013). TBM Tunnelling-Induced Settlements in Coarse-Grained Soils: The Case of the New Milan Underground Line 5. Tunnelling and Underground Space Technology 38: p.336–347.

Gálvez, J. (2012). Análisis de la respuesta de edificios unifamiliares adosados de obra de fábrica sometidos a asentamientos inducidos por tunelación, Master Thesis. Universitat Politècnica de Catalunya.

Ganz, H.R. (1985). Masonry Walls Under Normal Force and Shear. Report No. 148, Institute of Structural Engineering. ETH Zurich. Zurich, Switzerland.

Gatti, M.C. and Cassani, G. (2007). Ground Loss Control in EPB TBM Tunnel Excavation. Underground Space – the 4th Dimension of Metropolises, TUST.

Gesto, J.M. and Gens, A., (2008). Estimation of Building Damage due to Tunneling: an Analytical Approach, pp. 141. Jornada Técnica de Movimientos de Edificios Inducidos por Excavaciones, Aula Payma Cotas.

Giardina G. (2013). Modelling of Settlement Induced Building Damage. PhD Thesis. Technische Universiteit Delft (The Netherlands).

Giardina G., Van de Graaf, A.V., Hendriks, M.A.N, Rots, J.G. and Marini A. (2013). Numerical Analysis of a Masonry Façade Subject to Tunnelling-Induced Settlements. Engineering Structures 54 (2013): p.234–247.

Giardina G., Marini A., Hendriks, M.A.N, Rots, J.G. and Rizzardini, F., Giuriani, E. (2012). Experimental Analysis of a Masonry Façade Subject to Tunnelling-Induced Settlements. Engineering Structures 45 (2012): p.421–434.

Giardina, G., Boldrini, S., Max, A.N., Hendriks, J., Rots, G. (2012). Pile Foundation in 3D Modelling of Bulding Damage due to Settlement. Proc. 8th Int. Conf. on Structural Analysis of Historical Constructions (Wrocklaw, Poland).

Gong, W., Luo, Z., Juang, C. H., Huang, H., Zhang, J., Wang, L. (2014). Optimization of Site Exploration Program for Improved Prediction of Tunneling-Induced Ground Settlement in Clays. Computers and Geotechnics 56 (2014) p.69–79.

Graham, A. (2002). Three-dimensional analysis of tunnelling effects on structures to develop design methods. PhD Thesis. University of Oxford.

Guglielmetti, V., Grasso, P., Mahtab, A. and Xu, S. (2008). Mechanized Tunnelling in Urban Areas: Design Methodology and Construction Control. Taylor and Francis Group, London, UK. ISBN 978-0-415-42010-5.

Huber, M., Hicks, M, Vermeer, P.A. and Moormann, C. (2010). Probabilistic calculation of differential settlement due to tunneling. Gucma, van Gelder and Proske: Proceedings of the 8th International Probabilistic Workshop, Szczecin 2010.

Jiménez Salas, J.A. (1982). Geotecnia y Cimientos, Vol. III: Cimentaciones, excavaciones y aplicaciones de la Geotecnica (Ed. Rueda).

Kappen, J.M.J. (2012). Three-dimensional Numerical Analysis of Tunnelling Induced Damage: the Influence of Masonry Building Geometry and Location. Master Thesis. Delft University of Technology (The Netherlands).

Kappen, J.M.J., Giardina, G., Max, A.N., Hendriks and J., Rots, G. (2013). 3D Numerical Analysis of Tunnelling Induced Damage: the Influence of the Alignment of a Masonry Building with the Tunnel Axis. Proc. 3rd Int. Conf. on Computational Methods in Tunnelling and Subsurface Engineering (Ruhr University Bochum, Germany).

Kym, C.Y., Bae, G.J., Hong, S.W., Park, C.H., Moon, H.K. and Shin, H.S. (2001). Neural Network Based Prediction of Ground Surface Settlement due to Tunneling. Computers and Geotechnics (2001) 28, p.517-547.

Lee, K.M. and Rowe, R.K. (1990). Finite Element Modelling of the Three-Dimensional Ground Deformations due to Tunnelling in Soft Cohesive Soils. Computers and Geotechnics, 10 (2), p.87-109.

Liu, G. (1997). Numerical Modelling of Damage to Masonry Buildings due to Tunnelling. PhD Thesis. University of Oxford.

Lourenço, P.B. (1996). Computational Strategies for Masonry Structures. PhD Thesis, Delft University of Technology (The Netherlands).

Mair, R.J., Taylor, R.N. and Burland, J.B. (1996). Prediction of Ground Movements and Assessment of Risk of Building Damage due to Bored Tunneling. Proc. Int. Symp. on Geotechnical Aspects of Underground Construction in Soft Ground, p. 713.

Melchers, R. E. (1999). Structural Reliability Analysis and Prediction, 2nd Ed., John Wiley, Chichester; New York.

Molins, C. and Camós C. (2013). Study of the Sensitivity of Different Building Structures to Tunneling Induced Settlements. Proceedings of the Second International Conference on Structures and Architecture, Guimaraes, Portugal, 24-26 July 2013. CRC Press Taylor & Francis Group, 2013, p. 704-711.

Möller, S. (2006) Tunnel Induced Settlements and Structural Forces in Lining. Mitteilung 54 des Instituts für Geotechnik Herausgeber P.A. Vermeer.

Mollon, G., Dias, D. and Soubra, A. (2013) Probabilistic analyses of tunneling-induced ground movements. Acta Geotechnica (2013), 8, pp.181-199.

Muzás Labad, F. (2002). Consideraciones sobre la elección de coeficientes de balasto. Revista de Obras Públicas,nº 3427, p. 45.

Netzel, H. (2009). Building Response due to Ground Movements. PhD Thesis, Delft University of Technology (The Netherlands).

Netzel, H. and Kaalberg, F.J. (1999). Numerical Damage Risk Assessment Studies on Masonry Structures due to TBM-Tunnelling in Amsterdam. In: Geotechnical Aspects of Underground Construction in Soft Ground, An International Symposium, Tokyo, 21-23 July.

Nomoto, T., Mori, H., Matsumoto, M., (1995). Overview on Ground Movements during Shield Tunnelling – a Survey on Japanese Shield Tunnelling. In: Proc. Int. Symposium on Geotechnical Aspects of Underground Construction in Soft Ground, Balkema, p. 345–35.

O'Reilly, M. P. and New, M. (1982). Settlements above Tunnels in the United Kingdom—Their Magnitude and Prediction. In Proceedings of Tunnelling '82. London, UK: Institution of Mining and Metallurgy, 173–181.

Papaioannou, I. and Straub. D (2012). Reliability Updating in Geotechnical Engineering Including Spatial Variability of Soil. Computers and Geotechnics 42: p.44–51.

Peck, R.B. (1969). Deep Excavations and Tunneling in Soft Ground. SOA Report, 7th Int. Conf. SM&FE.

Potts, D.M. and Addenbrooke, T.I (1997). A Structure's Influence on Tunneling-Induced Ground Movements. Proc. Instn. Civ. Engrs. Geotech. Engng., (125), p. 109.

Rankin, W.J. (1988). Ground Movements Resulting from Urban Tunneling; Predictions and Effects. Engineering Geology Special Publication, 5, pp. 79.

Roca, P., Cervera, M., Gariup, G., Pela', L. (2010). Structural Analysis of Masonry Historical Constructions. Classical and Advanced Approaches. Archives of Computational Methods in Engineering 17 (3), p.299-325.

Rots, J.G. (1989). Crack Models for Concrete: Discrete or Smeared? Fixed, Multi-Directional or Rotating? Heron, vol. 34, num. 1. TNO-Institute for Building Materials and Structures.

Rots, J.G. and Invernizzi, S. (2005). Prevision of Settlement-Induced Cracking in Historical Building Masonry Façades. Structural Analysis of Historical Constructions, Taylor & Francis Group.

Rowe, R.K., Lo, K.Y. and Kack, G.J. (1983). A Method of Estimating Surface Settlement Above Tunnels Constructed in Soft Ground. Canadian Geotechnical Journal, 20:11-22.

Samarasinghe, W., Page, A.W. and Hendry, A.W. (1982). A Finite Element Model for the in Plane Behavior of Brickwork. Proc. Inst. Civ. Eng., 71(2), p.171.

Sandoval, C., Roca, P., Bernat, E., and Gil, L. (2011). Testing and numerical modelling of buckling failure of masonry walls. Construction and building materials (25), pp. 4394-4402.

Smyth, G.K. (2006). Nonlinear Regression. Encyclopedia of Environmetrics 3: p.1405–1411. John Wiley & Sons, Ltd. Chichester, UK.

Špačková, O. and Straub, D. (2013). Dynamic Bayesian Network for Probabilistic Modelling of Tunnel Excavation Processes. Journal of Computer-Aided Civil and Infrastructure Engineering 28 (1), p.1-21.

Standing, J.R. **(2008).** Building Response to Tunneling: the Importance of Monitoring. Jornada Técnica: Movimientos de edificios inducidos por excavaciones: criterios de daño y gestión del riesgo. Aula Payma Cotas.

Straub, D. (2011). Reliability Updating with Equality Information. Probabilistic Engineering Mechanics 26: p.254-258.

Straub D., and Papaioannou I. (2014). Bayesian Updating with Structural Reliability Methods. Journal of Engineering Mechanics, Trans. ASCE, in print.

Skempton, A.W. and MacDonald, D.H. (1956). The Allowable Settlements of Buildings. ICE Proceedings: Engineering Divisions, Volume 5, Issue 6, p.727 –768.

Timoshenko, S. (1957). Strength of Materials Part I, D van Nostrand Co, Inc. London.

TNO (2005). Diana User's Manual. Release 9. http://www.tnodiana.com.

TYPSA (2003). Análisis de los movimientos del terreno producidos por la excavación mecánica del túnel de la L9 en la zona de Santa Coloma de Gramanet. Construction project of the L9 Metro Line in Barcelona. Bon Pastor – Can Zam. Stations and Infrastructure. Annex 8.

Vermeer and Brinkgreve (1993). PLAXIS Version 5 Manual. Rotterdam, a. a. Balkema edition.

Yoo, C., Kim, Y. (2003). A Web-Based Tunneling-Induced Building Utility Damage Assessment System: TURISK. Tunnelling and Underground Space Technology 18: p.497–511.

ANNEXES

A. Derivative of the ground horizontal movement U_x with respect to y.

Application of Eq. (4.19) requires the calculation of the term $\frac{\partial U_x}{\partial y}$, given in Eq. (4.21). For its determination, it has been assumed that:

$$\frac{\partial U_x}{\partial y} = \frac{\partial \left(\frac{x}{z_0 - z} \cdot S\right)}{\partial y} = \frac{x}{z_0 - z} \cdot \frac{\partial S}{\partial y} \tag{A.1}$$

where:

$$\frac{\partial S}{\partial y} = -S_{max} \cdot exp\left[-\frac{x^2}{2 \cdot K_x^2 \cdot (z_0 - z)^2}\right] \cdot \tag{A.2}$$

$$\cdot \frac{\partial}{\partial y}\left(\left[\Phi\left(\frac{y - (y_s + y_0)}{K_y \cdot (z_0 - z)}\right) - \Phi\left(\frac{y - y_f}{K_y \cdot (z_0 - z)}\right)\right]\right)$$

Focusing on the derivatives:

$$\frac{\partial}{\partial y}\left(\left[\Phi\left(\frac{y - (y_s + y_0)}{K_y \cdot (z_0 - z)}\right) - \Phi\left(\frac{y - y_f}{K_y \cdot (z_0 - z)}\right)\right]\right) \tag{A.3}$$

$$= \frac{\partial\left[\Phi\left(\frac{y-(y_s+y_0)}{K_y \cdot (z_0 - z)}\right)\right]}{\partial y} - \frac{\partial\left[\Phi\left(\frac{y-y_f}{K_y \cdot (z_0 - z)}\right)\right]}{\partial y}$$

Renaming these two derivatives as *C* and *D*:

$$C = \frac{\partial\left[\Phi\left(\frac{y-(y_s+y_0)}{K_y\cdot(z_0-z)}\right)\right]}{\partial y} \tag{A.4}$$

$$D = \frac{\partial\left[\Phi\left(\frac{y-y_f}{K_y\cdot(z_0-z)}\right)\right]}{\partial y} \tag{A.5}$$

Φ corresponds to the standard normal cumulative distribution function:

$$\Phi = \int_{-\infty}^{f(y)} \frac{1}{\sqrt{2\pi}} e^{-\frac{m^2}{2}} dm \tag{A.6}$$

where m is an auxiliary integration variable.

The field of ground displacements (and hence, the strain tensor $\boldsymbol{\varepsilon}$) at a particular depth z is given for each combination of ground conditions and tunnel geometry values (K_x, K_y, y_0, z_0, V_L, D, y_s and y_f). Therefore, the derivatives *C* and *D* in Eq. (A.3) will depend only on the variable y. The functions $f_C(y)$ and $f_D(y)$ at C and D are:

$$f_C(y) = \frac{y-(y_s+y_0)}{K_y\cdot(z_0-z)} \tag{A.7}$$

$$f_D(y) = \frac{y-y_f}{K_y\cdot(z_0-z)} \tag{A.8}$$

In this case, the Leibniz integral rule applies (Abramowitz *et al*., 1972):

$$\frac{d}{dy}\left(\int_{f_1(y)}^{f_2(y)} g(m)dm\right) = g[f_2(y)]\cdot f_2'(y) - g[f_1(y)]\cdot f_1'(y) \tag{A.9}$$

where f_1, f_2 are g are generic functions that depend on y and f_1' and f_2' are the correspondent derivatives respect to y. Since the lower bound of both integrals in C and D is $-\infty$, $f_1' = 0$ and Eq. (A.9) results in:

$$\frac{d}{dy}\left(\int_{-\infty}^{f_2(y)} g(m)dm\right) = g[f_2(y)]\cdot f_2'(y) \tag{A.10}$$

So that, if $f_2 \equiv f_C(y)$,

$$C = \frac{d\left[\Phi\left(\frac{y-(y_s+y_0)}{K_y\cdot(z_0-z)}\right)\right]}{dy} = \frac{1}{\sqrt{2\pi}} e^{-\frac{\left(\frac{y-(y_s+y_0)}{K_y\cdot(z_0-z)}\right)^2}{2}} \cdot \left(\frac{1}{K_y \cdot (z_0 - z)}\right) \tag{A.11}$$

And if $f_2 \equiv f_D(y)$,

$$D = \frac{d\left[\Phi\left(\frac{y-y_f}{K_y\cdot(z_0-z)}\right)\right]}{dy} = \frac{1}{\sqrt{2\pi}} e^{-\frac{\left(\frac{y-y_f}{K_y\cdot(z_0-z)}\right)^2}{2}} \cdot \left(\frac{1}{K_y \cdot (z_0 - z)}\right) \tag{A.12}$$

Then, the component of the strain tensor is finally obtained:

$$\frac{\partial U_x}{\partial y} = \frac{x}{z_0 - z} \cdot (-S_{max}) \cdot \left(exp\left(-\frac{x^2}{2 \cdot K_x^2 \cdot (z_0 - z)^2}\right)\right) \cdot (C - D) \tag{A.13}$$

which is equivalent to Eq. (4.21).

B. Notation

a	Height of the equivalent beam fiber where strains are calculated
A	Cross-section area per unit length of the beam
A_{exc}	Area of excavation
b	Distance between two locations within a quasi-homogeneous section
B	Beam half-length
c	Scaling constant
C	Cohesion
C.V.	Coefficient of variation
C_0	Cutt-off 0 (settlements lower than 1mm are included)
C_1	Cutt-off 1 (settlements lower than 1mm are disregarded)
d	Tunnel diameter
d_{axis}	Distance from tunnel longitudinal axis to a parallel building wall
d_{orig}	Distance from origin of coordinates to building reference point $\hat{A}$
e	Distance between tunnel axis and building centerline
E	Young modulus of material
E/G	Material elastic / shear modulus ratio
E_s	Representative soil stiffness
E_x	Horizontal elastic modulus of the material
E_y	Vertical elastic modulus of the material
E_y/E_x	Ratio between vertical and horizontal modulus of elasticity of the material
$E_{\varepsilon_{br}}$	Error of resultant extreme fiber strain in bending, accounting for ground strain
$E_{\varepsilon_{dr}}$	Error of resultant extreme fiber strain in shear, accounting for ground strain
$E_{br}^{hog,1}$	Error of maximum bending strain in hogging zone 1
$E_{br}^{hog,2}$	Error of maximum bending strain in hogging zone 2
E_{br}^{sag}	Error of maximum bending strain in sagging zone
$E_{dr}^{hog,1}$	Error of maximum shear strain in hogging zone 1

$E_{dr}^{hog,2}$	Error of maximum shear strain in hogging zone 2
E_{dr}^{sag}	Error of maximum shear strain in sagging zone
E_E	Error including the ground model error and the settlement measurement error
E_f	Ground model error for settlement prediction
E_m	Settlement measurement error
$F_{\varepsilon_{lim}}$	Failure of the construction process producing intolerable damage
f_{cx}	Horizontal compressive strength of the material
f_{cy}	Vertical compressive strength of the material
f_{cy}/f_{cx}	Ratio between vertical and horizontal compressive strength of the material
f_E	Probability density function of E_E
f_{t_i}	Tensile strength of interface elements
f_{tx}	Horizontal tensile strength of the material
f_{ty}	Vertical tensile strength of the material
G	Shear modulus of material
H	Building height
i_x (or i)	Distance from origin to inflection point in the transverse direction to tunnel axis
i_y	Distance from origin to inflection point in the longitudinal direction to tunnel axis
I	Inertia per unit length of the equivalent beam
k	Realization of trough width parameter
k_i	Trough width parameter at location of measurement s_i
k_m	Trough width parameter at location of measurement s_m
k_n	normal stiffness modulus of interface elements
k_t	shear stiffness modulus of interface elements
K_x (or K)	Trough width parameter in the transverse direction to tunnel axis
K_s	Compression stiffness of non-linear springs
K_y	Trough width parameter in the longitudinal direction to tunnel axis
K_0	Coefficient of lateral earth pressure
l	Horizontal distance between two reference points
l_{build}	Building length
l_{hog_1}	Building length in hogging zone 1
l_{hog_2}	Building length in hogging zone 2
l_{sag}	Building length in sagging zone
L_i	Likelihood function
M	Modification factors of Potts and Addenbrooke

M^{DRhog}	Modification factor of Potts and Addenbrooke to be applied on the deflection ratio of hogging
M^{DRsag}	Modification factor of Potts and Addenbrooke to be applied on the deflection ratio of sagging
$M^{\varepsilon_{hc}}$	Modification factor of Potts and Addenbrooke to be applied on the compressive ground strain
$M^{\varepsilon_{ht}}$	Modification factor of Potts and Addenbrooke to be applied on the tensile ground strain
p	Uniform radial pressure applied to tunnel lining
p_h	Horizontal pressure applied to tunnel lining
p_n	Resultant normal pressure applied to tunnel lining
p_v	Vertical pressure applied to tunnel lining
p_T	Probability of intolerable damage
Pr (F)	Probability of failure
q	Cylinder thickness
r	Horizontal distance between the z-axis and whichever point
$r_{\hat{P}}$	Horizontal distance between the z-axis and whichever ground point $\hat{P}$
R	Tunnel radius
R_K	Constant autocorrelation function for variable K
R_{V_L}	Constant autocorrelation function for variable V_L
s_i	Value of i-th settlement measurement
s_{lim}	Allowable value of settlement
s^*_{lim}	Updated allowable value of settlement
s_m	Realization of settlement measurement
S	Settlement
$\boldsymbol{S}$	Vector of settlement measurements
S_m	Settlement measurement
S_{max}	Maximal settlement
S_{par}	Settlement for buildings walls parallel to tunnel axis
t	Position of neutral axis in the equivalent beam
t_{hog}	Position of neutral axis in the hogging zone of the equivalent beam
t_{sag}	Position of neutral axis in the sagging zone of the equivalent beam
u	Realization of normal standard variable
u_i	Realization of normal standard variable at location of measurement s_i
U_x	Ground horizontal movements in the transverse direction (to tunnel axis)
U_y	Ground horizontal movements in the longitudinal direction (to tunnel axis)
$U_{y,par}$	Ground horizontal movements for buildings walls parallel to tunnel axis

v_{L_i}	Volume loss at location of measurement s_i
v_{L_m}	Volume loss at location of measurement s_m
v_L	Realization of ground volume loss
V_L	Ground volume loss
V_s	Generated volume loss per unit length
x	x-coordinate
$\hat{x}$	$\hat{x}$-coordinate
x_i	x-coordinate of measurement s_i
x_m	x-coordinate of measurement s_m
X	Vector of random variables
XRD	X-Ray Diffraction
y_f	Location of tunnel origin
y_i	y-coordinate of measurement s_i
y_m	y-coordinate of measurement s_m
y_s	Location of tunnel face
z	z-coordinate
z_0	Depth of tunnel axis
z_i	Depth of measurement s_i
z_m	Depth of measurement s_m
$z_{\hat{P}}$	Depth of whichever ground point $\hat{P}$
α	Central angle of tunnel section
α^*	Relative axial stiffness of the beam
δ	Ratio between surface settlement above tunnel face and maximal settlement at infinite distance of the face
δ_R	Radial variation of length in a cylinder
Δ	Relative deflection between two reference points
Δ/l	Deflection ratio
Δ_{hog_1}/l_{hog_1}	Deflection ratio in hogging zone 1
Δ_{hog_2}/l_{hog_2}	Deflection ratio in hogging zone 2
Δ_{sag}/l_{sag}	Deflection ratio in sagging zone
ΔV_{tube}	Volume reduction per unit length of a cylinder
ε_{bmax}	Maximum tensile strain in the equivalent beam due to bending
$\varepsilon_{br}^{hog,1}$	Maximum bending strain in hogging zone 1
$\varepsilon_{br}^{hog,2}$	Maximum bending strain in hogging zone 2
ε_{br}^{sag}	Maximum bending strain in sagging zone
ε_{br}	Resultant extreme fiber strain in bending, accounting for ground strain
ε_{dmax}	Maximum tensile strain in the equivalent beam due to shear
$\varepsilon_{dr}^{hog,1}$	Maximum shear strain in hogging zone 1

$\varepsilon_{dr}^{hog,2}$	Maximum shear strain in hogging zone 2
ε_{dr}^{sag}	Maximum shear strain in sagging zone
ε_{dr}	Resultant extreme fiber strain in shear, accounting for ground strain
ε_{h,hog_1}	Resultant horizontal ground strain at surface in hogging zone 1
ε_{h,hog_2}	Resultant horizontal ground strain at surface in hogging zone 2
$\varepsilon_{h,sag}$	Resultant horizontal ground strain at surface in sagging zone
ε_{h}^{sag}	Resultant horizontal ground strain at surface in sagging zone
ε_{h}	Resultant horizontal ground strain
ε_{h+}	Tensile horizontal ground strain
ε_{h-}	Compressive horizontal ground strain
$\varepsilon_{h,mean}$	Mean value of horizontal ground strain at surface level
$\varepsilon_{h,par}$	Resultant horizontal ground strain for buildings walls parallel to tunnel axis
ε_{lim}	Limit strain value for damage classification
ε_{max}	Maximum strain in the equivalent beam
$\varepsilon_{max,fit}$	Adjusted maximum strain in the equivalent beam (non-linear regression model)
$\varepsilon_{h,xx}$	Component xx of ground strain infinitesimal tensor
$\hat{\varepsilon}_{h,\widehat{xx}}$	Component $\widehat{xx}$ of ground strain infinitesimal tensor
$\hat{\varepsilon}_{h,\widehat{xx},par}$	Component $\widehat{xx}$ of ground strain infinitesimal tensor for buildings walls parallel to tunnel axis
$\varepsilon_{h,xy}$	Component xy of ground strain infinitesimal tensor
$\varepsilon_{h,yy}$	Component yy of ground strain infinitesimal tensor
ε_{p_1}	Plastic strains
ε_{x}	Principal strains
θ	Building alignment respect to x axis
$\theta_{\hat{P}}$	Alignment of whichever ground point $\hat{P}$
μ_{V_L}	Lognormal parameter of V_L
μ'_{V_L}	Modified lognormal parameter of V_L
μ_K	Lognormal parameter of K
μ'_K	Modified lognormal parameter of K
ν	Poisson's ratio
ρ^*	Relative bending stiffness of the beam
ρ_K	Correlation coefficient of K
ρ_{V_L}	Correlation coefficient of V_L
σ_{E_E}	Standard normal deviation of E_E
σ_{V_L}	Lognormal parameter of V_L
σ'_{V_L}	Modified lognormal parameter of V_L

σ_K	Lognormal parameter of K
σ'_K	Modified lognormal parameter of K
ϕ	Internal friction angle
$\Phi(\cdot)$	Cumulative standard normal distribution function
Ω_0	Observation domain
ψ	Dilatancy angle
Ω_F	Failure domain
Ω_i	Corresponding observation domain for measurement s_i